

การเปรียบเทียบสมบัติเชิงโครงสร้างของฟิล์มควิบิกแกลเลียมไนไตรด์ที่ปลูกผลึกโดยเมทอล
ออร์แกนิกเวเปอ์เฟสเอพิแทกซีลงบนชั้นสเตรตแกลเลียมอาร์เซไนด์ที่ระนาบ (311) และ (001)

นายณัฐพงศ์ ดิษฐเจริญ

วิทยานิพนธ์นี้เป็นส่วนหนึ่งของการศึกษาตามหลักสูตรปริญญาวิทยาศาสตรมหาบัณฑิต
สาขาวิชาฟิสิกส์ ภาควิชาฟิสิกส์
คณะวิทยาศาสตร์ จุฬาลงกรณ์มหาวิทยาลัย
ปีการศึกษา 2551
ลิขสิทธิ์ของจุฬาลงกรณ์มหาวิทยาลัย

COMPARISON OF STRUCTURAL PROPERTY OF CUBIC GaN FILMS GROWN BY
METALORGANIC VAPOR PHASE EPITAXY ON (311) AND ON (001) GaAs SUBSTRATES

Mr. Nuttapong Discharoen

A Thesis Submitted in Partial Fulfillment of the Requirements
for the Degree of Master of Science Program in Physics

Department of Physics

Faculty of Science

Chulalongkorn University

Academic year 2008

Copyright of Chulalongkorn University

510874


Thesis Title COMPARISON OF STRUCTURAL PROPERTY OF
CUBIC GaN FILMS GROWN BY METALORGANIC
VAPOR PHASE EPITAXY ON (311) AND ON (001) GaAs
SUBSTRATES

By Mr. Nuttapong Discharoen


Field of Study Physics


Advisor Assistant Professor Sakuntam Sanorpim, Ph.D.

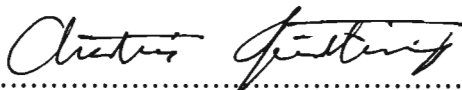
Accepted by the Faculty of Science, Chulalongkorn University in Partial
Fulfillment of the Requirements for the Master's Degree


.....Dean of the Faculty of Science
(Professor Supot Hannongbua, Ph.D.)

THESIS COMMITTEE

..... Chairman
(Assistant Professor Chaisingh Poo-Rakkiat, Ph.D.)

..... Advisor
(Assistant Professor Sakuntam Sanorpim, Ph.D.)

..... Examiner
(Chatchai Srinithiwawong, Ph.D.)

..... Examiner
(Assistant Professor Somchai Kiatgamolchai, Ph.D.)

ณัฐพงศ์ ดิษฐเจริญ : การเปรียบเทียบสมบัติเชิงโครงสร้างของฟิล์มควมิกแกลเลียมไนไตรด์ที่ปลูกผลึกโดยเมททอลออร์แกนิกเวเปอร์เฟสเอพิแทกซีลงบนซับสเตรตแกลเลียมอาร์เซไนด์ที่ระนาบ (311) และ (001). (COMPARISON OF STRUCTURE PROPERTY OF CUBIC GaN FILMS GROWN BY METALORGANIC VAPOR PHASE EPITAXY ON (311) AND ON (001) GaAs SUBSTRATES) อ. ที่ปรึกษาวิทยานิพนธ์หลัก: ผศ. ดร. สกฤตธรรม เสนาะพิมพ์, 77 หน้า.

ความเครียดและการก่อเกิดของโครงสร้างแบบเฮกซะโกนัลในชั้นของควมิกแกลเลียมไนไตรด์ที่ปลูกโดยเมททอลออร์แกนิกเวเปอร์เฟสเอพิแทกซีลงบนซับสเตรตแกลเลียมอาร์เซไนด์ที่ระนาบ (001) และ (311) ถูกตรวจสอบโดยการเลี้ยวเบนรังสีเอกซ์กำลังแยกสูงและการกระเจิงแบบรามาน พบว่าฟิล์มควมิกแกลเลียมไนไตรด์อยู่ในสภาวะความเครียดแบบอัดซึ่งตรงกันข้ามจากที่คาดการณ์ว่าจะอยู่ในสภาวะความเครียดแบบดึง นอกจากนี้โครงสร้างแบบควมิกแกลเลียมไนไตรด์มีการก่อเกิดบนระนาบ (001) และ (311) รวมกับโครงสร้างแบบเฮกซะโกนัลแกลเลียมไนไตรด์ที่ก่อเกิดบนระนาบ {111} จากผลการเลี้ยวเบนรังสีเอกซ์กำลังแยกสูงพบความเครียดที่เกิดขึ้นในฟิล์มควมิกแกลเลียมไนไตรด์มีความซับซ้อน ขึ้นกับเงื่อนไขการปลูก เราอธิบายได้ว่าเกิดจากการรวมกันของสองอิทธิพลระหว่างความแตกต่างของค่าคงที่โครงผลึกและค่าความแตกต่างของอุณหภูมิ ค่าคงที่โครงผลึกของควมิกแกลเลียมไนไตรด์ขณะไม่มีอิทธิพลของความเครียดมีค่าเท่ากับ $4.5045 \pm 0.0021 \text{ \AA}$ ซึ่งมีค่าสอดคล้องกับทางทฤษฎีเท่ากับ 4.503 \AA โครงสร้างควมิกแกลเลียมไนไตรด์มีโครงสร้างเฮกซะโกนัลแกลเลียมไนไตรด์รวมอยู่ $H_{XRD} = 25-85\%$ แม้ว่าารรวมของโครงสร้างแบบเฮกซะโกนัลในโครงสร้างแบบควมิกแกลเลียมไนไตรด์ที่ปลูกบนแกลเลียมอาร์เซไนด์ที่ระนาบ (311) ไม่สามารถตรวจสอบด้วยการเลี้ยวเบนรังสีเอกซ์ แต่ในทางตรงกันข้ามการกระเจิงแบบรามานยืนยันการมีอยู่ของโครงสร้างแบบเฮกซะโกนัลได้ โครงสร้างแบบเฮกซะโกนัลที่ได้จากการกระเจิงแบบรามาน H_{Raman} แสดงถึงความสัมพันธ์แบบสมการเส้นตรงที่ทำให้เป็นมาตรฐานกับการเลี้ยวเบนของรังสีเอกซ์ H_{XRD} เพื่อใช้พิจารณาหาปริมาณของโครงสร้างแบบเฮกซะโกนัลแกลเลียมไนไตรด์ในโครงสร้างแบบควมิกแกลเลียมไนไตรด์

ภาควิชา..... ฟิสิกส์..... ลายมือชื่อนิสิต..... ณัฐพงศ์.....
 สาขาวิชา..... ฟิสิกส์..... ลายมือชื่อ อ. ที่ปรึกษาวิทยานิพนธ์หลัก..... SK.....
 ปีการศึกษา..... 2551.....

4872280023: MAJOR PHYSICS

KEYWORDS: HIGH RESOLUTION X-RAY DIFFRACTION / METALORGANIC VAPOR PHASE EPITAXY / RAMAN SCATTERING / STRAIN / CUBIC GaN

NUTTAPONG DISCHAROEN: COMPARISON OF STRUCTURAL PROPERTY OF CUBIC GaN FILMS GROWN BY METALORGANIC VAPOR PHASE EPITAXY ON (311) AND ON (001) GaAs SUBSTRATES. ADVISOR: ASST. PROF. SAKUNTAM SANORPIM, Ph.D., 77 pp.

Strains and hexagonal phase generation in c-GaN layers grown by metalorganic vapor phase epitaxy on (001) GaAs and on (311) GaAs substrates were investigated using HRXRD and Raman scattering. The results show that c-GaN films are compressive. This contrasts with results which should be under tensile strain. In addition, c-GaN films have a cubic structure which is generated on the (001) and (311) planes and contain some amount of hexagonal phase generated on {111} plane. From HRXRD results, it is found that the relief of strains in the c-GaN layers has a complicated dependence on the growth conditions. We interpreted this as the interaction between the lattice mismatch and thermal mismatch stresses. The fully relaxed lattice constants of cubic GaN are determined to be $4.5045 \pm 0.0021 \text{ \AA}$, which is in agreement with the theoretical prediction of 4.503 \AA . The c-GaN layers contain 25-85% hexagonal phase inclusion. Although, the hexagonal phase inclusion in c-GaN layers on GaAs (311) cannot be determined by HRXRD measurement. On the other hand, Raman scattering is a very sensitive method for measuring an existence of hexagonal phase. The hexagonal phase inclusion determined by Raman spectroscopy technique, H_{Raman} , exhibits a linear dependence on the H_{XRD} , providing a useful calibration method to determine the hexagonal phase inclusion in c-GaN layers.

Department:Physics.....

Field of Study:Physics.....

Academic Year:2008.....

Student's Signature.....

Advisor's Signature.....

Acknowledgements

I would like to sincerely express my gratitude to my advisor, Assistant Professor Dr. Sakuntum Sanorpim for his valuable suggestions, encouragement, continued assistance and time throughout the length of thesis. He gave me good experience, participating in an conference (presentation) in Thailand and English writing (journal and thesis).

I am deeply indebted to Assistant Professor Dr. Chaisingh Poo-Rakkiat, Dr. Chatchai Srinitivawong and Assistant Professor Dr. Somchai Kiatgamolchai for being my thesis committees. Their comments on this thesis are very gratefully appreciated. I wish to thank Assistant Professor Dr. Sukkanaste Tungasmita for usefully suggestion and additional information to support my work. In particular, I am grateful to Mr. Manop Tiraratanasomphod for his technique assistance in operation of HRXRD instrument at Scientific and Technology Research Equipment Center, Chulalongkorn University.

I would like to acknowledge the financial supports from the Thailand-Japan Technology Transfer Project-Overseas Economic Cooperation Found (TJTTP-OECF) and Graduate Schools of Chulalongkorn University. I would like to acknowledge Department of Physic, Faculty of Science, Chulalongkorn University for providing teaching assistantship. Special thank goes to Professor Dr. Kentaro Onabe, Department of Advanced Materials Science, Graduate Schools of Frontier Sciences, the University of Tokyo, Japan, for providing the great sample to analyze and correcting my manuscripts.

I would like to thank my colleagues: Pawinee, Dares, Kwang, Ying, tum, Rut, Pin, Nene', Koy, Bingo, Ging and many friends for helpful discussions and joyful moments.

I would like to pay my heartfelt thanks to my family; my father, my mother and my brother for love, understanding and supports.

CONTENTS

	Page
Abstract (Thai)	iv
Abstract (English)	v
Acknowledgements	vi
Contents	vii
List of Tables	ix
List of Figures	xi
 Chapter	
I Introduction	1
1.1 Gallium Nitride.....	1
1.2 Objectives and organization of the thesis.....	6
II Characterization techniques and their principle	7
2.1 High-resolution X-ray diffraction.....	7
2.2 Scan modes in HRXRD.....	8
2.2.1 $2\theta/\omega$ -scan mode.....	8
2.2.2 ω -scan mode.....	8
2.2.3 X-ray reciprocal lattice space mapping.....	10
2.3 Determination of strain in epitaxial film.....	11
2.4 Determination of the hexagonal phase inclusion.....	15
2.5 Raman scattering.....	15
III Materials and Experiment	20
3.1 Sample details.....	20
3.1.1 c-GaN on GaAs (001).....	21

Chapter	Page
3.1.2 c-GaN on GaAs (311).....	27
3.2 High resolution XRD diffraction measurements.....	32
3.3 Raman scattering spectroscopy measurements.....	33
IV Anomalous Strain in c-GaN.....	35
4.1 Strain in c-GaN on GaAs (001).....	35
4.2 Strain in c-GaN on GaAs (311).....	45
4.3 Summary.....	50
V Hexagonal phase generation in c-GaN.....	51
5.1 hexagonal phase generation in c-GaN on GaAs (001).....	51
5.1.1 Detection of an inclined hexagonal-phase	52
5.1.2 Estimation of hexagonal phase inclusion.....	55
5.1.3 Correlation between vibrational properties and hexagonal phase generation.....	61
5.2 Hexagonal phase generation in c-GaN on GaAs (311).....	64
5.3 Summary.....	68
VI Conclusions.....	69
References.....	71
Appendix.....	76
Regional conference presentations.....	76
Vitae.....	77

List of Tables

Table	Page
1.1 Lattice constants, lattice mismatch and thermal expansion coefficients for substrate materials of c-GaN film.....	6
2.1 Phonon frequencies of GaN crystals including both hexagonal and cubic crystal lattices(h-TO and c-TO are transverse optical mode of hexagonal and cubic structure, respectively. And h-LO and c-LO are longitudinal optical mode of hexagonal and cubic structure, respectively.).....	18
3.1 Growth condition of the c-GaN on GaAs (001), in this table T _g is growth temperature.....	22
3.2 Growth conditions and thicknesses of the c-GaN layers on GaAs (311) substrates.....	28
4.1 Measured $\Delta\omega$, thickness, in-plane and perpendicular lattice constants of c-GaN on GaAs (001) with different growth conditions. The in-plane strain $\varepsilon_{//}$ was calculated by $(a_{//}-a_r)/a_r$	41
4.2 Calculated fully “relaxed” lattice constants of all the samples using the different published elastic constants of c-GaN. Value of Δ represents the discrepancy between the maximum and minimum of calculated values using the different reported elastic constants of c-GaN.....	44
4.3 Measured values of d_{200} and d_{311} of c-GaN on GaAs (311) with different growth conditions. The ε_{200} and ε_{311} was calculated by $(d_{200}-d_{r,200})/d_{r,200}$ and $(d_{311}-d_{r,311})/d_{r,311}$, respectively. In the calculation here, $a_r = 4.503 \text{ \AA}$, $d_{r,200} = 2.2515 \text{ \AA}$ and $d_{r,311} = 1.3577 \text{ \AA}$ were used.....	49
4.4 Measured values of d_{200} and d_{311} of c-GaN on GaAs (311) with different growth conditions. The ε_{200} and ε_{311} was calculated by	

Table	Page
$(d_{200}-d_{r,200})/d_{r,200}$ and $(d_{311}-d_{r,311})/d_{r,311}$, respectively. In the calculation here, $a_r = 4.5045 \text{ \AA}$, $d_{r,200} = 2.2522 \text{ \AA}$ and $d_{r,311} = 1.3582 \text{ \AA}$ were used.....	49
5.1 Atomic scattering factors for Ga and N atom, which used in our calculation.....	58
5.2 Theoretical XRD intensities from several cubic and hexagonal phase for GaN crystal.....	59
5.3 Amounts of hexagonal phase inclusion determined by HRXRD (H_{XRD}) and Raman scattering (H_{Raman}) in c-GaN layers on GaAs (001) substrates with various growth conditions.....	60
5.4 Ratios of $I_{h\text{-TO}}/I_{c\text{-TO}}$ and H_{Raman} for c-GaN layers on GaAs (311) substrates with different growth conditions. Hexagonal phase inclusion was estimated using linear fit, $H_{\text{Raman}} = 2.4+0.5H_{\text{XRD}}$, obtained from Fig. 5.9.....	67

List of Figures

Figure	Page
1.1 Relationship between band gap energy and lattice constants of binary compound semiconductors. The blue line indicates the relationship for their alloys.....	2
1.2 Schematic illustration of GaN crystal structures, (a) cubic (zinc blend) structure, (b) hexagonal (wurtzite) structure, (c) cubic structure along $\langle 111 \rangle$ direction and (d) hexagonal structure along $\langle 0001 \rangle$ direction.....	2
1.3 Two-dimensional atomic models of crystal structure for GaN along (110) cross-section, (a) cubic structure and (b) hexagonal structure.....	4
1.4 Schematic view of possible structures of planar defects, namely a) stacking faults, (b) twin and (c) hexagonal-phase subdomain in cubic structure along (110) cross-section.....	5
2.1 Schematic illustrations of the HRXRD measurements in (a) $2\theta/\omega$ -scan and (b) ω -scan.....	9
2.2 Possible incorporation models of hexagonal phase in c-GaN layer classified in two different ways: (a) h-GaN (0002) // GaAs (002) or c-GaN (001) and (b) h-GaN (0001) // GaAs (111) or c-GaN (111).....	11
2.3 Strain (right) and relaxed (left) layers for (a) compressive and (b) tensile strain a_r , a_L and a_S are the fully relaxed lattice constants, lattice constant of layer and lattice constant of substrate, respectively.	12
2.4 (a) Two dimensional lattice structure of compressive strain, (b) Three dimensional lattice structures under compressive strain.....	13
2.5 Diagram of strain determination.....	14

Figure	Page
2.6 Schematic views of similar {111} planes in cubic crystal and crystalline relationship between c-GaN (002) and h-GaN (10-11) for the (a) [110] and (b) [1-10] azimuth axes.....	16
2.7 Schematic representation of Raman scattering of a phonon with a) emission and b) absorption of a phonon.....	17
2.8 Schematic drawing of Raman scattering system.....	17
3.1 Schematic diagram of MOVPE system. A typical system consists of four major parts, gas-handling system, reactor chamber, heating system (RF coil) and exhaust gases treatment system.....	21
3.2 (a) Schematic illustration of sample structure for c-GaN film grown on GaAs (001) substrate. (b) Example of c-GaN grown layer on GaAs (001) substrate measured by SEM.....	22
3.3 SEM images showing cross-section of the c-GaN films grown at different growth temperatures of GaN buffer layer and different V/III ratios for the c-GaN buffer layer (100 and 50) and the c-GaN main layer (25 and 12.5).....	24
3.4 SEM images showing surfaces of the c-GaN films grown at different growth temperatures of GaN buffer layer and different V/III ratios for the c-GaN buffer layer (100 and 50) and the c-GaN main layer (25 and 12.5).....	25
3.5 AFM images showing surface morphologies of the c-GaN films grown at different growth temperatures of GaN buffer layer and different V/III ratios for the c-GaN buffer layer (100 and 50), c-GaN main layers (25 and 12.5).....	26
3.6 (a) Schematic illustration of sample structure of c-GaN film grown on GaAs (311) substrate. (b) Cross-section sample structure recorded by SEM.....	28
3.7 SEM images showing a cross-section of the c-GaN films grown at different growth temperatures of GaN buffer layer and the V/III ratios for the c-GaN buffer layer, epitaxial layer.....	29

Figure	Page
3.8 SEM images surface morphology of the c-GaN films grown at different growth temperatures of GaN buffer layer and the V/III ratios for the c-GaN buffer, epitaxy layer.....	30
3.9 AFM images surface morphology of the c-GaN films grown at different growth temperatures of GaN buffer layer and the V/III ratios for the c-GaN buffer layer, epitaxial layers.....	31
3.10 High resolution X-ray diffraction instrument installed at Scientific and Technology Research Equipment Center, Chulalongkorn University.....	33
3.11 Raman spectroscopy system at the Gem and Jewelry Institute of Thailand (Public Organization), Chulalongkorn University.....	34
4.1 (a) A typical high resolution X-ray diffraction (002) 2θ - ω scan of c-GaN film on GaAs (001) substrate grown with V/III ratios of c-GaN buffer and c-GaN main layers of 100 and 25, respectively, at growth temperature of buffer layer of 600°C; (b) Reciprocal space map of (002) c-GaN.....	37
4.2 The (002) c-GaN peak positions fitted by Gaussian-line shape.....	38
4.3 (a) Reciprocal space map of the (113) reflection of c-GaN film on GaAs (001) substrate (the same sample used in Figs. 4.1 and 4.2). (b) Diffraction peaks 2θ - ω scan of (113) reflection.....	39
4.4 (a) Reciprocal space map of the (113) reflection of only the c-GaN region and (b) the (113) reflection of ω -scan fitted by Gaussian-line shape.....	40
4.5 $\Delta\omega$ variation of $\varepsilon_{//}$ for growth temperature (a) V/III ratio 100:25 and (b) V/III ratio 50:12.5 of c-GaN on GaAs (001).....	42
4.6 Thickness variation of $\varepsilon_{//}$ for growth temperature (a) V/III ratio 100:25 and (b) V/III ratio 50:12.5 of c-GaN on GaAs (001).....	44

Figure	Page
4.7 Diffraction peak 2θ - ω scans of (a) (311) and (b) (200) reflections from c-GaN layer grown on GaAs (311) substrate with V/III ratios of c-GaN buffer and c-GaN main layers of 100 and 25, respectively, and growth temperature of c-GaN buffer layer was 575°C (sample No.8).....	46
4.8 The peak positions of (a) c-GaN (311) and (b) c-GaN (200) reflections of the sample used in Fig. 4.7 fitted by Gaussian-line shape.....	48
5.1 (002) $2\theta/\omega$ scan profiles of the c-GaN films on GaAs (001) substrates grown with different growth conditions (see details in Chapter III).....	52
5.2 Typical (002) X-ray reciprocal space mappings of the GaN films growth condition GaN buffer layer 550°C and V/III ratio 100:25 and the growth condition GaN buffer layer 575°C and V/III 50:12.5 measured along the [110] azimuth axis.....	53
5.3 ω -scan profile of the c-GaN (002) ($2\theta = 40.01^\circ$) and h-GaN (10-11) ($2\theta = 34.56^\circ$) diffraction peaks extracted from the X-ray RSM measured along the [110] and [1-10] azimuth axis of sample condition GaN buffer layer 530°C and V/III ratio 50:12.5 (sample No. 4). The red circles and blue solid lines are the experimental and the Gaussian fitted curves, respective. The integration data of each diffraction peaks was calculated from the area under the Gaussian fitted curves.....	56
5.4 Atomic scattering factor for Ga and N atom as a function of $\sin\theta/\lambda$	58
5.5 $I_{h(10-11)}/I_{c(002)}$ as a function of hexagonal phase inclusion (%) of c-GaN layers on GaAs (001) substrates for (a) [1-10] azimuth and (b) [110] azimuth axes.....	60

Figure	Page
5.6 Raman spectra of the c-GaN films on GaAs (001) substrates grown with different growth conditions. Green-dotted lines and black-dotted lines indicate the characteristic phonon frequencies of c-GaN and h-GaN phase, respectively.....	62
5.7 I_{h-TO} / I_{c-TO} ratio as a function of hexagonal phase inclusion in c-GaN layers on GaAs (001): (a) V/III ratios of buffer and main layers are 100 and 25, respectively, and (b) V/III ratios of buffer and main layers are 50 and 12.5, respectively.....	63
5.8 Raman spectra of the c-GaN films on GaAs (001) substrates grown with V/III ratios of buffer and main layers are 100 and 25, respectively, at growth temperature of buffer layer of 575°C. Red circle, blue-dashes line and blue solid line are represented an experiment, fitting and total fitting, respectively.....	63
5.9 H_{Raman} as a function of the H_{XRD} , from our experiment. The data points are average data obtained from 3 spots on the sample. Error bars are standard deviations.....	65
5.10 Raman spectra of the c-GaN films on GaAs (001) substrates grown with different growth conditions. Red-dotted lines and black-dotted lines indicate the characteristic phonon frequencies of c-GaN and h-GaN phase, respectively.....	66
5.11 Raman spectra of the c-GaN films on GaAs (311) substrates grown with V/III ratios of buffer layer = 100 and main layer = 25 and at growth temperature of buffer layer = 575°C. Red circle, blue-dashes line and blue solid line is experiment, fitting and total fit, respectively.....	67

CHAPTER I

INTRODUCTION

1.1 Gallium Nitride

The physical properties of GaN make it an attractive semiconductor for many electronic and optoelectronic devices [1-4]. Its wide, direct band gap energy makes it suitable for short wavelength emitters such as light emitting diodes (LEDs), laser diodes (LDs) and detectors. The wide band gap energy and good thermal stability of GaN is also advantageous for high temperature and high power electronics [5]. GaN can form solid solutions with AlN and InN, making a wide range of band gap energy (0.8-6.2 eV), as shown in Fig. 1.1. This ability of GaN and its alloys is essential for producing specific wavelengths for emitters, and for creating hetero-junctions with potential barriers into the device structures. Heat dissipation in devices is facilitated by high thermal conductivity of GaN compared with Si and GaAs [6].

Commonly, GaN exhibits two polytypes, thermodynamically stable hexagonal structure (wurtzite structure: h-GaN) and metastable cubic structure (zincblende structure: c-GaN). Figures 1.2(a) and 1.2(b) show schematic illustration of the cubic structure and the hexagonal structure, respectively. These structures of GaN are strongly dependent on the substrate symmetry as well as growth condition. Actually, h-GaN, which is a stable phase, has been successfully grown on various substrates, such as sapphire, SiC and Si [7]. On the other hand, just only few research group work with metastable c-GaN. Although, the growth of metastable c-GaN layers is performed using cubic substrate such as GaAs, Si, 3C-SiC, and MgO [8-11]. However, the growth of high quality c-GaN layer is still difficult. It is due to metastability of c-GaN, the hexagonal phase is often unexpectedly introduced in the

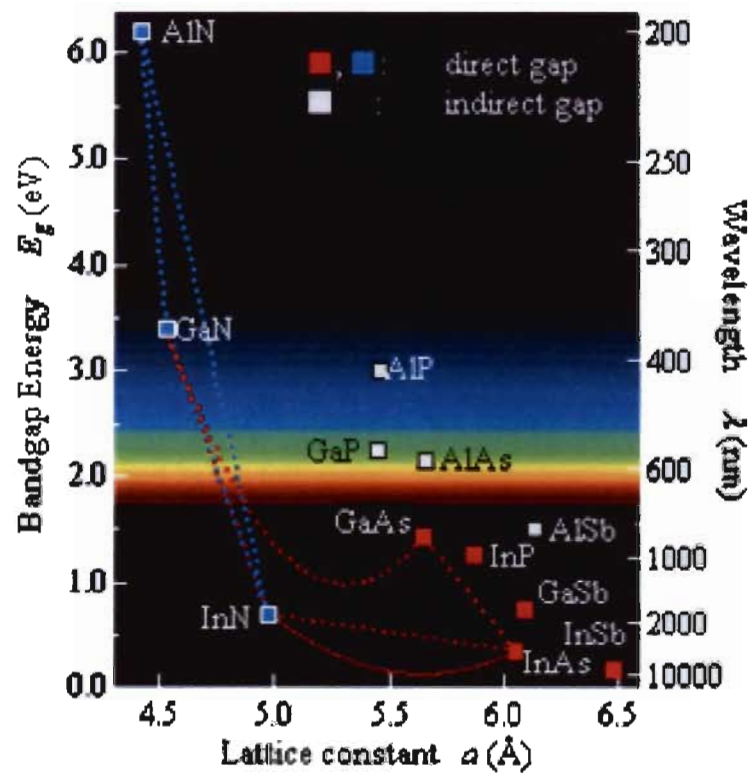


Figure 1.1: Relationship between bandgap energy and lattice constants of binary compound semiconductors. The blue line indicates the relationship for their alloys [11].

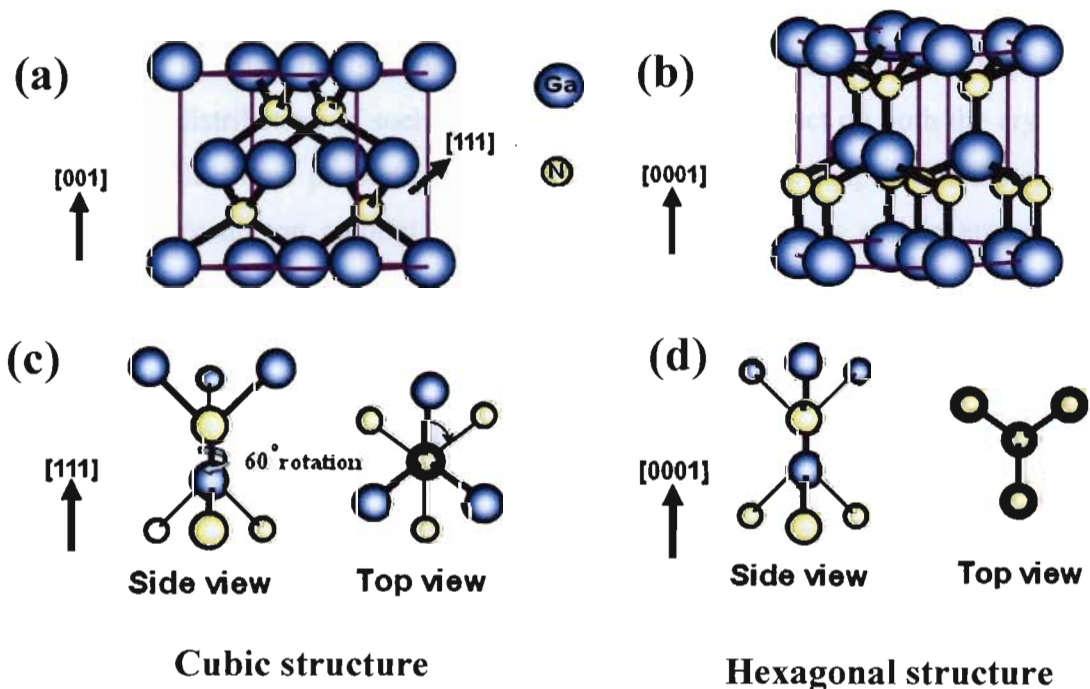


Figure 1.2: Schematic illustration of GaN crystal structures, (a) cubic (zinc blend) structure, (b) hexagonal (wurtzite) structure, (c) cubic structure along $\langle 111 \rangle$ direction and (d) hexagonal structure along $\langle 0001 \rangle$ direction [12].

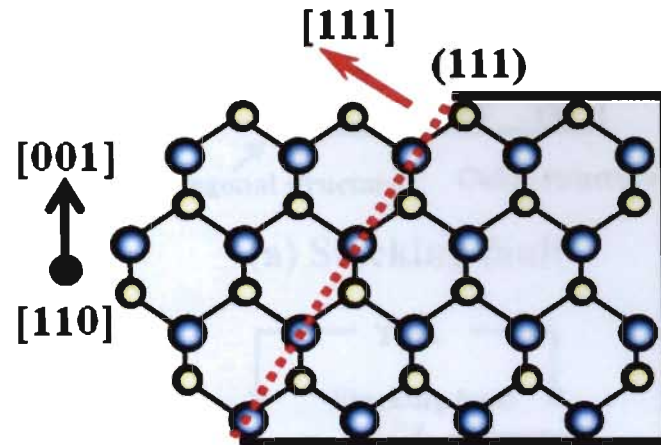
cubic layer. Several research groups reported that most of hexagonal phases has generated on the cubic $\{111\}$ planes as a formation of planar defects, such as stacking faults, twin and hexagonal phase inclusion. This is due to the fundamental difference between cubic and hexagonal structures, which is merely a 60° rotation along the hexagonal $\langle 0001 \rangle$ (Figs.1.2(c) and 1.3(b)) and cubic $\langle 111 \rangle$ (Figs. 1.2(d) and 1.3(a)) directions. Thus, the cubic $\{111\}$ plane can accommodate the growth of hexagonal structure along $\langle 0001 \rangle$ direction. Three possible models of the generation of hexagonal structure in the cubic structure are shown in Fig. 1.4. The description of each model is described as the following.

(1) Stacking faults on cubic $\{111\}$ planes is an insertion of 1 monolayer of hexagonal structure between two cubic structures, which are identical crystal orientation (Fig. 1.4(a)).

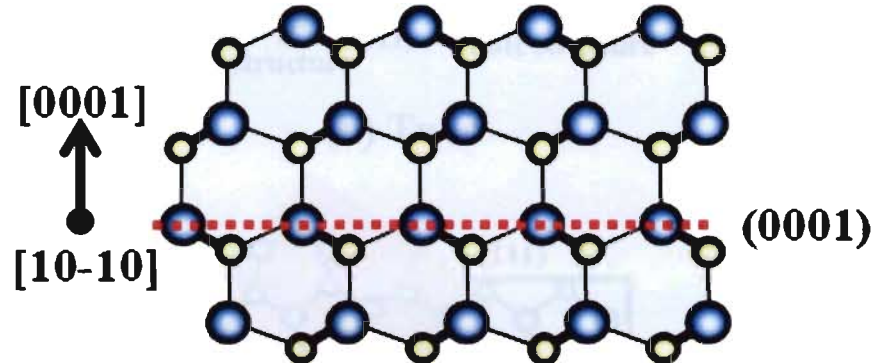
(2) Twins in cubic $\{111\}$ planes are formed by the insertion of $\frac{1}{2}$ monolayer of hexagonal structure between two of cubic structures, which are different crystal orientations (Fig. 1.4(b)).

(3) Hexagonal phase subdomain generated on the cubic $\{111\}$ planes is an extension of stacking faults to be a single crystal of hexagonal structure (Fig. 1.4(c)). Density and distribution of such planar defects seriously affect on both the crystalline quality and electronic properties of c-GaN. Thus, it will be helpful for the epitaxial growth to measure an amount of the mixed structural phases and to analyze their formation mechanism for future device improvements.

In addition, the crystal growth of c-GaN is a lack of suitable substrates. Table 1.1 summarizes the lattice constant and thermal expansion coefficients of c-GaN and some prospective substrate materials [14]. As shown in Table 1.1, there is a large difference of lattice constants and thermal expansion coefficients between c-GaN and the substrate materials. This large mismatch in the lattice constants and thermal expansion coefficients exist in GaN/GaAs while these mismatches result in strain relaxation, which leads to generation of defects. To improve the quality of c-GaN grown film, it is necessary to study the affecting parameters, such as growth methods, growth conditions, substrate material, etc.



(a) Cubic structure



(b) Hexagonal structure

Figure 1.3: Two-dimensional atomic models of crystal structure for GaN along (110) cross-section, (a) cubic structure and (b) hexagonal structure [12].

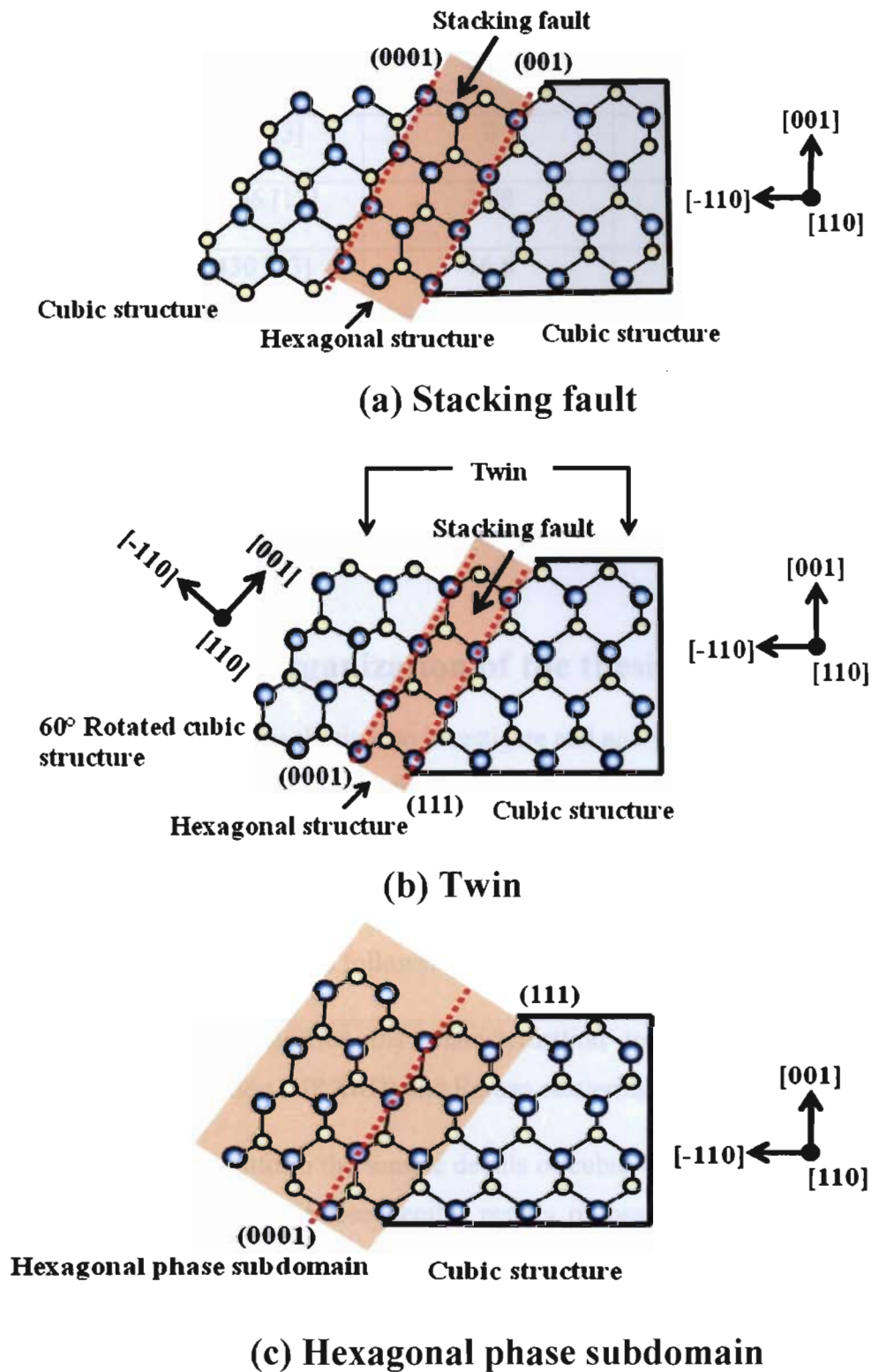


Figure 1.4: Schematic view of possible structures of planar defects, namely a) stacking faults, (b) twin and (c) hexagonal-phase subdomain in cubic structure along (110) cross-section [12].

Substrate materials	Lattice constants (Å)	Lattice mismatch (%)	Thermal expansion coefficients ($\times 10^{-6} \text{ K}^{-1}$)
c-GaN	4.52 [13]	0	3.17 [7]
3c-sic	3.3596 [13]	3.68	3.9 [13]
Si	5.430 [13]	16.8	3.59 [13]
GaAs	5.653 [13]	20.0	6.0 [13]
Mgo	4.216 [13]	7.21	10.5 [13]

Table 1.1: Lattice constants, lattice mismatch and thermal expansion coefficients for substrate materials of c-GaN

1.2 Objectives and organization of the thesis

The objectives of this thesis is to investigate and analyze the strain, film quality and generation of crystal defects in the c-GaN layer grown on GaAs (001) and on GaAs (311) substrate by metal organic vapor phase epitaxy (MOVPE) using high resolution x-ray diffraction and Raman scattering technique.

The thesis is organized as follows:

Chapter II: We describe the characterization techniques, including high resolution X-ray diffraction (HRXRD) and Raman scattering, and their principles.

Chapter III: We inform the sample details of cubic GaN layers on GaAs (001) and GaAs (311) substrates. Subsequently, results of basic characterizations using scanning electron microscopy (SEM), atomic force microscopy (AFM) were shown.

Chapter IV: Strain in c-GaN films on (001) GaAs and (311) GaAs substrates has been established.

Chapter V: The hexagonal phase generation in the c-GaN layers grown on GaAs (001) and GaAs (311) is discussed.

Finally, Chapter VI gives summary of the thesis.

CHAPTER II

CHARACTERIZATION TECHNIQUES AND THEIR PRINCIPLES

In this chapter, we discuss on characterization techniques, including high resolution X-ray diffraction (HRXRD) and Raman scattering, and on their principles. We then show how to derive the crystal structures, lattice constants, strains and vibrational property of c-GaN.

2.1 High resolution X-ray diffraction

It is well known that the epitaxial structures exhibit a high degree of crystalline perfection. However, there are still some deviations, which usually occur in epitaxial layer, from the perfect crystal. The measurement of such deviations is necessary in order to evaluate the crystal quality of the grown layers.

High resolution X-ray diffraction (HRXRD), which is known as an important technique that has a high accuracy, is commonly used to analyze crystal properties of the epitaxial layer, such as lattice constants, crystal orientations, strain, etc. Measurement is performed by projecting the X-ray beam onto the sample. The diffraction condition occurs according to Bragg's law

$$2d_{hkl} \sin(\theta_B) = \lambda, \quad 2.1$$

where d_{hkl} is the lattice plane spacing of the (hkl) plane, θ_B is Bragg's angle and λ is the wavelength of X-ray ($K_{\alpha 1}$: $\lambda=1.5406 \text{ \AA}$). Despite the implication that the

HRXRD technique is only applicable to very high perfection material, Tlafford *et al.* [15] reported that it is also highly appropriate to relatively poor epitaxy materials such as GaN.

2.2 Scan modes in HRXRD

2.2.1 $2\theta/\omega$ -scan mode

In HRXRD measurement, most frequently used mode is $2\theta/\omega$ -scan, which is used to clarify variations of lattice plane spacing. For epitaxial layer, only the lattice plane spacing parallel to the film surface is usually measured. The HRXRD measurement setup in the $2\theta/\omega$ -scan mode is shown in Fig 2.1(a). The diffraction pattern is collected by varying the incident angle θ of the incoming X-ray beam and the scattered angle 2θ , while the specimen is fixed. Then, the scattered X-ray intensity is measured as a function of the scattering angle " 2θ ". After, we obtain the values of d_{hkl} by using Eq. 2.1, the lattice constant for cubic structure can be determined by

$$d_{hkl} = \frac{a}{\sqrt{h^2 + k^2 + l^2}}. \quad 2.2$$

For the strained epitaxial layer, it is found that the cubic structure will transform to tetragonal structure. Thus, lattice constants can be determined by

$$d_{hkl} = \frac{a_{\parallel}}{\sqrt{h^2 + k^2}} + \frac{a_{\perp}}{\sqrt{l^2}}. \quad 2.3$$

2.2.2 ω -scan mode

Since, we have a set of samples comprising a GaN layer on a GaAs (001) substrate. The aim of the investigation is to determine the hexagonal phase inclusion in cubic phase GaN (c-GaN) by measuring a single reflection with the rocking technique or called " ω -scan". The measurement of a rocking curve is performed in the

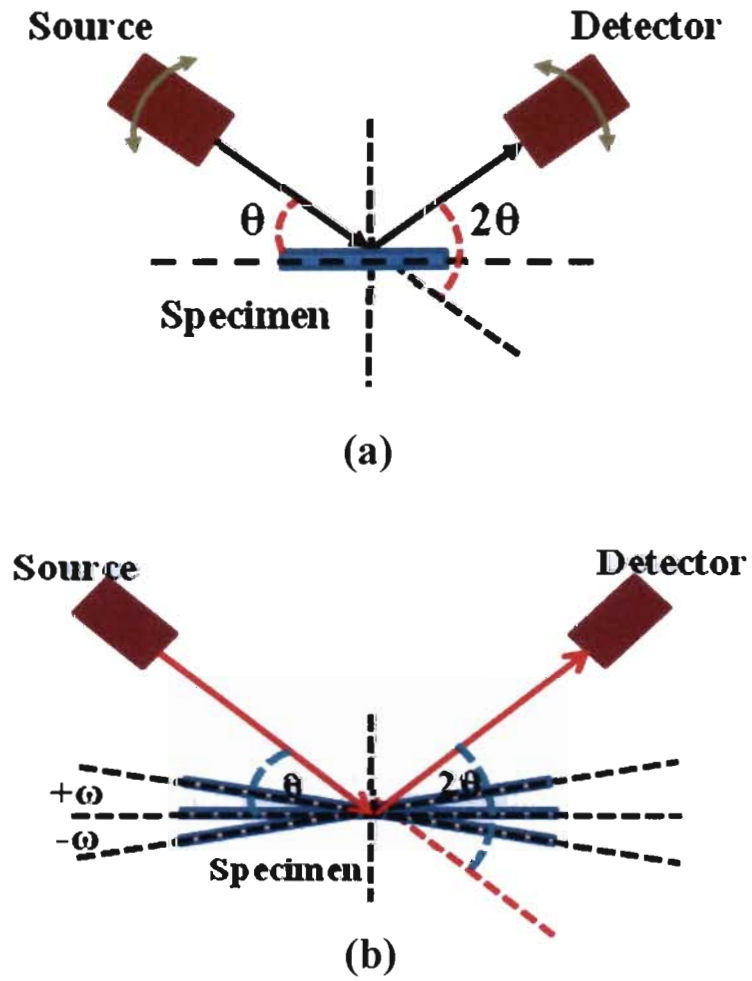


Figure 2.1: Schematic illustrations of the HRXRD measurements in (a) $2\theta/\omega$ -scan and (b) ω -scan [16].

conditions that the X-ray source and detector are fixed at the position of 2θ . On the other hand, the specimen is tilted along the ω -axis (see in Fig. 2.1 (b)) in the vicinity of the Bragg angle θ_B . Therefore, ω is defined as the difference between the incident and the reflection angles in to the specimen for a certain detection position. The HRXRD measurement in ω -scan mode is shown in Fig. 2.1(b). For the fixed value of $2\theta_B$, the value of ω is restricted to a range between $-\theta$ to $+\theta$. Thus, the peak position in the ω -scan mode refers to the inclination of epitaxial plane from the film surface. This allows us to obtain the diffraction from the tilted planes related to hexagonal phase structure in the cubic crystal. In addition, the full width at half maximum (FWHM) in the ω -scan mode reflects to the variations of crystal directions [16].

2.2.3 X-ray reciprocal lattice space mapping

Two-dimensional scan composed of $2\theta/\omega$ - and ω - scans give reciprocal lattice space mapping (RSM), which is used to characterize all the planes tilted from the film surface. According to our aim that is to determine the hexagonal phase in c-GaN layer, possible incorporation models of hexagonal phase GaN (h-GaN) in the c-GaN layer are classified in two different ways as shown in Fig. 2.2; (a) h-GaN (0002) // GaAs (002) or c-GaN (002) and (b) h-GaN (0001) // GaAs (111) or c-GaN (111). To detect all the diffraction from the hexagonal phase structure, the ω -scan mode is done for the fixed 2θ of each crystal planes, including (0002) and (10-11) planes. (I will present in Chapter V.) For the figure 2.2(a) the h-GaN (0002) generate on (002) plane in c-GaN and hexagonal (10-11) plane are tiled from c-GaN (001) plane about $\pm 7^\circ$. In this case, the $\langle 0001 \rangle$ axes of hexagonal structure in the layer is a hexagonal structure with the $[0001]$ direction perpendicular to the GaAs (001) surface. On the other hand, for the ω -scan profile of the h-GaN (10-11) planes is necessary to observe the h-GaN $\langle 0001 \rangle$ parallel to the $\langle 111 \rangle$ axes of the GaAs crystal or c-GaN. According to the crystal geography, the angles between the GaAs (001) and GaAs (111) planes and between hexagonal GaN (0002) and hexagonal GaN (10-11) planes are 54.7° and 61.8° , respectively. Therefore, the X-ray RSMs mode in HRXRD measurements is highly applicable to record all the crystal phases shown in Fig. 2.2.

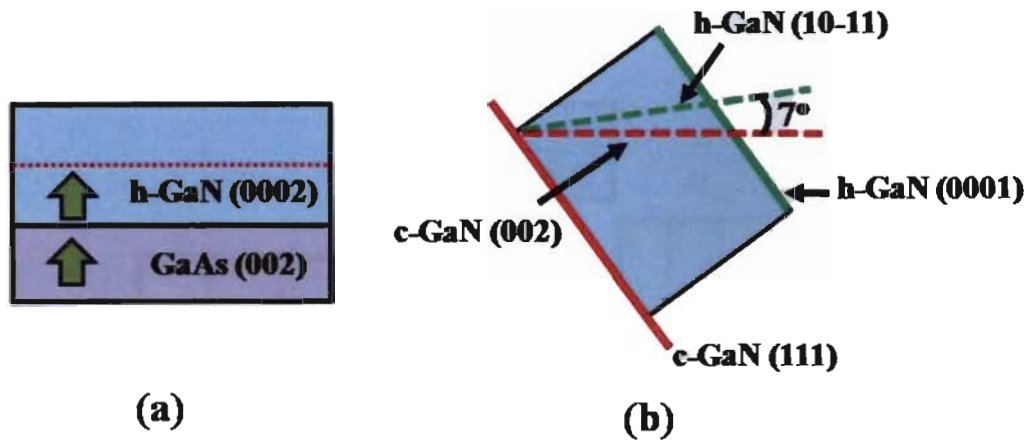
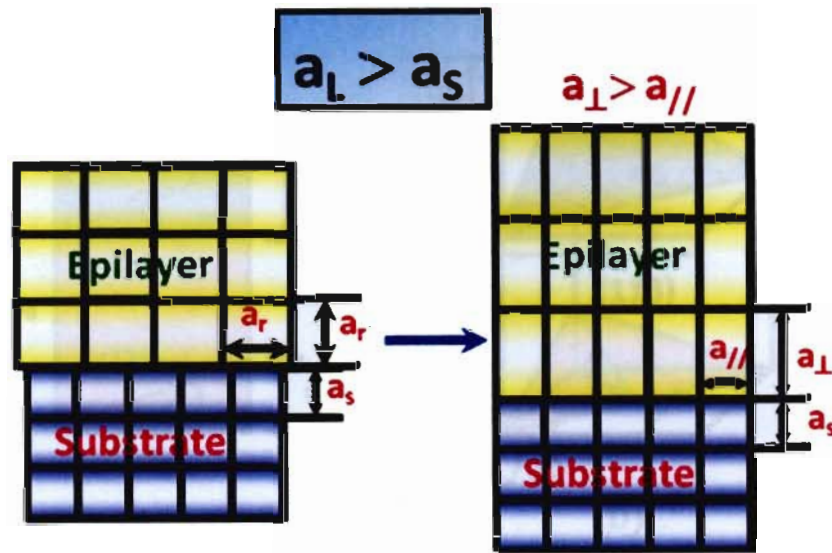


Figure 2.2: Possible incorporation models of hexagonal phase in c-GaN layer classified in two different ways: (a) h-GaN (0002) // GaAs (002) or c-GaN (001) and (b) h-GaN (0001) // GaAs (111) or c-GaN (111).

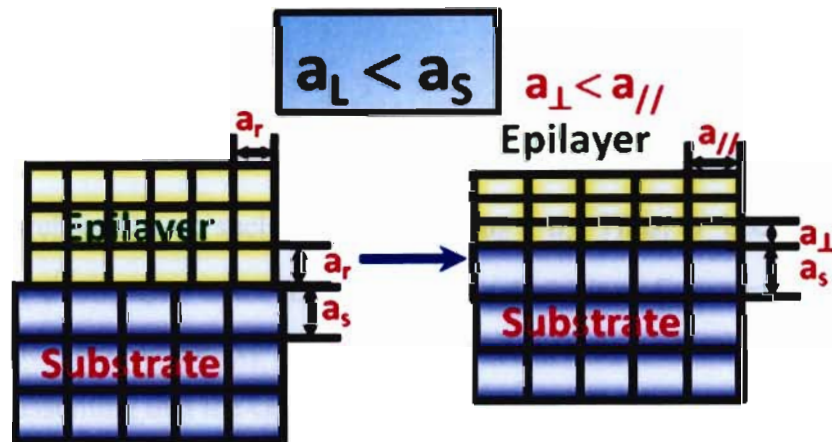
2.3. Determination of strain

The continuation of the substrate crystal lattice will be associated with the incorporation of strain into the epitaxial layer. In this case, the layer of c-GaN distorts along the growth direction to produce a tetragonal distortion as shown in Fig. 2.3. The value of d_{hkl} can be represented as in Equation 2.3. In order to analyze the lattice parameters parallel ($a_{//}$) and normal (a_{\perp}) to the substrate surface, both symmetric (002) and asymmetric (113) reflections were measured by the (002) $2\theta/\omega$ -scan and the (113) reciprocal space mapping modes [14].

The symmetric (002) $2\theta/\omega$ -scan was performed to examine the value of a_{\perp} for GaN strained layers. From the separation between the GaN and GaAs reflection peaks, a_{\perp} can be calculated using Bragg's law. To determine the value of $a_{//}$, asymmetric (113) reciprocal space mapping mode, as shown in Fig. 2.4(b), was performed. It is known that the inclination between the asymmetric plane of substrate and that of the epitaxial layer is commonly observed to be tetragonal distortion, as shown in Figure 2.4. The angle ψ between the (001) plane (113) of the strained layer



(a) Compressive strain



(b) Tensile strain

Fully relaxed

Fully strained

Figure 2.3: Strain (right) and relaxed (left) layers for (a) compressive and (b) tensile strain. a_r , a_L and a_S are the fully relaxed lattice constants, lattice constant of layer and lattice constant of substrate, respectively.

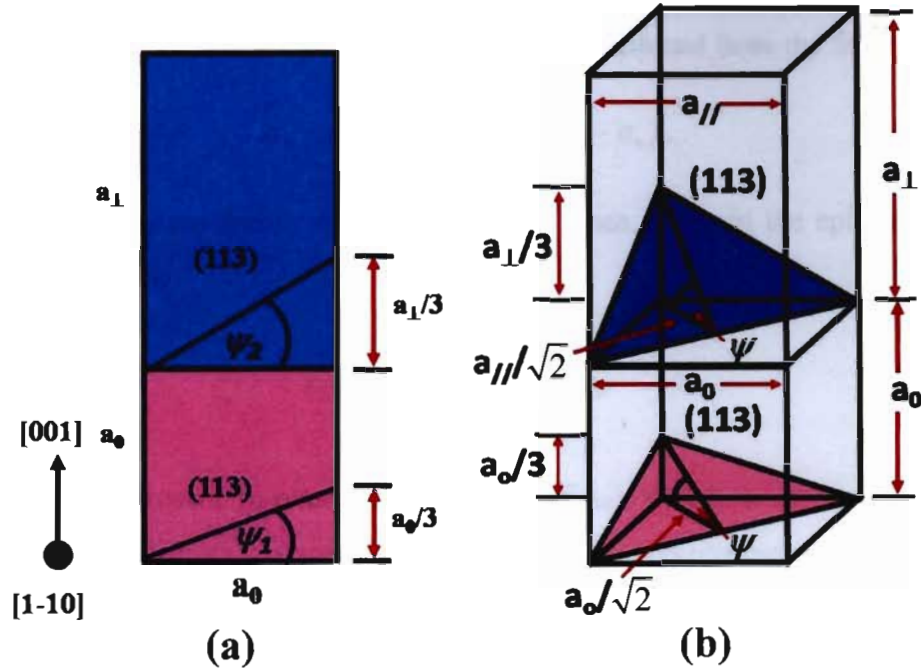


Figure 2.4: (a) Two dimensional lattice structure of compressive strain, (b) Three dimensional lattice structures under compressive strain

is give by [17]

$$\psi = \tan^{-1}(\sqrt{2} \cdot a_{\perp} / 3 \cdot a_{\parallel}). \quad 2.4$$

For the fully relaxed layer, such as GaAs, $a_{\perp} = a_{\parallel} = a_{\perp}$. Thus, ψ become a constant value of $\tan^{-1}(\sqrt{2}/3)$. Due to the tetragonal lattice distortion of the strained GaN layer ($a_{\parallel} \neq a_{\perp}$), the tilted angle $\Delta\psi$ between the GaAs (113) and GaN (113) plane is represented, assuming that the GaAs substrate is under full relaxation, as follows [14]

$$\Delta\psi \equiv \psi_{\text{GaAs}} - \psi_{\text{InGaAs}} \equiv \psi_0 - \psi_1 = \tan^{-1}(\sqrt{2}/3) - \tan^{-1}(\sqrt{2} \cdot a_{\perp} / 3 \cdot a_{\parallel}). \quad 2.5$$

In the experiment set up, the value of ω indicates a combination of the incident angle θ and the inclination angle (offset angle) between sample and stage holder of the instrument set up. Thus, with the fixed value of 2θ , the value of $\Delta\omega$ is equivalent to the tilted angle ($\Delta\psi$) between the (001) plane and (113) of the strained layer. Therefore, the high-resolution mapping technique can be applied to determine both the tilted angle $\Delta\psi$ and actual Bragg angle of the grown layer. In addition, the mosaic structure within the layers can also be observed.

The fully relaxed lattice constant (a_r) can be deduced from the following:

$$a_{\perp} - a_{\parallel} = 2(c_{11}/c_{12}) \cdot (a_{\parallel} - a_r), \quad 2.6$$

where c_{11} and c_{12} are elastic stiffness constants. Then, strain in the epitaxial layer can be calculated using

$$\varepsilon_{\parallel} = \frac{(a_{\parallel} - a_r)}{a_r} \times 100\%, \quad 2.7$$

where, ε_{\parallel} is represent in-plane strain (Strain of a_{\parallel}), which is in the direction that parallel to the substrate surface. The diagram of strain determination is shown in Fig. 2.5.

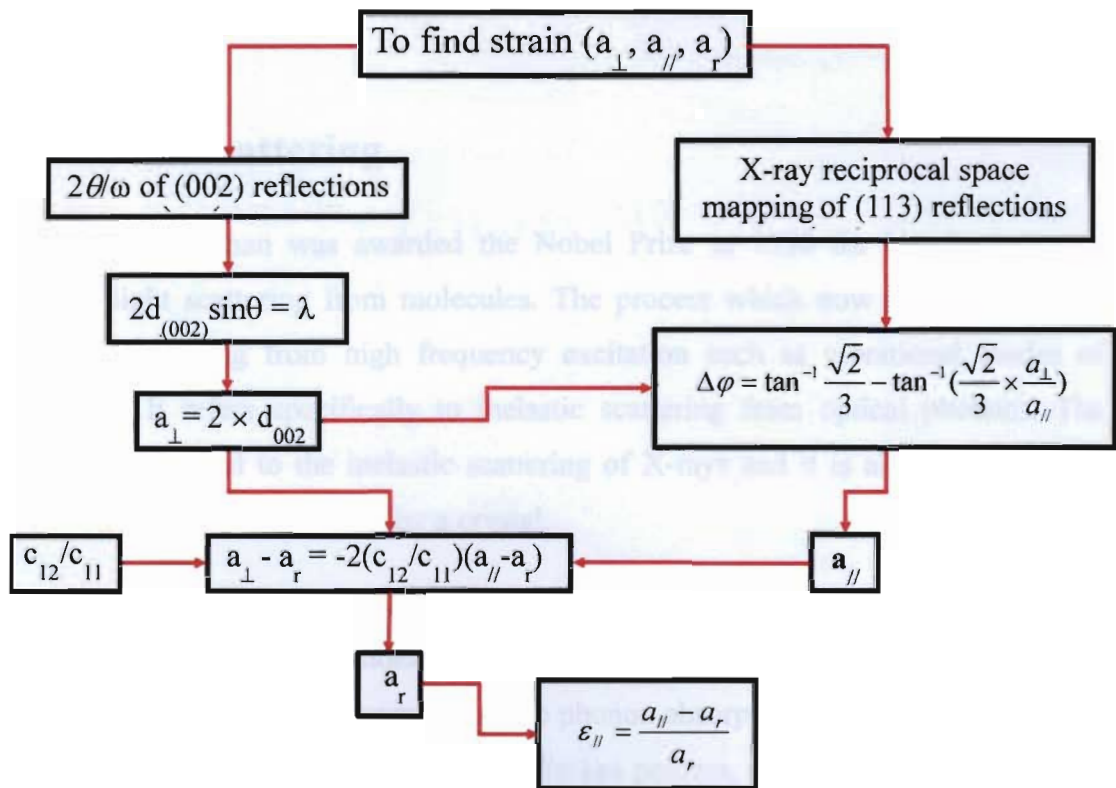


Figure 2.5: Diagram of strain determination

2.4 Determination of the hexagonal phase inclusion

In order to precisely investigate how and what extent h-GaN included in the c-GaN layers, X-ray RSMs were performed. The epitaxial relationship between the h-GaN and c-GaN is hexagonal (0001)//cubic (111). Furthermore, it is known that there are four equivalent [111] axes in the cubic structure. (1-11) and (-111) planes along the [110] direction or azimuth axis and (111) and (-1-11) planes along the [1-10] azimuth axis (show in Fig. 2.6) [18, 19]. In order to collect the diffraction peaks from all the hexagonal phase inclusion generated on the four similar {111} planes from cubic structure, the tilted angle between the cubic (002) and hexagonal (10-11) reflection in the c-GaN layers about $\pm 7^\circ$, as shown in Fig. 2.6, is confirmed [16] More details of determination of hexagonal phase inclusion in c-GaN layer will be discussed later in Chapter IV.

2.5 Raman scattering

C. V. Raman was awarded the Nobel Prize in 1930 for his discovery of inelastic light scattering from molecules. The process which now carries his name refers to scattering from high frequency excitation such as vibrational modes of molecules. It refers specifically to inelastic scattering from optical phonons. The process is identical to the inelastic scattering of X-rays and it is also similar to the inelastic scattering of neutrons by a crystal.

Inelastic light scattering can be subdivided into two types, Stokes scattering and anti-Stokes scattering. Stokes scattering corresponds to the emission of phonon, while anti-Stokes scattering corresponds to phonon absorption. The interaction shown in Figs. 2.7 (a) and (b) is Stokes and anti-Stokes process, respectively. Mostly Stokes scattering is used. Conservation of energy and momentum during the interaction requires that: $\omega = \omega_i \pm \omega_s$ and $\vec{k} = \vec{k}_i \pm \vec{k}_s$, where ω_i and \vec{k}_i are frequency and wave vector of the incident photon, respectively. ω_s and \vec{k}_s are frequency and wave vector

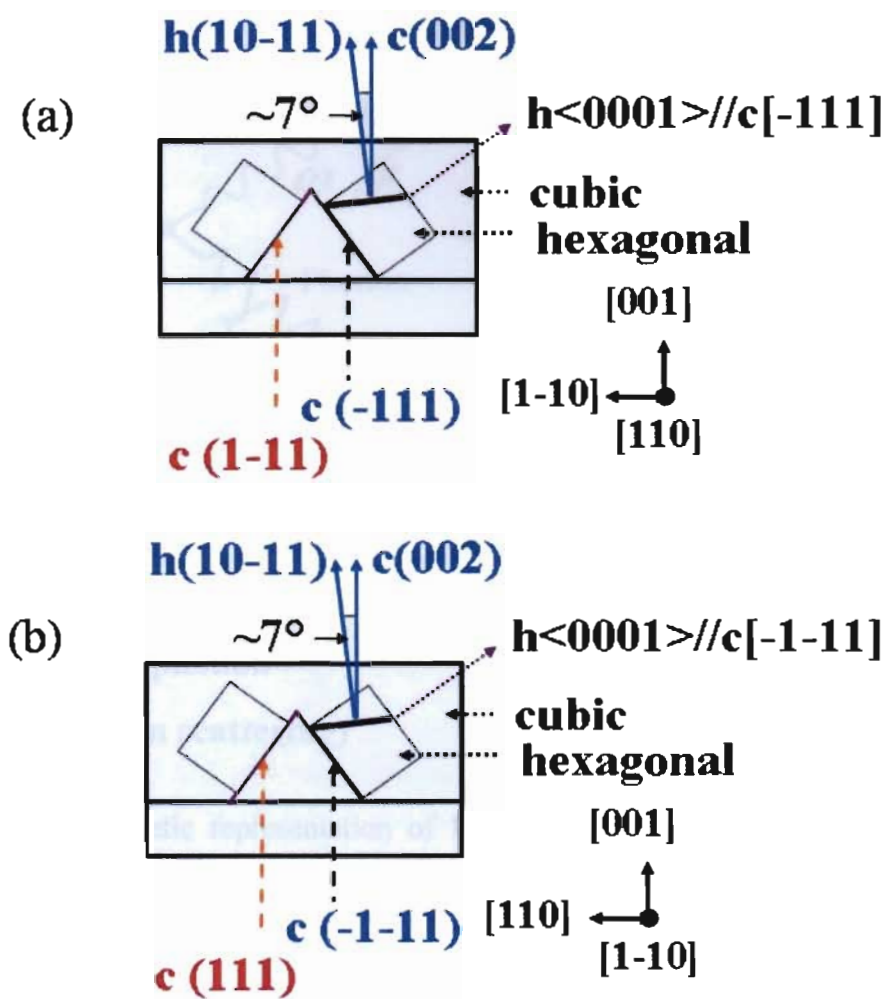


Figure 2.6: Schematic views of similar $\{111\}$ planes in the cubic crystal and crystalline relationship between c-GaN (002) and h-GaN (10-11) for the (a) $[110]$ and (b) $[1-10]$ azimuth axes.

of the scattered photon, respectively. The + signs correspond to phonon emission (Stokes scattering), while the - signs correspond to phonon absorption (anti-Stokes scattering). Thus the light is shifted down in frequency during a Stokes process and up in frequency in the anti-Stokes process. The frequency difference between incident photon and scattered photon is called “Raman frequency” or “Raman shift”. Thus the main use of inelastic light scattering is to measure phonon scattering. Raman scattering experiment requires a monochromatic light source, typically a laser, a

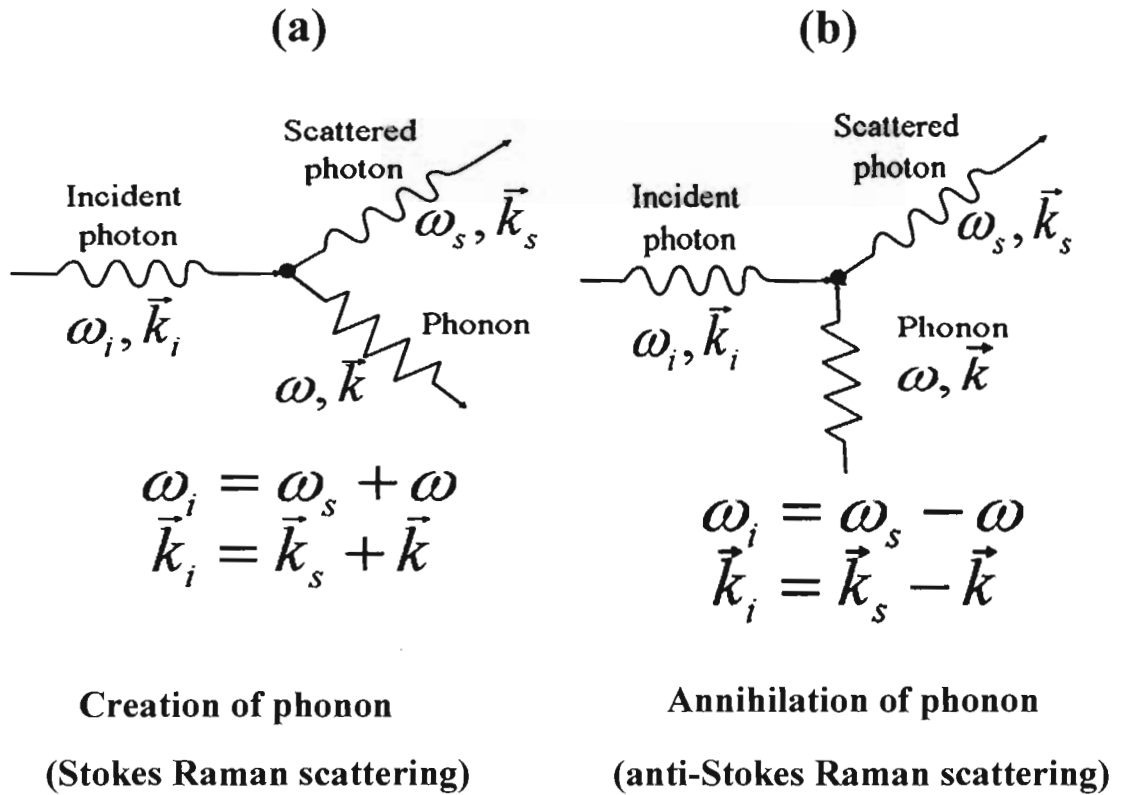


Figure 2.7: Schematic representation of Raman scattering of a phonon with a) emission and b) absorption of a phonon [22].

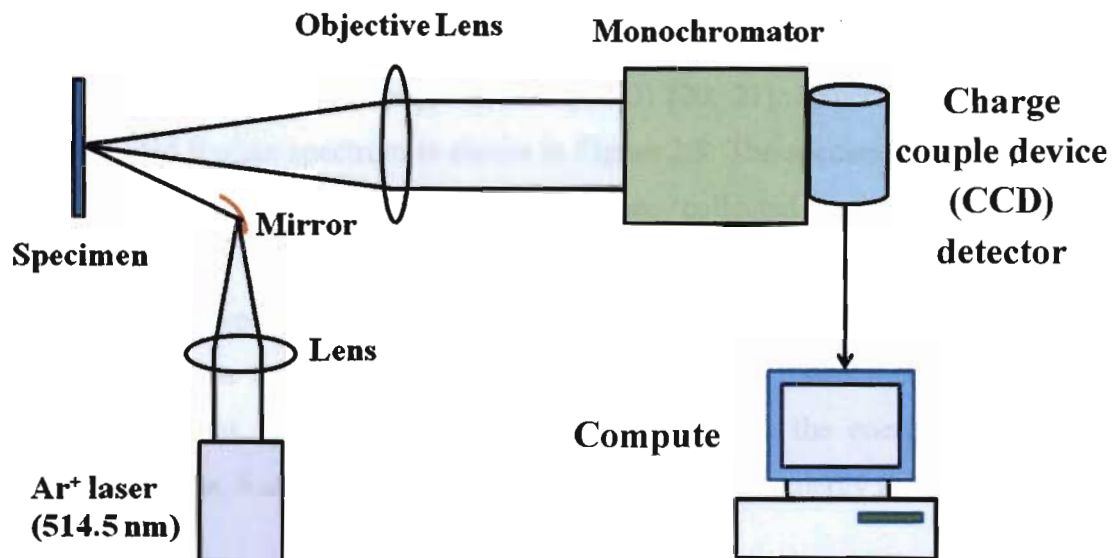


Figure 2.8: Schematic drawing of Raman scattering system

Structural phases	Phonon frequencies (cm ⁻¹)			
	h-TO	h- LO	c-TO	c-LO
h-GaN	568 [31]	733 [21]		
	568.9 [34]	735.3 [34]		
	567 [32]	-		
c-GaN			553 [21]	739 [21]
			551 [32]	740.3[34]
			-	740 [34]

Table 2.1: Phonon frequencies of GaN crystals including both hexagonal and cubic crystal lattices (h-TO and c-TO are transverse optical mode of hexagonal and cubic structure, respectively. And h-LO and c-LO are longitudinal optical mode of hexagonal and cubic structure, respectively.)

spectrometer and a sensitive photon-counting detector such as a photo multiplier tube or a multi- channel charge couple device (CCD) [20, 21]. Experimental apparatus used to record Raman spectrum is shown in Figure 2.8. The specimen is excited with a laser light, and the scattered phonons are collected and focused into a monochromator. The signals are recorded using a sensitive photon-counting detector. Raman spectra are usually plotted in term of the intensity of the scattered photons versus the Raman shift in wave number unit (cm⁻¹), which is a standard for vibrational studies. The unit of “cm⁻¹” is used to clarify the energy shift of the scattered photons. Raman shift of 1 cm⁻¹, corresponds to the energy shift of ~1/8 meV [23].

The scattering geometry is commonly written as $\vec{k}_i (e_i, e_s) \vec{k}_s$, which is so called Porto notation [23]; where \vec{k}_i and \vec{k}_s are the directions of incident and scattered photons; e_i and e_s are the polarizations of incident and scattered photons, respectively.

The simplest scattering geometry is the backscattering. From the conservation of wavevector, the wavevector \vec{k} must be along the [001] direction also for backscattering from a (001) surface of cubic crystal. The longitudinal optical (LO) phonon is polarized in the z direction (or [001] direction), while the transverse optical (TO) phonon is polarized in x-y plane (or (001) plane). Thus, the scattering geometries for backscattering from the (001) surface of cubic crystal are $z(x,y)\vec{z}$ or $z(y,x)\vec{z}$.

Recently, Raman spectroscopy has proved to be a power tool for the investigation of material properties such as doping concentration, crystal orientation and defect identifications, etc. X. L. Sun *et al.* [24] have used Raman spectroscopy to clarify the spatial distribution of the hexagonal and cubic phases in the GaN layers grown on 3C-SiC (001) substrates. They confirmed that the occurrence of optical phonon mode from hexagonal phase can be spectrally separated from the phonon mode of the cubic phase. Their result uniquely showed the presence of the hexagonal phase subdomain. In this study, Raman spectroscopy is used to clarify the spatial distribution of the hexagonal and cubic phases in the c-GaN films grown by MOVPE. The expected results are summarized in Table 2.1. For c-GaN, the frequency of the optical phonon is splitted into c-LO and c-TO components [25] associated with the incident photons. On the other hand, for h-GaN the LO and TO phonons are represented as the h-LO and h-TO phonons, respectively.

In this study, the Raman scattering measurements were carried out at room temperature using the Renishaw Ramanscope RM1000 at the Gem and Jewelry Institute of Thailand (Public Organization), Chulalongkorn University. A 514.5-nm line of an Ar⁺ laser is used as a monochromatic high frequency light source. The optical penetration depth, skin depth, $d = 1/2\alpha$; where α is the absorption coefficient of GaN is estimated to be about 70 nm [26]. The laser beam is focused on the sample with the spot sized of $\sim 2 \mu\text{m}$. The Raman spectra were obtained in the backscattering geometry $z(x,y)\vec{z}$ and recorded in the range of 250-800 wave number (cm^{-1}).

CHAPTER III

Materials and Experiment

In this chapter, we provide the sample details of cubic GaN films on GaAs (001) and GaAs (311) substrates, which were used in this study. Subsequently, the basic characterizations using scanning electron microscopy (SEM), atomic force microscopy (AFM) were done and described. High-resolution X-ray diffraction (HRXRD) sets up for characterization the c-GaN films on the GaAs (001) and GaAs (311) substrates.

3.1 Sample details

All the c-GaN layers used in this study were grown on GaAs (001) and GaAs (311) substrates by metalorganic vapor phase epitaxy (MOVPE) at laboratory of Prof. Dr. Kentaro Onabe, the University of Tokyo, Japan. The growth experiments were performed by low-pressure MOVPE using an ULVAC system MPM-254. This system employs the horizontal growth reactor with a water-cooled cold wall. RF power was used to heat up the carbon subsector. However, no substrate rotation is available in this system. Figure 3.1 shows a schematic diagram of our growth apparatus. High purity trimethylgallium (TMGa) was used as the group III precursors. Tertiarybutylamine (TBAs) and DMHy) were used as the group V precursors. The temperature-controlled bubblers of TMGa and DMHy were maintained at -10°C and 10°C , respectively. Pd-diffused H_2 was used as the carrier gas to bubble the metal-organic liquids and deliver them to reactor. These column III and V precursors enter the reactor and are decomposed in the hot region above or on the substrate surface itself.

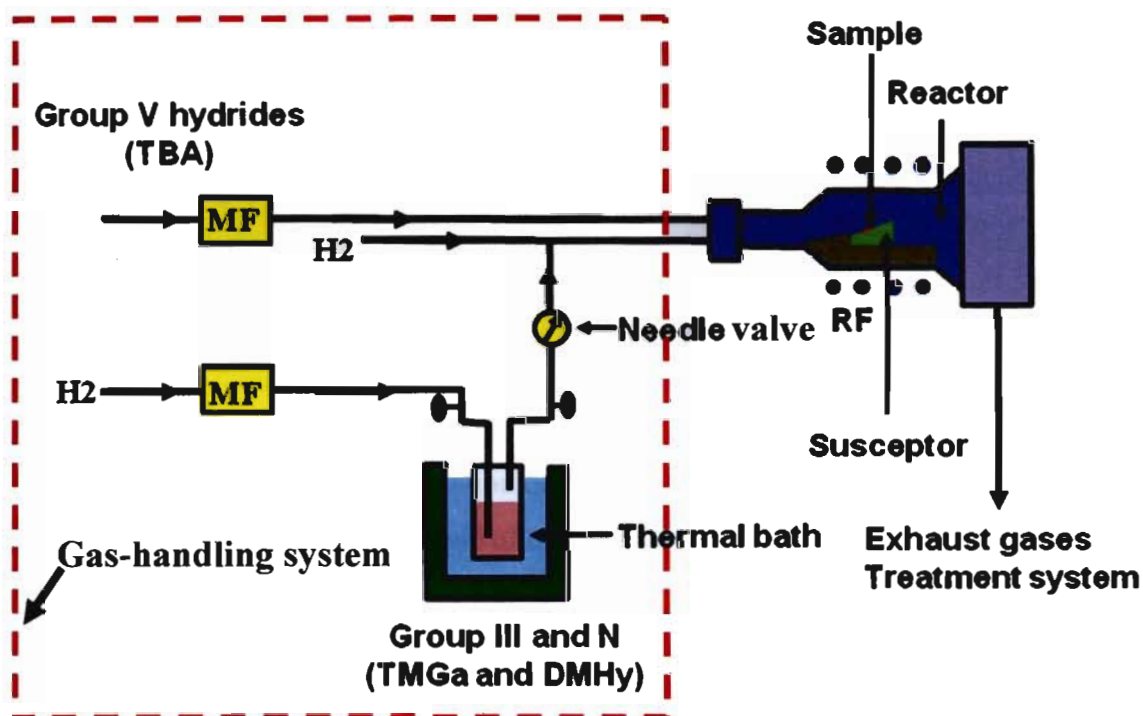


Figure 3.1: Schematic diagram of MOVPE system. A typical system consists of four major parts, gas-handling system, reactor chamber, heating system (RF coil) and exhaust gases treatment system.

3.1.1 c-GaN on GaAs (001)

The sample structure of c-GaN grown on GaAs (001) substrate is shown in Fig. 3.2. After the growth of the around 100 nm-thick GaAs buffer layer was grown by metal organic vapor phase epitaxy (MOVPE) at 650°C, then a 20 nm-thick GaN buffer layer was deposited at substrate temperatures in the range of 530-600°C. Finally, the c-GaN main layer was grown at 900°C. The V/III ratios for the c-GaN buffer layer and main layer were divided in to two series. First, V/III ratios for the c-GaN buffer layer and epitaxy layer were 100 and 25, respectively. Another, the V/III ratios for the c-GaN buffer layer and main layer were 50 and 12.5, respectively.

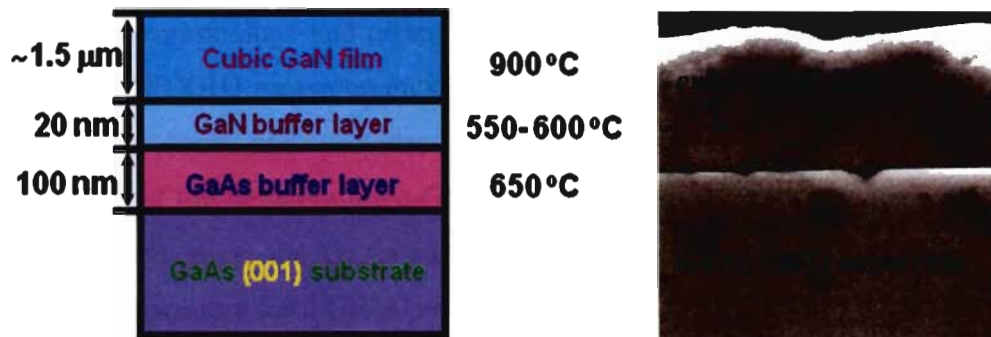


Figure 3.2: (a) Schematic illustration of sample structure for c-GaN film grown on GaAs (001) substrate. (b) Example of c-GaN grown layer on GaAs (001) substrate measured by SEM.

Sample No.	V/III ratios Buffer : layer	Tg buff. (°C)	Nominal thickness (μm)
1	100:25	550	1.50
2	100:25	575	2.05
3	100:25	600	1.28
4	50: 12.5	530	1.61
5	50:12.5	550	8.87
6	50:12.5	575	2.55

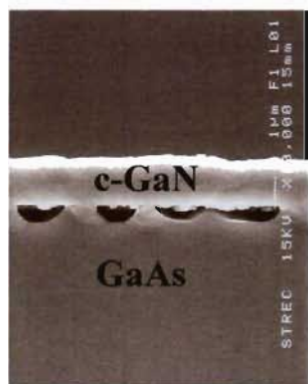
Table 3.1: Growth condition of the c-GaN on GaAs (001), in this table Tg is growth temperature.

Growth time of the main c-GaN layer was 20 mins for all the samples. Growth conditions of all the samples are summarized in Table 3.1. An overview of structural properties (morphology and crystal structures) of these c-GaN films were obtained by SEM and HRXRD measurements. A GaAs pre-layer is usually necessary to improve GaN main layer and provides an atomically smooth substrate surface before deposition of low-temperature c-GaN buffer layer [6]. This also reduced the effects of residual oxygen on the GaAs surface which affects on the nitride layers [6]. The growth temperature for a GaAs pre-layer is usually about 600-700°C and the thickness is typically 200 nm [27]. During the MOVPE growth, the presence of As ambient pressure is known to protect the surface from degradation at high substrate temperature and to enhance subsequent c-GaN growth [28]. It is known that the best c-GaN films are commonly produced when a thin GaAs layer is first deposited and then followed by the low-temperature GaN nucleation layer. This layer helps to maintain an atomically smooth surface, which is critical for minimizing generation of defects. Trampert *et al* [29] and Brandt *et al* [30] found that GaN nucleates in the cubic phase on atomically smooth 100 nm-thick GaAs (001) pre-layer. An atomically roughening of the GaN/GaAs interface generate structural defects, such as dislocation, stacking faults etc. The use of buffer layer of GaN grown at low-temperature, which acts as a nucleation layer, improves the quality of high-temperature GaN layer. Moreover, an initial deposition of GaN is usually conducted at relatively low-temperature (550-650°C) compared to that for the growth of GaN main layer. As a result, this film can protect the GaAs surface from thermal decomposition at relatively high growth temperatures (>700 °C).

Figure 3.3 shows cross-sectional SEM images of the c-GaN films on GaAs (001) substrates grown at different growth temperatures. It is clearly seen that the thickness of c-GaN layers is in the range of 1.5 μm depending on growth condition. Number of voids were clearly observed at the GaN/GaAs interface. The reason for occurrence of such voids is considered to relate to desorption of As-atoms from the GaAs surface at high growth temperature (900°C). This situation is similar for the GaP substrate [7]. Correlation between of size and density of the voids and the growth condition V/III ratio 100:25 (sample No. 1, 2 and 3) decreased with increasing the temperature of GaN buffer layer. In addition the size and density of the voids of the

V/III ratios [buffer layer: main layer]

[100:25]

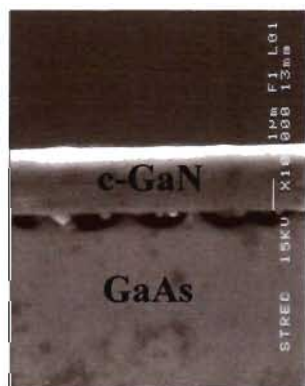


$T_g(\text{buff.}) = 550^\circ\text{C}$

[50:12.5]



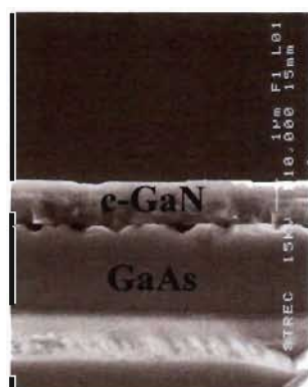
$T_g(\text{buff.}) = 530^\circ\text{C}$



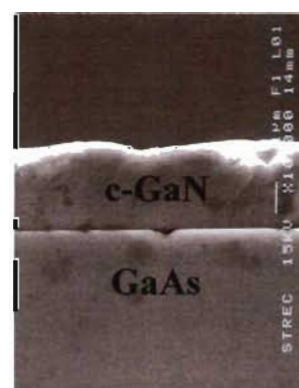
$T_g(\text{buff.}) = 575^\circ\text{C}$



$T_g(\text{buff.}) = 550^\circ\text{C}$



$T_g(\text{buff.}) = 600^\circ\text{C}$

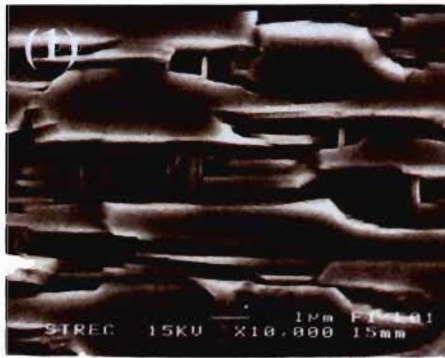


$T_g(\text{buff.}) = 575^\circ\text{C}$

Figure 3.3: SEM images showing cross-section of the c-GaN films grown at different growth temperatures of GaN buffer layer and different V/III ratios for the c-GaN buffer layer (100 and 50) and the c-GaN main layer (25 and 12.5).

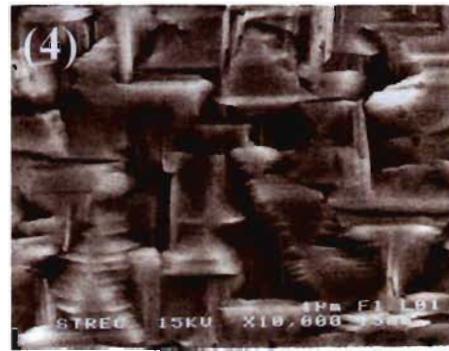
V/III ratios [buffer layer: main layer]

[100:25]

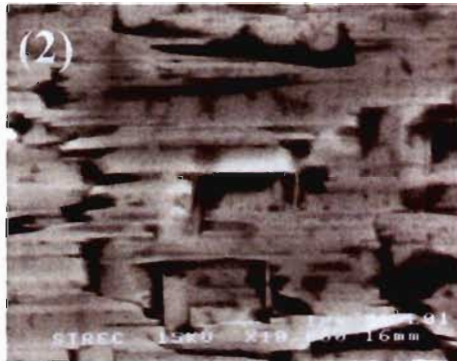


T_g (buff.)= 550°C

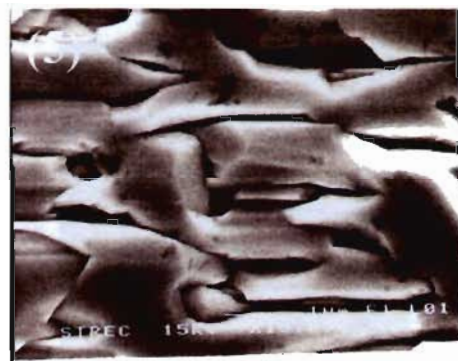
[50:12.5]



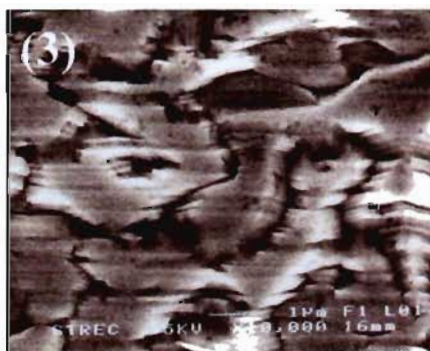
T_g (buff.)= 530°C



T_g (buff.)= 575°C



T_g (buff.)= 550°C



T_g (buff.)= 600°C



T_g (buff.)= 575°C

Figure 3.4: SEM images show surfaces of the c-GaN films grown at different growth temperatures of GaN buffer layer and different V/III ratios for the c-GaN buffer layer (100 and 50) and the c-GaN main layer (25 and 12.5).

V/III ratios [buffer layer: main layer]

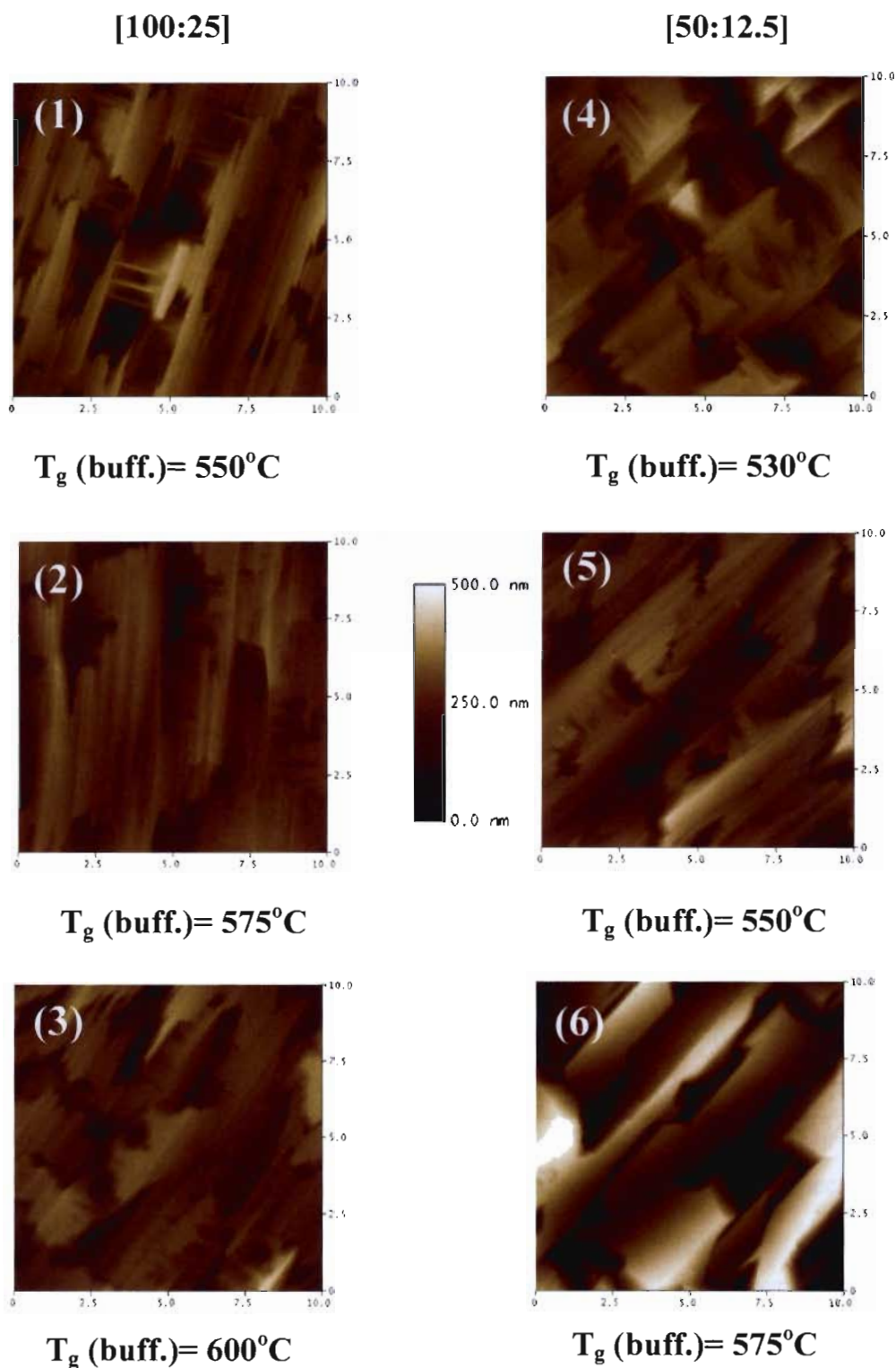


Figure 3.5: AFM images show surface morphologies of the c-GaN films grown at different growth temperatures of GaN buffer layer and different V/III ratios for the c-GaN buffer layer (100 and 50), c-GaN main layers (25 and 12.5).

growth condition V/III ratio 50:12.5 (samples No. 4, 5 and 6) were less than the growth condition V/III ratio 100:25.

Figures 3.4 and 3.5 respectively show the SEM and AFM images of surface morphology of the c-GaN films on GaAs (001) substrates grown under different growth conditions. It can be observed the film is rough with facets. This may result from the voids, which the decomposed of GaAs between the surface of GaN buffer layer and GaAs substrate has an influence on the rough of the c-GaN film. As shown in these figure, the roughness of surface morphology of films decreased with increasing the temperature of GaN buffer layer as shown in the growth condition V/III ratio 100:50 (sample No. 1, 2 and 3) and the growth condition V/III ratio 50:12.5 (samples No. 4, 5 and 6).

Figure 3.5 shows the AFM images of surface morphology of the c-GaN films on the GaAs (001) substrates. For condition V/III ratio 100:50 (samples No. 1, 2 and 3), surface root mean square (RMS) roughness of the films decreases with an increasing the growth temperature of GaN buffer later. On the other hand, the surface RMS roughness of the films grown under the growth conditions with V/III ratio of 50:12.5 (samples No. 4, 5 and 6) increases with an increasing the temperature of GaN buffer layer.

3.1.2 c-GaN on GaAs (311)

c-GaN layer was grown on GaAs (311) substrate, which has a 100 nm-thick GaAs buffer layer grown from TMGa and AsH₃ at 650°C on the GaAs (311) substrate. Then, GaN buffer layer was deposited for 2 mins at temperatures in the range of 530-600°C. Finally, c-GaN epitaxial layer was grown at 900°C. The V/III ratios for the c-GaN buffer layer and epitaxial layer were 100 and 25, respectively and the V/III ratio for the c-GaN buffer layer and epitaxy layer were 50 and 12.5, respectively. The growth time was 20 mins. The thickness of the grown c-GaN layers was 1.5 μm. Sample structure is shown in Fig. 3.6: growth condition and thickness of all the samples of c-GaN on GaAs (311) are summarized in Table 2.2. An overview of surface morphology of c-GaN grown films was obtained by SEM and AFM measurements, as shown in Figs. 3.7-3.9. Figure 3.7 shows cross-sectional SEM

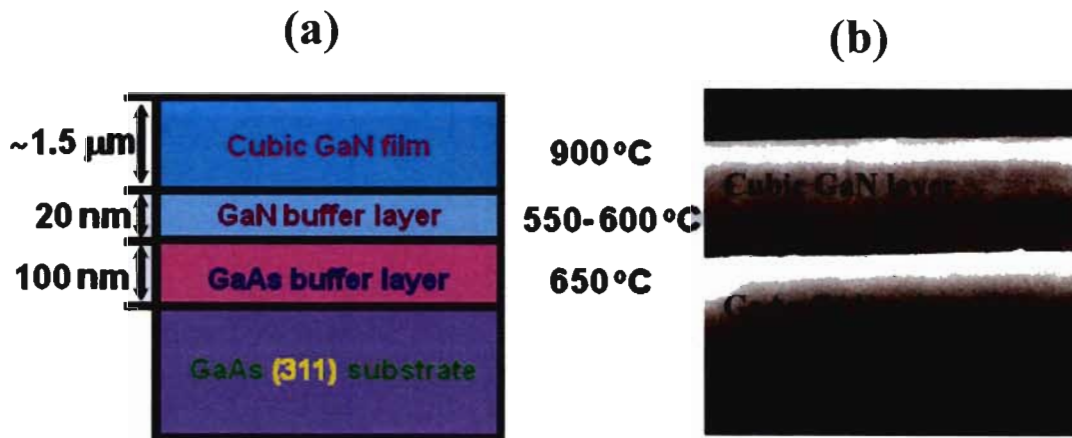


Figure 3.6: (a) Schematic illustration of sample structure of c-GaN film grown on GaAs (311) substrate. (b) Cross-section sample structure recorded by SEM.

Sample No.	V/III ratios Buffer : layer	Tg buff. (°C)	Nominal thickness (μm)
7	100:25	550	3.33
8	100:25	575	3.38
9	100:25	600	2.25
10	50:21.5	530	1.64
11	50:1.25	550	1.48
12	50:1.25	575	1.64

Table 3.2: Growth conditions and thicknesses of the c-GaN layers on GaAs (311) substrates.

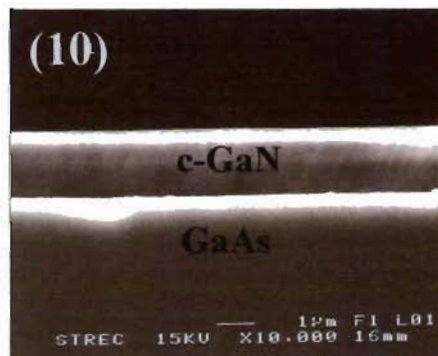
V/III ratios [buffer layer: main layer]

[100:25]

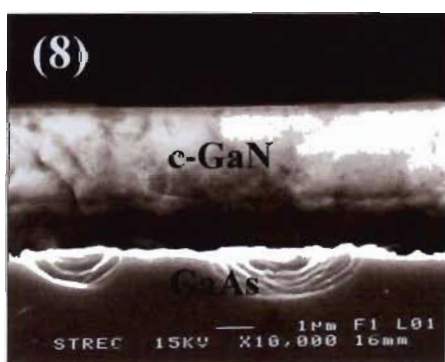


T_g (buff.)= 550°C

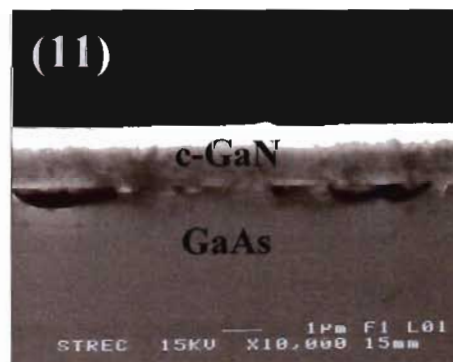
[50:12.5]



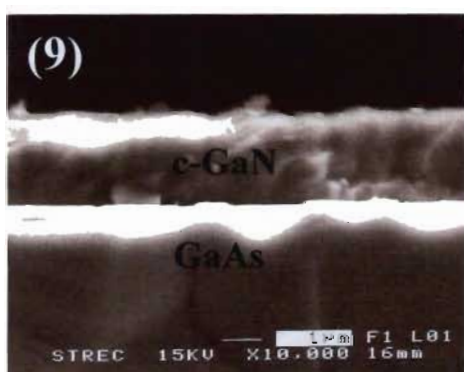
T_g (buff.)= 530°C



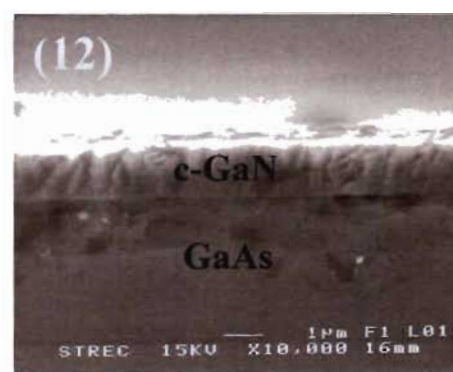
T_g (buff.)= 575°C



T_g (buff.)= 550°C



T_g (buff.)= 600°C



T_g (buff.)= 575°C

Figure 3.7: SEM images show a cross-section of the c-GaN films grown at different growth temperatures of GaN buffer layer and the V/III ratios for the c-GaN buffer layer, epitaxial layer.

V/III ratios [buffer layer: main layer]

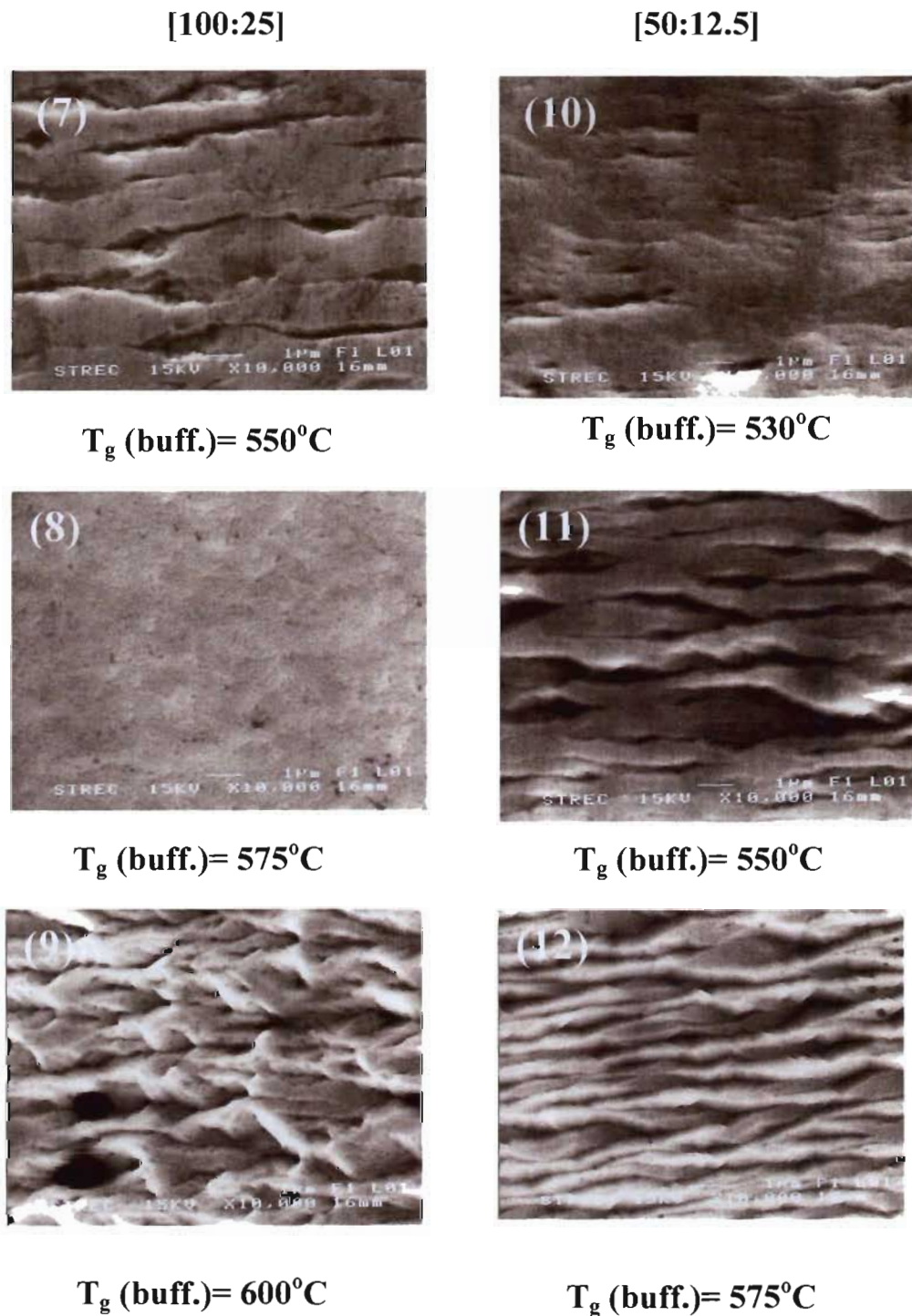


Figure 3.8: SEM images surface morphology of the c-GaN films grown at different growth temperatures of GaN buffer layer and the V/III ratios for the c-GaN buffer, epitaxy layer.

V/III ratios [buffer layer, main layer]

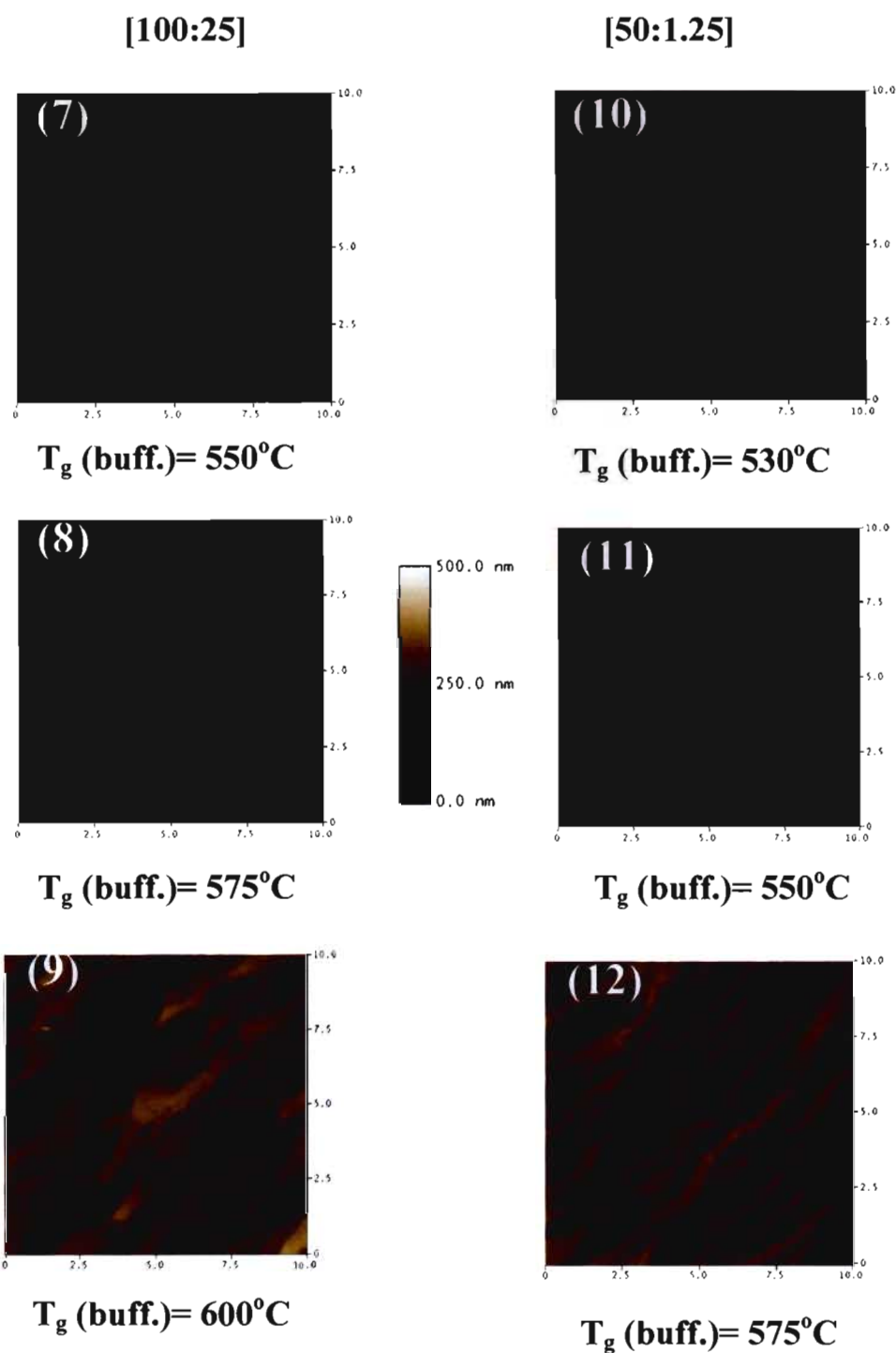


Figure 3.9: AFM images surface morphology of the c-GaN films grown at different growth temperatures of GaN buffer layer and the V/III ratios for the c-GaN buffer layer, epitaxial layers.

images of c-GaN films on GaAs (311) buffer and main layers. It is clearly seen that the voids were observed at the GaN/GaAs interface only the sample 8 (at 550°C, V/III ratios: 50 and 12.5). This indicates that flatter interface without generation of any voids can be obtained by use of the GaAs (311) substrate.

Figures 3.8 and 3.9 respectively show SEM and AFM images of surface morphology obtained from c-GaN films on GaAs (311) substrates. It can be observed the film is rougher than the c-GaN films on GaAs (311). As shown the Figs. 3.8 and 3.9, the growth condition V/III ratio 100:25, growth temperature of GaN buffer layer is 575°C (sample No.8). Films are rougher than any films in the same condition. AFM images of surface morphology of the c-GaN films on the GaAs (311) substrates. As shown in figure, it is seen that in order condition V/III ratio 100:25 (sample No. 7, 8 and 9). The surface root mean square (RMS) rough of the films much more than c-GaN films on GaAs (001) substrate.

3.2 High resolution X-ray diffraction measurements

In this study, HRXRD measurements were performed using the Bruker-AX8 D8 DISCOVER at Scientific and Technology Research Equipment Center (STREC), Chulalongkorn University. Figure 3.10 shows the HRXRD instrument with a conventional Cu target operated at 40 kV and 40mA. The CuK_α radiation is monochromatized into the wavelength of $K_{\alpha 1}$ ($\lambda=1.5406 \text{ \AA}$ with $\Delta\lambda/\lambda = 3\times 10^{-4}$ [13]) by a four-crystal Ge (022) channel-cut monochromator. In addition, a two-crystal Ge (022) channel-cut analyzer was placed in front of the detector to restrict the angular acceptance of the detector.

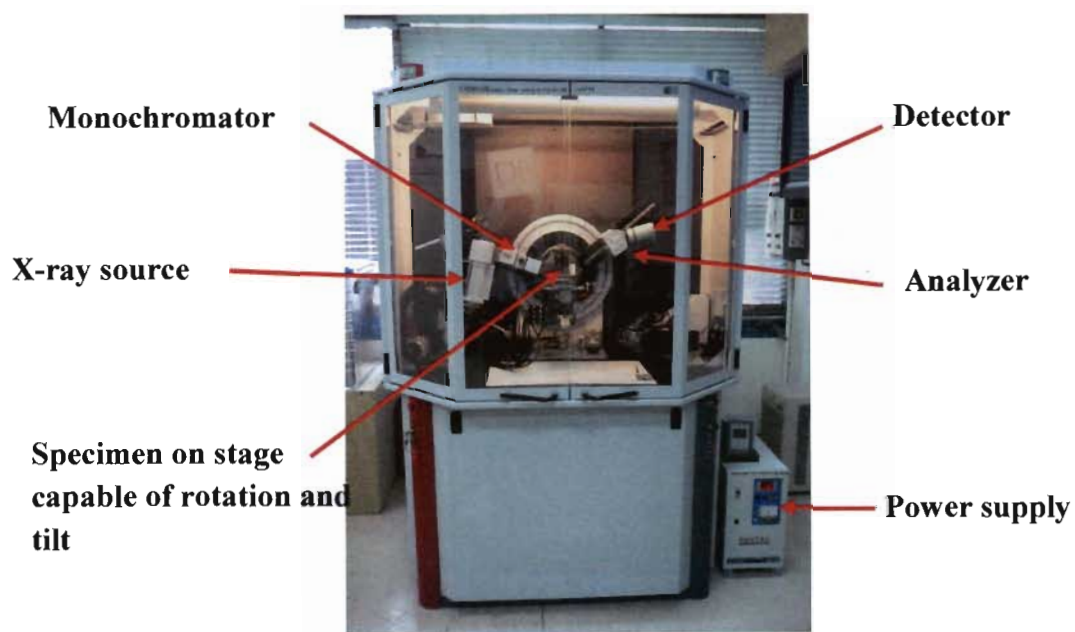


Figure 3.10: High resolution X-ray diffraction instrument installed at Scientific and Technology Research Equipment Center, Chulalongkorn University.

3.3 Raman scattering spectroscopy measurements

Micro-Raman scattering used in this study were done with the Renishaw ramanoscope RM1000 at the Gem and Jewelry Institute of Thailand, Faculty of Science, Chulalongkorn University (Fig. 3.11). Raman spectra were recorded at room temperature in backscattering geometry on the (001) growth surface of samples. The scattering configuration of $z(x, y)\bar{z}$ is used, where x , y and z correspond to the (100), (010) and (001) crystal directions, respectively. The spectral range was set at the wave number of 250 - 700 cm^{-1} . The Ar^+ 514.5-nm laser line was used as an excitation light source. The excitation laser beam was focused by a microscope lens system yielding a spot size $\sim 2 - 4 \mu\text{m}$ in diameter. Raman spectroscopy set up is shown in Fig. 2.8.

In the case of GaAs, the optical penetration depth ($d = 1/\alpha$; where α is the absorption coefficient) is about 100 nm for a photon energy of 2.41 eV (or 514.5-nm

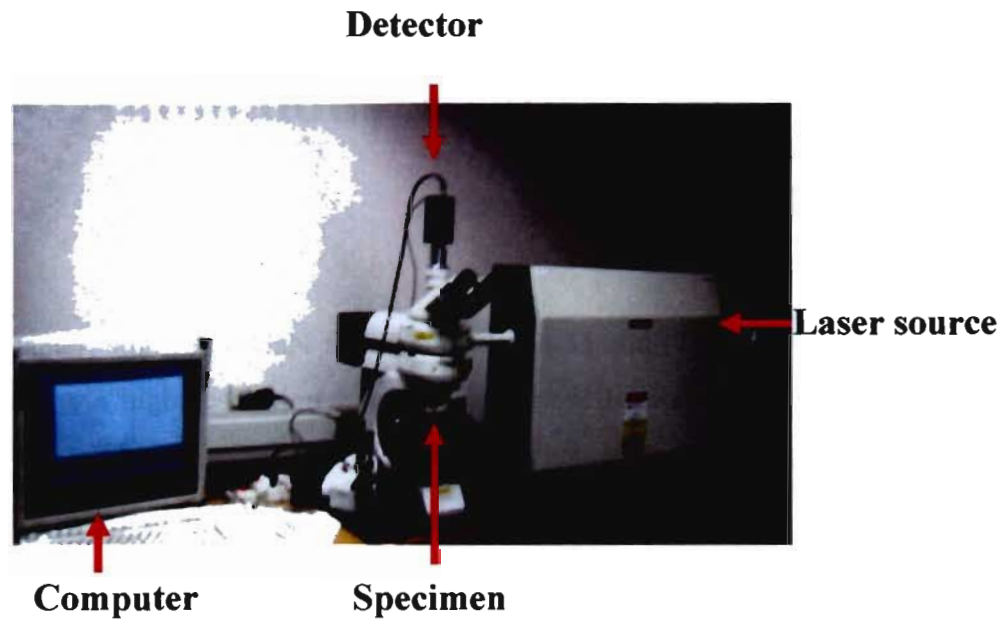


Figure 3.11: Raman spectroscopy system at the Gem and Jewelry Institute of Thailand (Public Organization), Chulalongkorn University.

wavelength, corresponding to the green line of Ar^+ laser) [26]. Thus, Raman scattering with incident light wavelength 514.5 nm is a great technique to study the regions of thin GaN films with thickness as thin as 100 nm. The number of samples used in this study is 12 samples. Raman spectra were recorded from five different areas (five spots) for each sample.

CHAPTER IV

Anomalous Strain in c-GaN

In this chapter, strain in c-GaN films on (001) GaAs and (311) GaAs substrates was investigated via high resolution X-ray diffraction (HRXRD). GaAs substrates have been mostly used as a substrate material for c-GaN. A large mismatch in the lattice parameters and thermal expansion coefficients results in a residual strain, which induces generation of defects that degrade layer quality. Thus, measurement and analysis of the residual strain is of great interest. It is known that the buffer layer, the growth temperature, the V/III ratio, and the thickness are the key parameters that control the lattice and the strain of hexagonal GaN [6, 42]. In this study, thus, $2\theta/\omega$ -scan and reciprocal space mapping modes in HRXRD were selected as a techniques to measure the lattice parameters and strain of c-GaN layers grown on (001) GaAs and (311) GaAs substrates with different growth conditions and thicknesses.

4.1 Strains in c-GaN on GaAs (001)

Six c-GaN samples with different thicknesses, V/III ratios of c-GaN buffers and main layers, and growth temperatures of buffer layer were investigated to clarify the lattice parameters and strain in c-GaN. Details and initial investigational results of all the samples, such as layer thicknesses and surface morphologies, were demonstrated in Chapter III. To calculate the strain, as described in Chapter II, the fully relaxed lattice constant (a_r) should be known first. It can be deduced from Eq. 2.6 that is:

$$a_{\perp} - a_{\parallel} = 2(c_{11} / c_{12}) \cdot (a_{\parallel} - a_r), \quad 4.1$$

where a_{\perp} and a_{\parallel} are the perpendicular and in-plane lattice parameters, which were

measured using symmetric (002) reflections and asymmetric (113) reflections, respectively, and c_{11} and c_{12} are the elastic constants. Eq. 4.1 can be applied to calculate a “relaxed” lattice constant, provided the value of c_{11}/c_{12} is known. Here we take c_{11}/c_{12} to be 0.57955 [39]. While, remarkable variations exist in the elastic constants reported [40, 41], fortunately, they had little effect on the calculated values of a_r . The discrepancy in those calculated values obtained based on different elastic constants will be discussed later. The in-plane strain, which is in the direction that parallel to the GaAs substrate surface, which is the (001) plane, was calculated by

$$\varepsilon_{//} = \frac{(a_{//} - a_r)}{a_r} \times 100\%. \quad 4.2.$$

To determine the value of a_{\perp} , $2\theta/\omega$ -scans of symmetric (002) reflection were performed. Figure 4.1(a) shows a typical result of (002) $2\theta/\omega$ -scan recorded from sample No. 3 (V/III ratio of c-GaN buffer layer = 100 at growth temperature = 600°C, V/III ratio of c-GaN main layer = 25 at growth temperature = 900°C). Two diffraction peaks detected at $2\theta = 31.6263^\circ$ and 39.9781° were identified as (002) GaAs and (002) c-GaN orientations, respectively. The results from HRXRD determine that the GaN layers used in this study had cubic structure with (001) surface parallel to the GaAs (001) substrate surface. Moreover, reciprocal space map (RSM) of symmetric (002) reflection was performed to examine an orientation tilting of the c-GaN (002) plane. Figure 4.1(b) shows the RSM of the symmetric (002) reflection obtained from the same sample as used in Fig. 4.1(a). The various colors of the contour line represent the different intensities of X-ray diffraction. Red contours refer to the high intensities, but on the other hand blues contours refer to relatively low intensities. Since this sample mainly consists of the c-GaN and GaAs crystalline structures, thus, there exist only two Bragg reflections, one of the (002) GaAs substrate and one which is due to (002) c-GaN layer are observed, as indicated by arrows. Since, $\Delta\omega = 0$, indicating that no crystal tilting was observed. Thus we can conclude that the epitaxial relationship was shown that (001) c-GaN is parallel to (001) GaAs crystal.

The peak position was obtained by fitting a Gaussian function to the experimental data. Figure 4.2 shows Gaussian fitting result of (002) c-GaN, which was used to determine peak position (002) c-GaN diffraction to be $2\theta = 39.9781^\circ$.

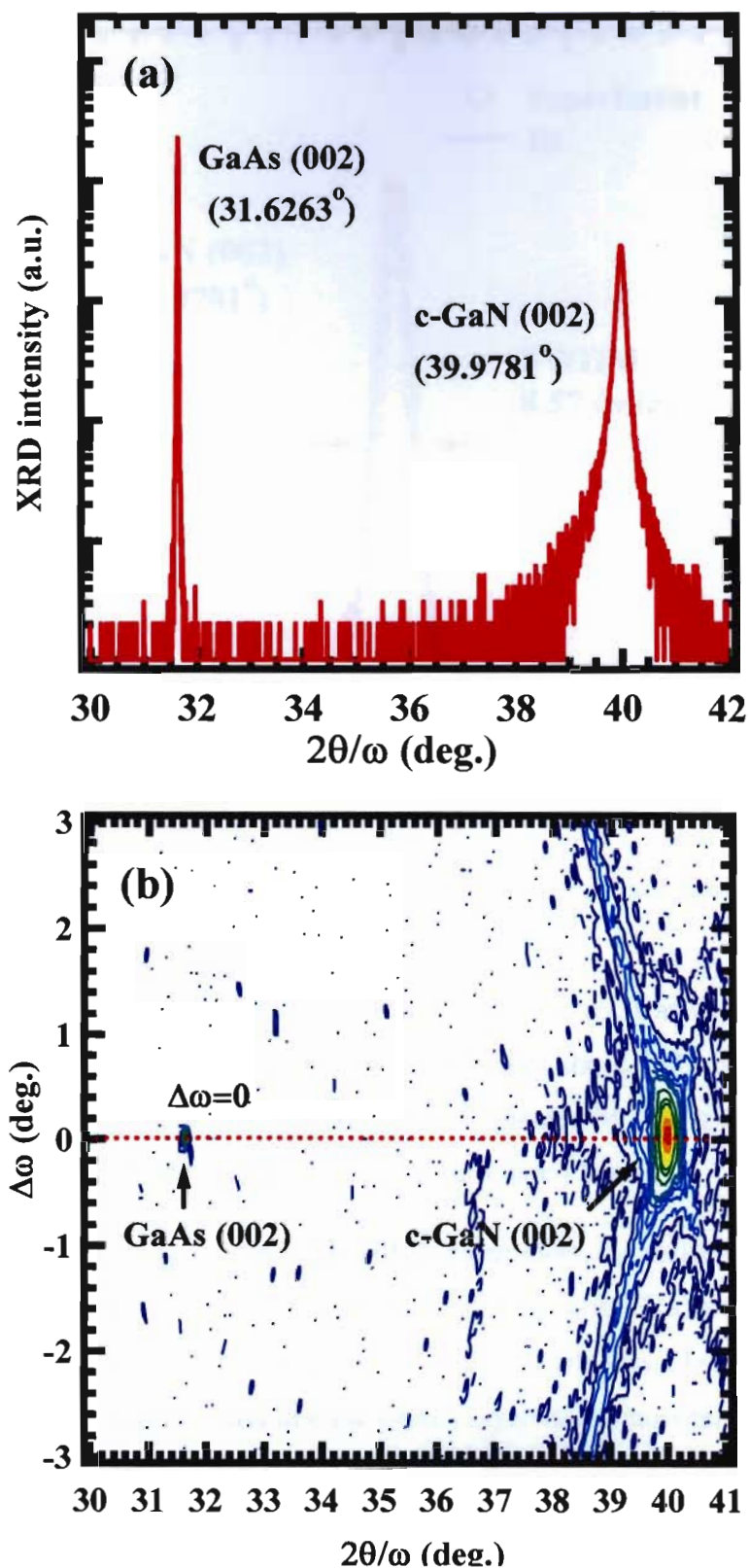


Figure 4.1: (a) A typical high resolution X-ray diffraction (002) $2\theta-\omega$ scan of c-GaN film on GaAs (001) substrate grown with V/III ratios of c-GaN buffer and c-GaN main layers of 100 and 25, respectively, at growth temperature of buffer layer of 600°C ; (b) Reciprocal space map of (002) c-GaN.

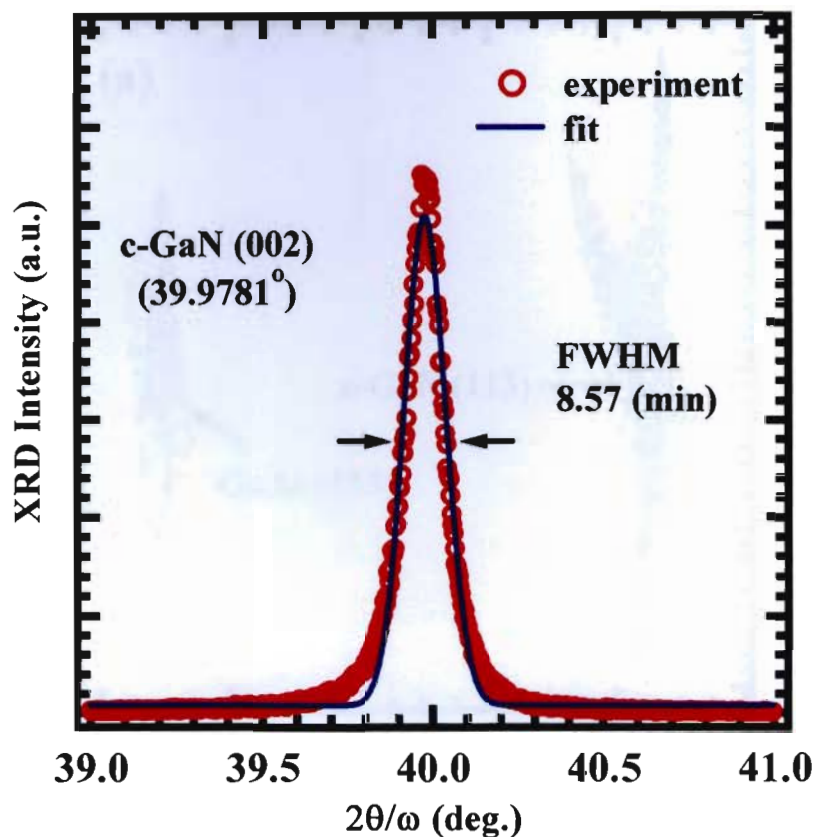


Figure 4.2: The (002) c-GaN peak positions fitted by Gaussian-line shape.

Using Eq. 2.3, the perpendicular lattice parameter, a_{\perp} , was determined to be 4.5068 Å indicating small compressive strain, whereas the c-GaN layer was fully relaxed with lattice constant of 4.503 [14]. Errors originated by fitting and their effect on the determination of lattice parameters will be discussed later.

In order to determine the in-plane lattice parameters, a_{\parallel} , reciprocal space map (RSM) of asymmetric (113) reflection was performed. Figures 4.3(a) and 4.3 (b) show the RSM and $2\theta-\omega$ scan of the asymmetric (113), which was observed from the sample used in Fig. 4.1. It is found that the c-GaN layer was almost relaxed on GaAs. This makes a possible observation of asymmetric (113) reflections from substrate and layer in the same measurement, as shown in Fig. 4.3(b). However, the small inclination, which is clearly visible in Fig. 4.3(a) and 4.4 (a), arises due to a small tilt of $\Delta\omega = -0.0243^\circ$ of the (113) plane with respect to that of the GaAs substrate. As shown in Fig. 4.4 (b), the values of $\Delta\omega$ were obtained from Gaussian fitting result of (113) reflection in ω -scan mode. Using the calculated value of a_{\perp} and Eq. 2.5,

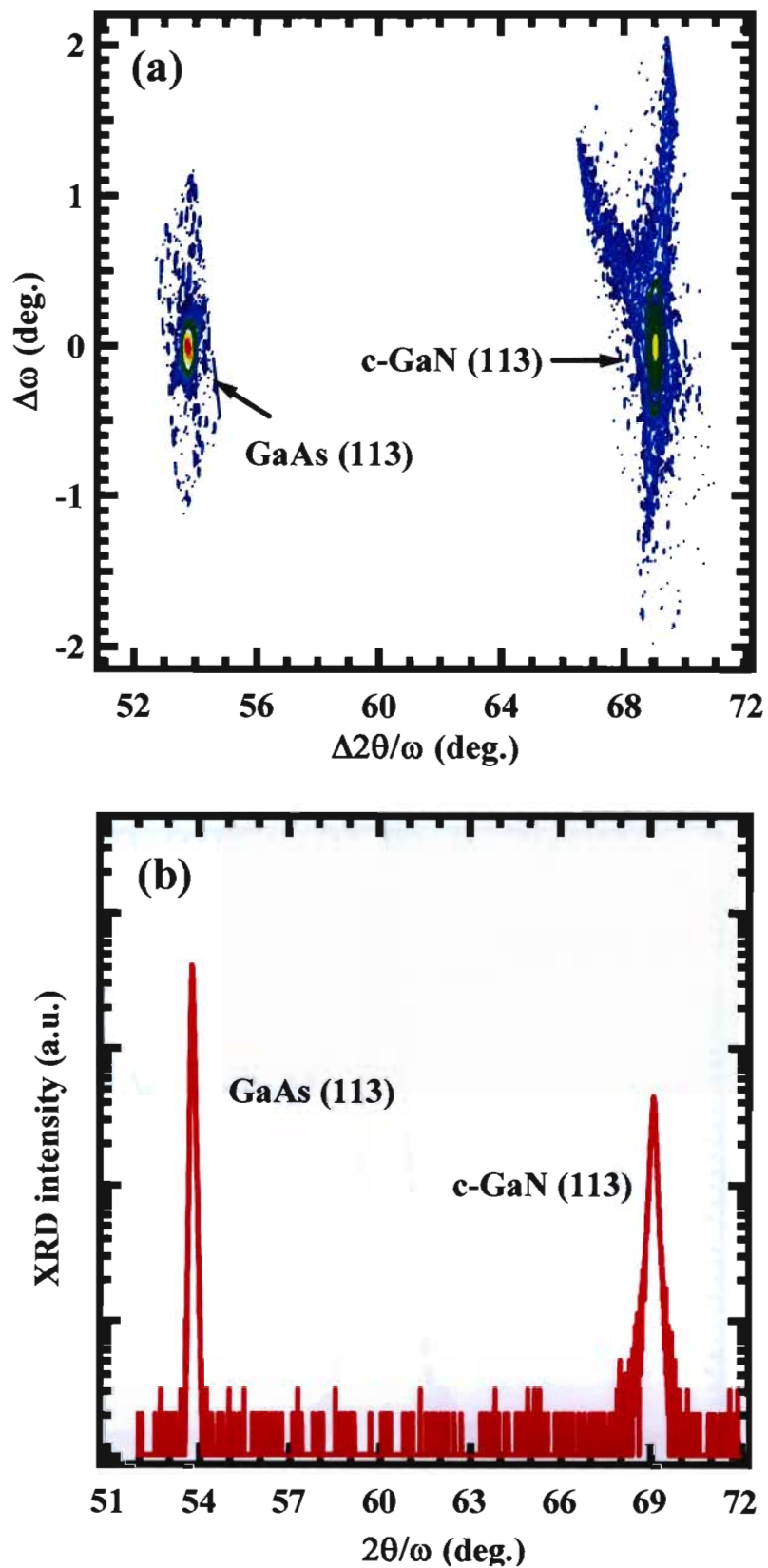


Figure 4.3: (a) Reciprocal space map of the (113) reflection of c-GaN film on GaAs (001) substrate (the same sample used in Figs. 4.1 and 4.2). (b) Diffraction peaks 2θ - ω scan of (113) reflection.

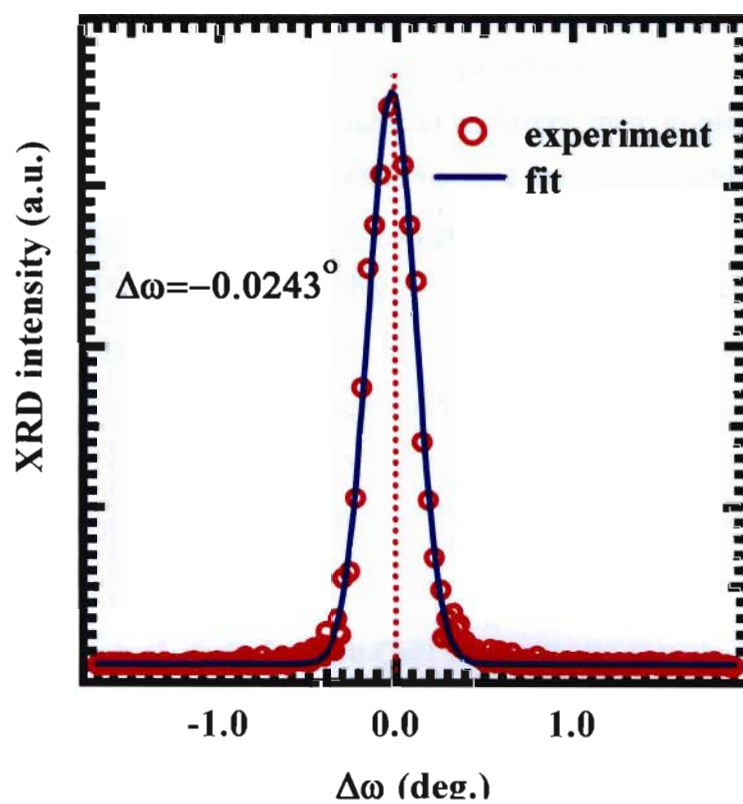
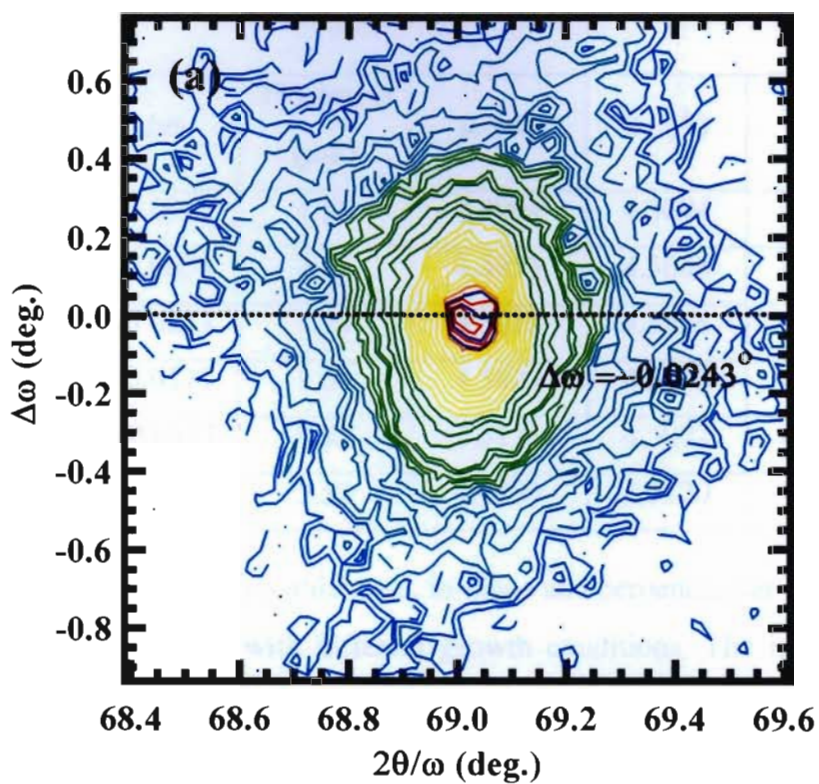


Figure 4.4: (a) Reciprocal space map of the (113) reflection of only the c-GaN region and (b) the (113) reflection of ω -scan fitted by Gaussian-line shape.

Samples No.	$\Delta\omega$	Thickness (μm)	$a_{//}(\text{\AA})$	$a_{\perp}(\text{\AA})$	$a_r(\text{\AA})$	$\varepsilon_{//}$
1	-0.0942	1.50	4.4904	4.5094	4.4992	-2.0×10^{-3}
2	-0.0658	2.05	4.4955	4.5088	4.5016	-1.4×10^{-3}
3	-0.0243	1.28	4.5018	4.5068	4.5041	-0.5×10^{-3}
4	-0.0379	1.61	4.5022	4.5098	4.5057	-0.8×10^{-3}
5	+0.0517	8.87	4.5178	4.5072	4.5129	$+1.1 \times 10^{-3}$
6	-0.0871	2.55	4.4939	4.5120	4.5023	-1.9×10^{-3}

Table 4.1: Measured $\Delta\omega$, thickness, in-plane and perpendicular lattice constants of c-GaN on GaAs (001) with different growth conditions. The in-plane strain $\varepsilon_{//}$ was calculated by $(a_{//}-a_r)/a_r$.

$$\Delta\omega = \tan^{-1}(\sqrt{2}/3) - \tan^{-1}(\sqrt{2} \cdot a_{\perp} / 3 \cdot a_{//}), \quad 4.3$$

thus, we can determine the in-plane lattice parameter to be $a_{//} = 4.5018 \text{ \AA}$. It is clearly visible that the perpendicular parameter is larger than in-plane lattice parameter, indicating that strain in this c-GaN layer is compressive, which is contrary to the expected tensile strain caused by the large lattice mismatch ($\sim 20\%$) between c-GaN layers and GaAs substrates. Table 4.1 summarized all determined parameters, including $\Delta\omega$, thickness, a_{\perp} , $a_{//}$, a_r and $\varepsilon_{//}$. It is found that relationship between $\Delta\omega$ and $\varepsilon_{//}$ is linear dependent. As shown in Fig. 4.5, we can distinguish the situation of strain in c-GaN into tensile and compressive strain regions. Almost c-GaN layers are under compressive strain situation, excluding the layer with the highest thickness of $8.87 \mu\text{m}$ (sample No. 5).

This unusual strain in the c-GaN layers shows that the residual strain in the layer was not dominated by the resulting lattice-mismatch strain. It is known that GaAs substrates and GaN layers also have thermal mismatch. After growth of c-GaN main layer at 900°C , the sample's temperature was cooled down to room temperature.

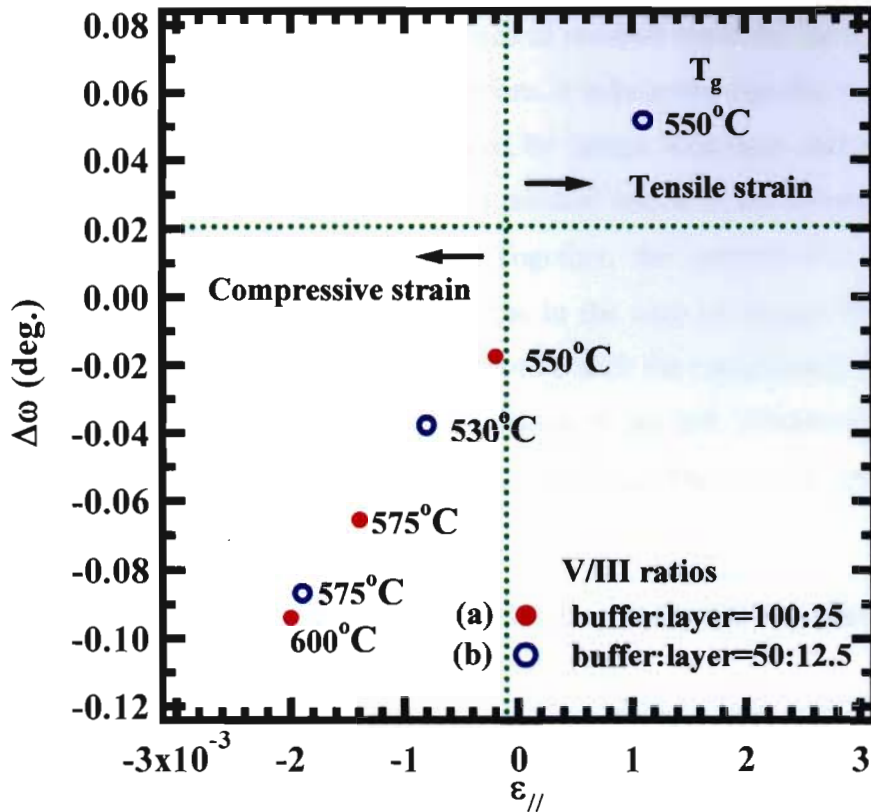


Figure 4.5: $\Delta\omega$ variation of $\varepsilon_{//}$ for growth temperature (a) V/III ratio 100:25 and (b) V/III ratio 50:12.5 of c-GaN on GaAs (001).

The difference of thermal expansion coefficients between c-GaN and GaAs results in compressive stresses. In the following, we estimate the strain ε induced by the thermal mismatch. This strain is given as [14]

$$\varepsilon = \Delta T(\alpha_1 - \alpha_2), \quad 4.4$$

where α_1 and α_2 are thermal expansion coefficients of GaAs and c-GaN, respectively. ΔT is difference between room temperature and the growth temperature, which is typically about 900°C. We take ΔT , α_1 and α_2 as 875 K, $6.0 \times 10^{-6} \text{ K}^{-1}$ and $3.17 \times 10^{-6} \text{ K}^{-1}$ [14], respectively, and obtain this strain value to be 2.5×10^{-3} . Compared with the residual strain in c-GaN layers shown in Table 4.1, this value is larger. Thus, this expects that the compressive strains observed in this work come from the difference of thermal expansion coefficients. But, we cannot assume that the resulting lattice-mismatch strain was relieved with the growth proceeded. If the residual strain was totally composed by thermal mismatch strain, it will be only dependent on the thickness of films (the growth temperature is the same for all samples). However, this

was not the case and the direct dependence of residual strain on the thickness of films was not found as seen in Fig. 4.6. Therefore, it is believed that the residual strain is a combination of the tensile strain induced by lattice mismatch and the compressive strain induced by thermal mismatch. The residual tensile strain counteracts part of the compressive thermal mismatch strain. Together, the compressive strain was also relaxed as the film thickness increased (as in the case of sample No. 8, which has layer thickness of 8.8 μm). Thus, we cannot identify the contributing factor. However, the tensile stresses caused by lattice mismatch are not completely relieved with increasing thickness, and have a complicated dependence on the growth conditions concerned in this thesis.

Now, we discuss the factors which may influence the precision of lattice constants.

(i) c_{12}/c_{11} affects the lattice parameters according to Eq. 4.1. The accurate value of c_{12}/c_{11} is still not obtained yet. As is shown in Table 4.2, the reported c_{12}/c_{11} values ranged from 0.634869 to 0.48659 [39, 40, 41]. However, the difference between the calculated lattice parameters induced by c_{12}/c_{11} is less than 0.0013 Å. It is very possible that the precise value of c_{12}/c_{11} is in the region of 0.634 869–0.486 59, and the errors induced by c_{12}/c_{11} may be estimated to be 0.0013 Å.

(ii) Diffraction angles will also affect on the lattice constants. We can determine the lattice constant, which is simply related to the Bragg angle of the measurement and the accuracy Δa in the peak position as

$$\Delta a = a_r \cot(\theta) \Delta \theta \quad 4.5$$

where a_r is the relaxed lattice constant, and θ is the diffraction angle of c-GaN. With the instrument used in our study, the precision in determining the peak position is 0.06 arc min for a typical peak width value of 1.2 arc min. The absolute peak was obtained by a Gaussian-line fit. The fitting errors are 0.006–0.024 arc min. According to Eq. 4.5, the errors of lattice constants are less than 0.0008 Å.

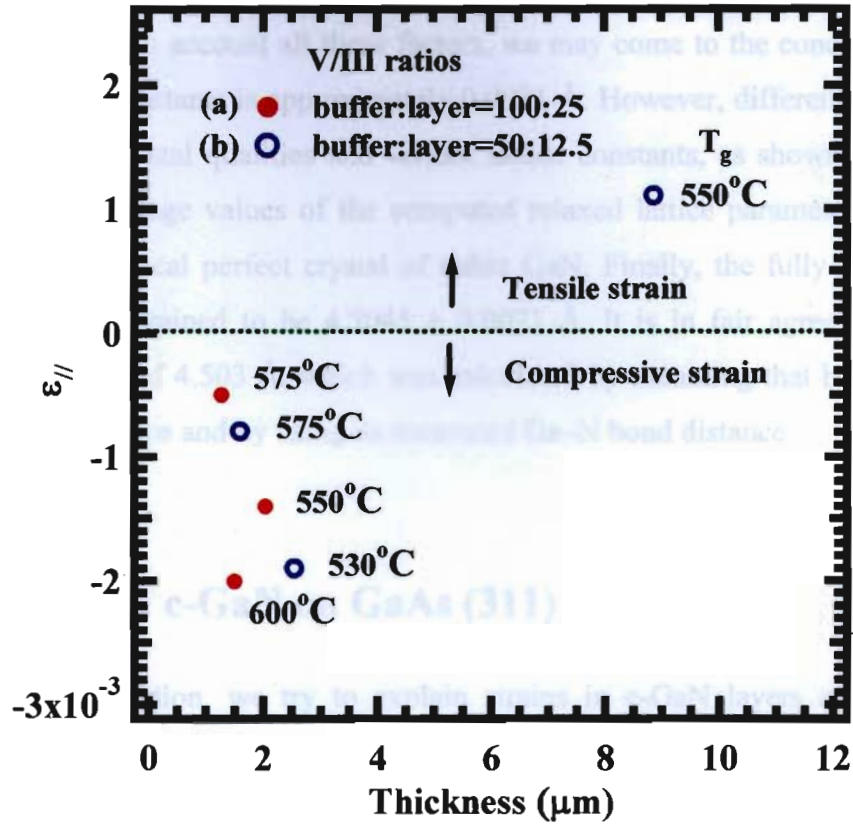


Figure 4.6: Thickness variation of $\epsilon_{//}$ for growth temperature (a) V/III ratio 100:25 and (b) V/III ratio 50:12.5 of c-GaN on GaAs (001)

Sample No.	a_r (Å) [28] ($c_{12}/c_{11}=0.57955$)	a_r (Å) [28] ($c_{12}/c_{11}=0.63489$)	a_r (Å) [28] ($c_{12}/c_{11}=0.48659$)	Δa (Å)
1	4.4992	4.4988	4.5001	0.0013
2	4.5016	4.5013	4.5022	0.0009
3	4.5041	4.5040	4.5043	0.0002
4	4.5057	4.5056	4.5060	0.0004
5	4.5129	4.5131	4.5124	0.0007
6	4.5023	4.5019	4.5030	0.0011

Table 4.2: Calculated fully “relaxed” lattice constants of all the samples using the different published elastic constants of c-GaN. Value of Δ represents the statistical discrepancy between the maximum and minimum of calculated values using the different reported elastic constants of c-GaN.

Taking into account all these factors, we may come to the conclusion that the error of lattice constants is approximately 0.0021 Å. However, different c-GaN layers have different crystal qualities and variant lattice constants, as shown in Table 4.2. We used the average values of the computed relaxed lattice parameters to estimate those of hypothetical perfect crystal of cubic GaN. Finally, the fully relaxed lattice parameter was obtained to be 4.5045 ± 0.0021 Å. It is in fair agreement with the theoretical value of 4.503 Å, which was calculated by assuming that hexagonal GaN forms a cubic lattice and by using its measured Ga–N bond distance

4.2 Strains in c-GaN on GaAs (311)

In this section, we try to explain strains in c-GaN layers on GaAs (311) substrates grown with different growth conditions based on the method of X-ray diffraction as in the case of c-GaN on GaAs (001) substrate. In this case, unlike c-GaN on GaAs (001), symmetric reflections ($\Delta\omega=0$) for the c-GaN layer and the GaAs substrate can be measured from (311) and (200) planes. The (200) reflection is known as symmetric reflections due to $\Delta\omega=0$. However, the c-GaN (200) plane is tilted from the c-GaN (311) plane by about 25.2° , while $\Delta\omega$ is kept at 0. The diffracted intensities by $2\theta/\omega$ -scan mode were recorded and after the c-GaN layers were rotated around the axis parallel to the surface of GaAs (311) substrate and the plane of incident and reflected X-ray beams.

As an example, HRXRD $2\theta/\omega$ -scans of the (311) and (200) reflections measured from sample No. 8 (V/III ratio of c-GaN buffer layer = 100 at growth temperature of 575°C , V/III ratio of c-GaN main layer = 25 at growth temperature of 900°C) are shown in Fig. 4.7. Single peak diffractions from the c-GaN layer are clearly observed and any other peaks including hexagonal GaN are not observed in each reflection. This result suggests that the GaN layers had cubic structure with epitaxial relationship of c-GaN (311)//GaAs (311) and c-GaN (200)//GaAs (200). Compared to c-GaN on GaAs (001), c-GaN layer on GaAs (311) shows equivalently crystal quality: FWHM values of the c-GaN on GaAs (311) in $2\theta/\omega$ -scan is 8.67

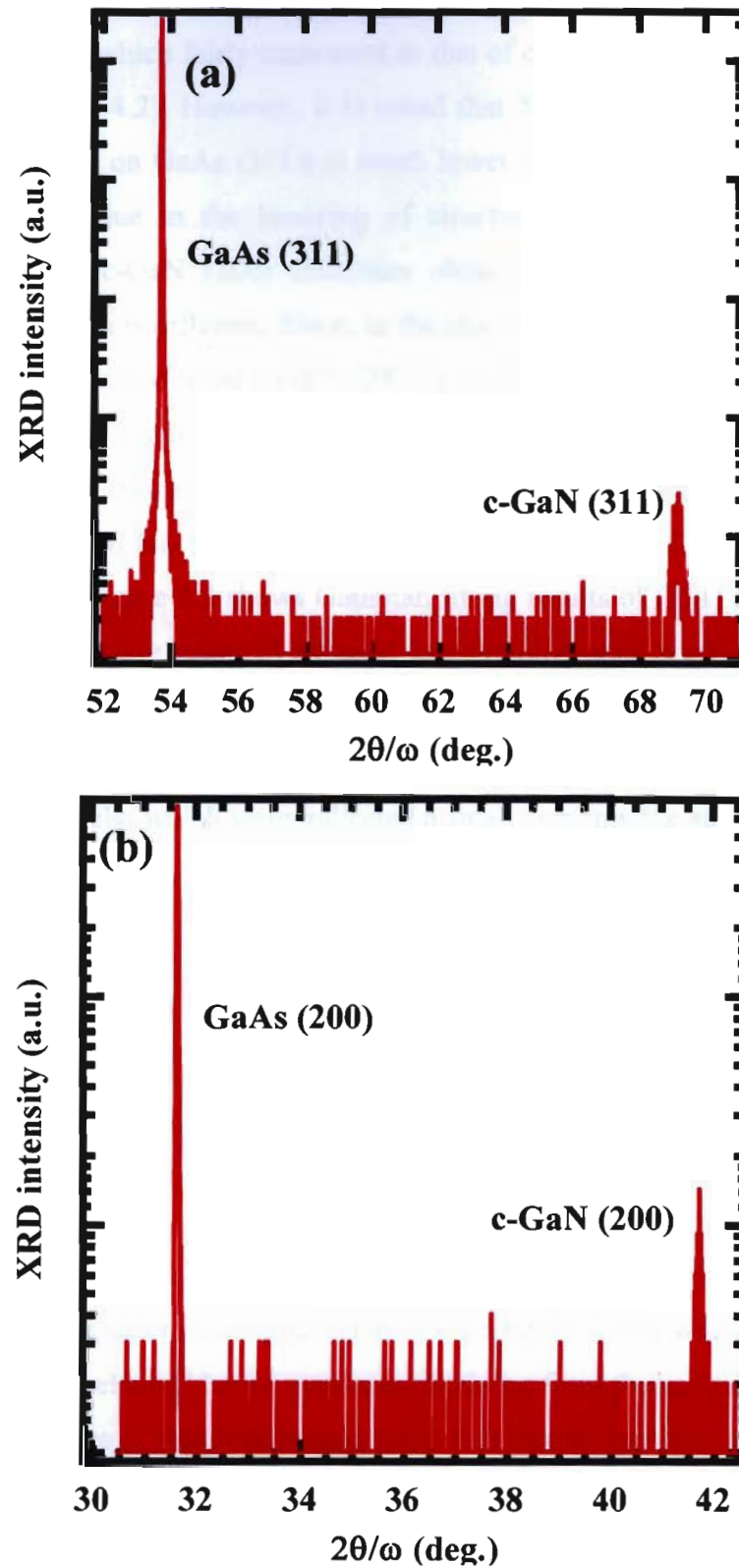


Figure 4.7: Diffraction peak 2θ - ω scans of (a) (311) and (b) (200) reflections from c-GaN layer grown on GaAs (311) substrate with V/III ratios of c-GaN buffer and c-GaN main layers of 100 and 25, respectively, and growth temperature of c-GaN buffer layer was 575°C (sample No. 8).

arc min (Fig. 4.8), which fairly equivalent to that of c-GaN layer on GaAs (001) (8.57 arcmin, see in Fig. 4.2). However, it is noted that X-ray diffracted intensity from c-GaN (311) (c-GaN on GaAs (311)) is much lower than that of c-GaN (002) (c-GaN on GaAs (001)), due to the lowering of structure factor. Although, this is also observed for the c-GaN (200) reflection obtained from c-GaN on GaAs (311) substrate, but reason is different. Since, in the case of c-GaN on GaAs (311) substrate, the irradiated volume of tilted c-GaN (200) is much lower than that in the case of c-GaN on GaAs (001), that the c-GaN (002) is in-plane with the substrate surface. To calculate the lattice spacings of c-GaN on GaAs (311), the peak position was obtained by fitting a Gaussian function to the experimental data obtained from both (311) and (200) reflections. Figure 4.8 shows Gaussian fitting results of (311) and (200) c-GaN reflections, which were respectively used to determine peak positions of (311) and (200) diffraction peak to be $2\theta = 69.106^\circ$ and 41.698° . With using Bragg's law (Eq. 2.1), the values of lattice spacings, d_{200} and d_{311} , were determined to be 2.164 Å and 1.359 Å, respectively, which were indicated a small compressive strain. The values of lattice spacing of the fully relaxed c-GaN layer were $d_{r,311} = 1.3577$ Å and $d_{r,200} = 2.2515$ Å.

The strain, which is in the direction that parallel to the GaAs (311) and GaAs (200), was calculated by

$$\varepsilon_{hkl} = \frac{(d_{hkl} - d_{r,hkl})}{d_{r,hkl}} \times 100\%. \quad 4.2.$$

Here, (hkl) index as (311) and (200) were used in our calculation. Tables 4.3 and 4.4 summarized all the determined parameters, including thickness, d_{200} , d_{311} , ε_{200} and ε_{311} , calculated using “relaxed” lattice constants obtaining from theoretical (Table 4.3) and experimental values (Table 4.4), respectively. It is clearly seen that the values of d_{200} and d_{311} of c-GaN layers are smaller and larger than those of the relaxed c-GaN layer, indicating that strain in this c-GaN layer is also compressive as observed in the c-GaN layer on the GaAs (001) substrate. This is contrary to the expected tensile strain caused by the large lattice mismatch between c-GaN layers and GaAs substrates. We believed that the strain in c-GaN on GaAs (311) is compressive induced by the

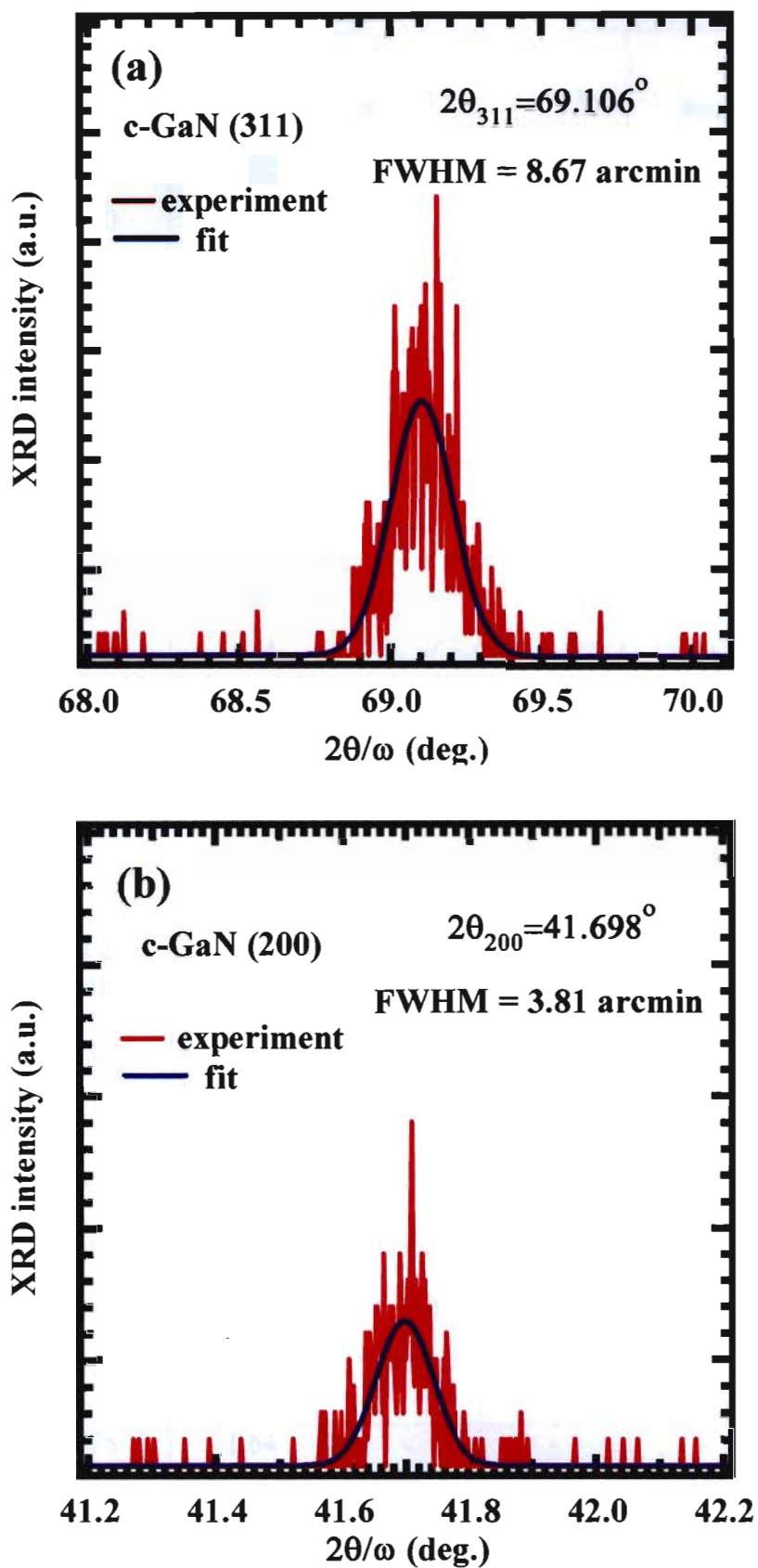


Figure 4.8: The peak positions of (a) c-GaN (311) and (b) c-GaN (200) reflections of the sample used in Fig. 4.7 fitted by Gaussian-line shape.

Samples No.	Tg buffer (°C)	Thickness (μm)	d_{200} (Å)	d_{311} (Å)	ϵ_{311}	ϵ_{200}
7	550	3.33	1.359	2.138	+0.000	-0.050
8	575	3.38	1.359	2.164	+0.000	-0.039
9	600	2.25	1.359	2.090	+0.000	-0.072
10	530	1.64	1.359	2.166	+0.000	-0.038
11	550	1.48	-	-	-	-
12	575	1.64	-	-	-	-

Table 4.3: Measured values of d_{200} and d_{311} of c-GaN on GaAs (311) with different growth conditions. The ϵ_{200} and ϵ_{311} was calculated by $(d_{200}-d_{r,200})/d_{r,200}$ and $(d_{311}-d_{r,311})/d_{r,311}$, respectively. In the calculation here, $a_r = 4.503$ Å, $d_{r,200} = 2.2515$ Å and $d_{r,311} = 1.3577$ Å were used.

Samples No.	Tg buffer (°C)	Thickness (μm)	d_{200} (Å)	d_{311} (Å)	ϵ_{311}	ϵ_{200}
7	550	3.33	1.359	2.138	+0.000	-5.1×10^{-2}
8	575	3.38	1.359	2.164	+0.000	-3.9×10^{-2}
9	600	2.25	1.359	2.090	+0.000	-7.2×10^{-2}
10	530	1.64	1.359	2.166	+0.000	-3.8×10^{-2}
11	550	1.48	-	-	-	-
12	575	1.64	-	-	-	-

Table 4.4: Measured values of d_{200} and d_{311} of c-GaN on GaAs (311) with different growth conditions. The ϵ_{200} and ϵ_{311} was calculated by $(d_{200}-d_{r,200})/d_{r,200}$ and $(d_{311}-d_{r,311})/d_{r,311}$, respectively. In the calculation here, $a_r = 4.5045$ Å, $d_{r,200} = 2.2522$ Å and $d_{r,311} = 1.3582$ Å were used.

thermal mismatch strain during the cooling down process. Thus, we propose the same explanation of this anomalous strain as in the case of c-GaN on (001) substrate.

4.2 Summary

We investigated the difference in lattice constants and strain of c-GaAs layers grown by MOVPE on GaAs substrates using HRXRD with regard to the influence of growth conditions, including V/III ratio and growth temperature of an intermediate c-GaN buffer layer and V/III ratios of c-GaN main layer, and substrate surface orientations. A c-GaN buffer layer directly grown on the GaAs substrates used to modify the quality of upper c-GaN layer. In our samples, compressive strain existed in the c-GaN layers. It was found that growth temperatures of 575°C trends to reduce the residual strain of the c-GaN layers grown on both the GaAs (001) and GaAs (311) substrates. However, with a buffer we cannot identify types of strain, since strain type is changed with thickness. Actually, the strain of c-GaN layers is compressive due to thermal mismatch strain and is induced during the cooling down process. Additionally, this residual strain is not only dependent on the layer thickness, thus on the other hand, the tensile strain induced by the mismatch in lattice constants of c-GaN and GaAs also contributed to the total strain in the studied c-GaN layers. Therefore we concluded that the residual compressive strain appears as the result of interaction between lattice mismatch and thermal mismatch. We also determined the fully “relaxed” lattice constants of c-GaN to be $4.5045 \pm 0.0021 \text{ \AA}$.

CHAPTER V

Hexagonal Phase Generation in c-GaN

In this chapter, we report that the ratio of cubic to hexagonal components in c-GaN layers on GaAs (001) substrates. It can be estimated from the ratio of integrated X-ray diffraction intensities of the cubic (002) (I_{c-002}) and hexagonal (10-11) ($I_{h-10-11}$) planes measured using ω -scan extracted from RSM in HRXRD, as far as the h-GaN is grown with [0001] axis parallel to the cubic [111] direction. We tried to estimate the dependence of hexagonal phase inclusion in c-GaN layer on GaAs (001) substrate on the growth condition by this method. The hexagonal generations was also confirmed by the results of Raman scattering. Correlation between amounts of hexagonal inclusion estimated using HRXRD (H_{XRD}) and the ratio of integrated Raman scattering intensities of cubic related transverse optical (c-TO) phonon (I_{c-TO}) and hexagonal related h-TO phonon (I_{h-TO}) modes. This correlation was used to estimate an amount of hexagonal phase inclusion (H_{Raman}) in the c-GaN layers on GaAs (311) substrates via Raman scattering due to a lack of X-ray diffraction from hexagonal (10-11) plane.

5.1 Hexagonal phase generation in c-GaN on GaAs (001)

Figure 5.1 shows the (002) $2\theta/\omega$ -scan profiles of the c-GaN films on GaAs (001) substrates. Growth conditions: V/III ratios of c-GaN buffer (V/III=100) and main (V/III=25) layers are indicated as red solid lines and V/III ratios of c-GaN buffer (V/III=50) and main (V/III=12.5) layers are indicated as blue solid lines. The cubic (002) diffractions are clearly observed at $2\theta \sim 40^\circ$, whereas the hexagonal (0002) diffractions are absent. The diffraction peaks related to h-GaN (10-11) were also

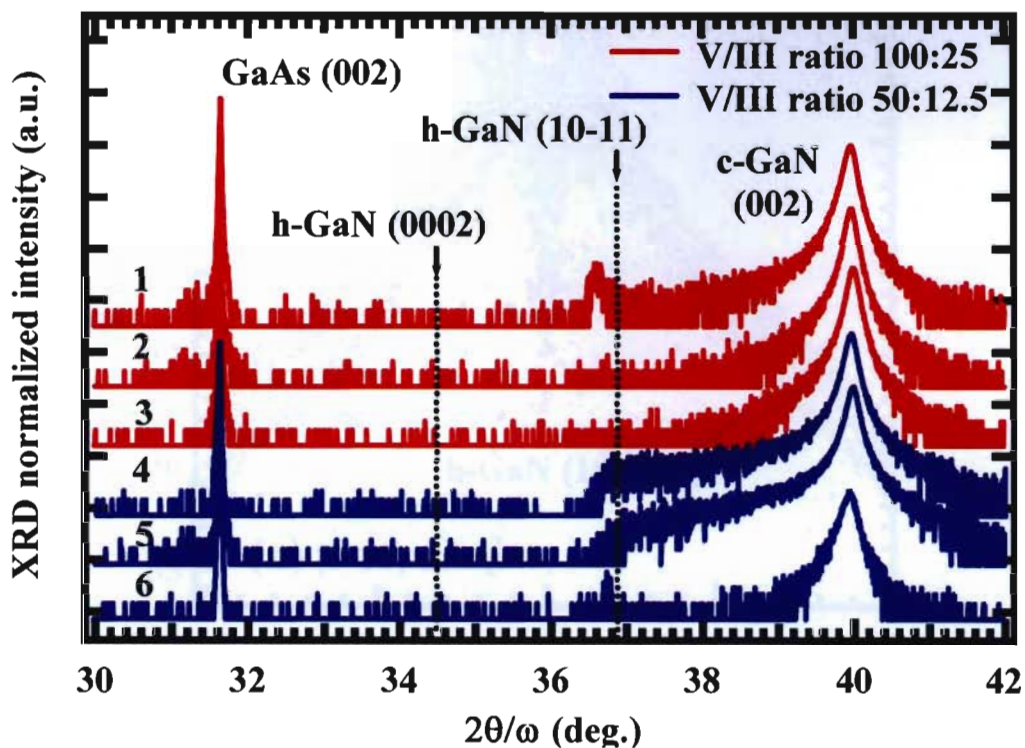


Figure 5.1: (002) $2\theta/\omega$ scan profiles of the c-GaN films on GaAs (001) substrates grown with different growth conditions (see details in Chapter III).

observed for some layers, excluding samples No. 2 and 3. This demonstrates that the GaN grown films have cubic structures and prefer to have hexagonal (10-11) grains parallel to the GaAs (001) substrate. Thus, it cannot be concluded that no generation of hexagonal crystal in these c-GaN films as described in Chapter II. The way to prove this situation is measured the RSM around the (002) reflection and try to cover the reflection from h-GaN (10-11) [18].

5.1.1 Detection of an inclined hexagonal-phase

In order to detect the inclined hexagonal phase subdomains in the c-GaN films, X-ray RSMs were performed. Figure 5.2 shows the X-ray RSMs around the (002) diffraction point measured along the [110] and [1-10] azimuth axis from sample No.4 (V/III ratio of c-GaN buffer layer = 50 at 530°C, V/III ratio of main layer = 12.5). The related diffractions from different plane are labeled in the figure 5.2. The

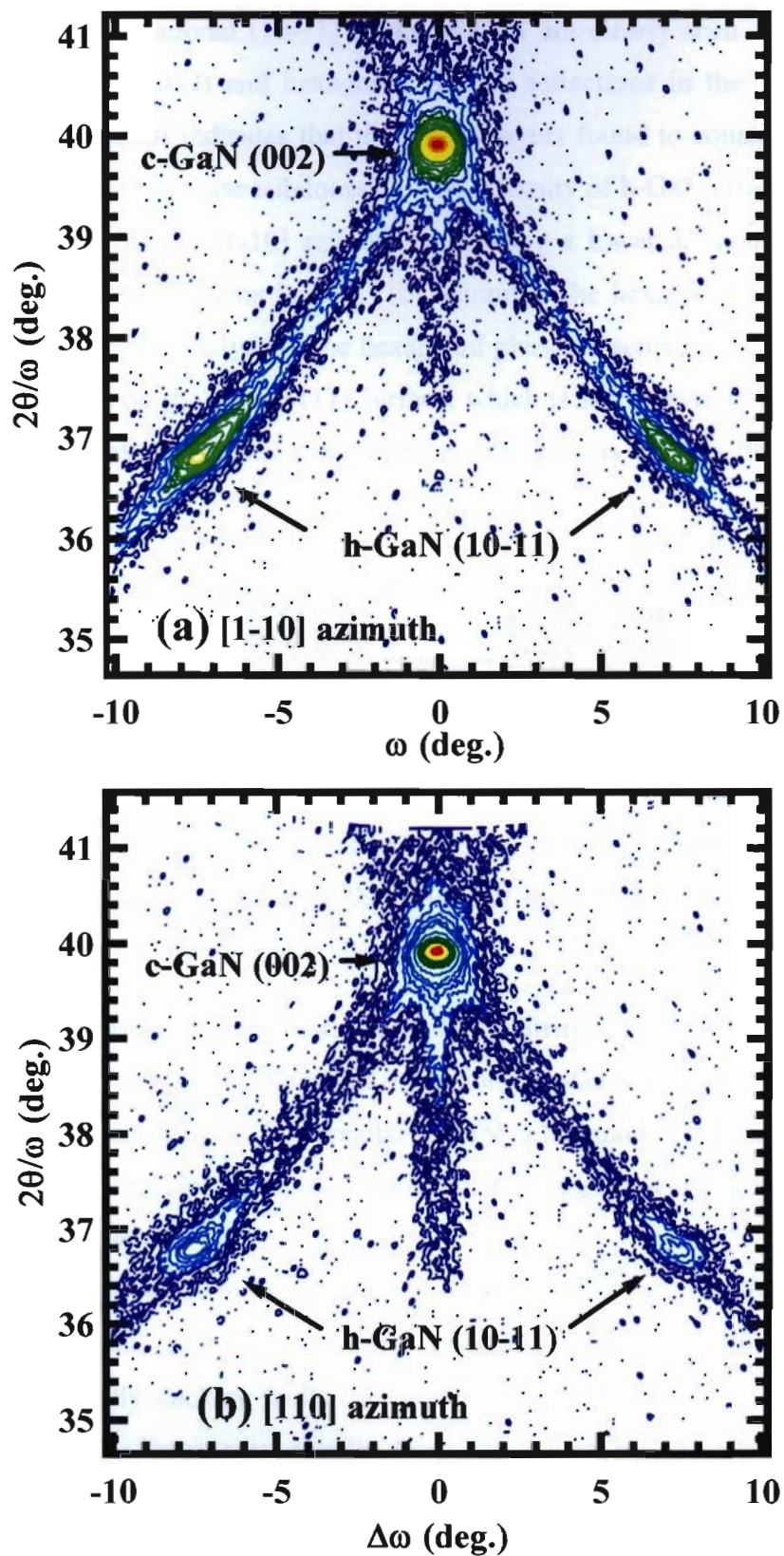


Figure 5.2: Typical (002) X-ray reciprocal space mappings of the GaN films growth condition GaN buffer layer 550°C and V/III ratio 100:25 and the growth condition GaN buffer layer 575°C and V/III 50:12.5 measured along the [110] azimuth axis.

cubic (002) and hexagonal (10-11) peaks of GaN are clearly seen. The tilted angle between the cubic (002) and hexagonal (10-11) reflections in the c-GaN layers is about $\pm 7^\circ$. This result indicates that the c-GaN layers found to contain some amount of inclined hexagonal-phase subdomains. The intensity of h-GaN (10-11) reflection is smaller than that of the [1-10] azimuth, suggesting a lower amount of the inclined hexagonal-phase subdomains in the [110] azimuth. The hexagonal (10-11) peaks as seen in Figure 5.2 are analyzed. The hexagonal phase presented in the c-GaN layer is mainly generated on the cubic (111) surface, which is shown schematically in Figure 2.5. The orientation of hexagonal phase subdomains are in the direction of $[0001]//[111]$.

In addition, the shape characteristic of the hexagonal (10-11) peaks can be clarified. As an example, it is clearly seen in Figure 5.2 that there is a streak connecting the c-GaN (002) reciprocal lattice point to the h-GaN (10-11) points. This diffraction pattern indicates that there are a few hexagonal phases with different lattice constants and crystal orientations. Since, the atomic arrangement (0001) surfaces are the same as those of the cubic (111) surfaces. For this reason, there are three possible way as to interpret the structural modifications of c-GaN along the $\langle 111 \rangle$ directions.

1. The streak consists of (10-11) diffraction peaks of h-GaN with different lattice constants. The strain relaxation in h-GaN domain will vary with the size of h-GaN subdomain. For smaller h-GaN subdomain, the lattice constant and orientation will be close to those of c-GaN. For larger h-GaN domains, they will approach to those of h-GaN.

2. The domain boundaries between h-GaN and c-GaN are deformed regions with its crystalline structure changing gradually cubic to hexagonal structures, namely stacking faults.

3. The layer may contain layer-like c-GaN/h-GaN material. From this reasons, we obtain that the average lattice plane spacing would vary from c-GaN to that of h-GaN due to the different amounts of hexagonal phase inclusion.

5.1.2 Estimation of hexagonal phase inclusion

The intensity of the h-GaN (10-11) reflections varies on the growth condition, suggesting variation of amount of hexagonal phase inclusion in the c-GaN layers. In order to give a quantitative estimation of an amount of hexagonal phase inclusion, we calculated the integrated XRD intensities of the cubic (002) and hexagonal (10-11) diffractions measured by the ω -scan [19]. Figures 5.3 show the ω -scan profiles of c-GaN (002) planes ($2\theta = 40.01^\circ$) and h-GaN (10-11) planes ($2\theta = 34.56^\circ$) of sample No. 4. The red circles and solid blue lines are the experimental and the Gaussian fitted curves, respectively. The integration data of each diffraction peaks was calculated from area under the Gaussian fitted curves as shown in Figures 5.3.

It has been well known that XRD peak intensities are usually different for different lattice planes [36]. However, there is no report on the XRD intensity of c-GaN compared with that of h-GaN, owing to a lack of a high quality thick c-GaN layer. Thus, we calculated the theoretical XRD intensities of the ω -scan for both the c-GaN (002) and h-GaN (10-11) planes. The integrated XRD intensity I is expressed as [19]:

$$I = I_0 \times |F(hkl)|^2 \times P \times V \times L_p \times N^2 \times e^{-2M}, \quad 5.1$$

where I_0 , P , V , L_p , N and e^{-2M} are the incident X-ray intensity, multiplicity factor, irradiated volume, Lorentz polarization factor, number of unit cell per unit volume and temperature factor, respectively.

If there are N atoms in unit cell, the coordinates of the n -th atom are defined as (x_n, y_n, z_n) and f_n is the atomic scattering factor for the n -th atom, then structure factor $F_{(hkl)}$ can be expressed as

$$F_{hkl} = \sum_{n=1}^N f_n \exp[2\pi i(hx_n + ky_n + lz_n)], \quad 5.2$$

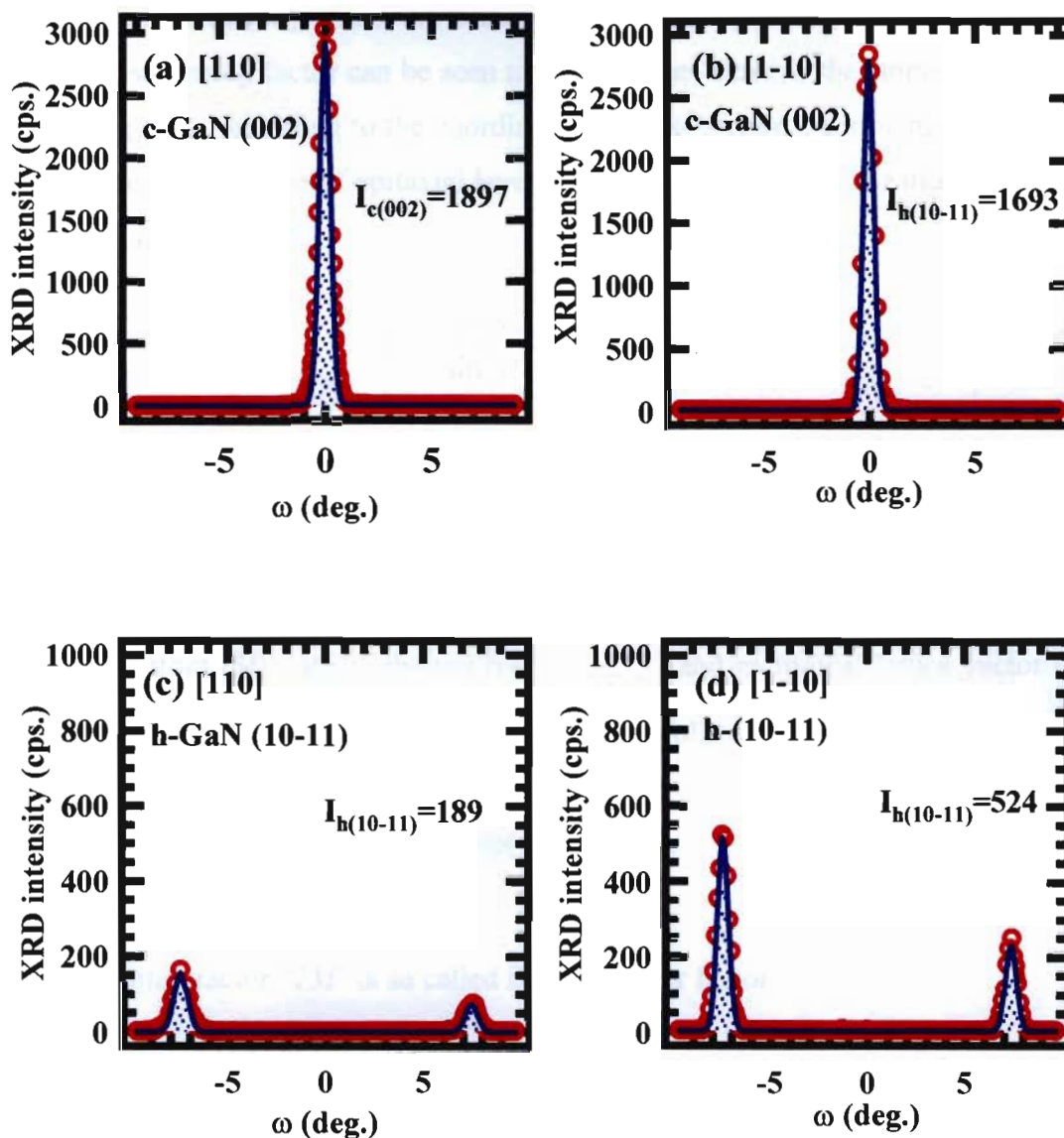


Figure 5.3: ω -scan profile of the c-GaN (002) ($2\theta = 40.01^\circ$) and h-GaN (10-11) ($2\theta = 34.56^\circ$) diffraction peaks extracted from the X-ray RSM measured along the [110] and [1-10] azimuth axis of sample condition GaN buffer layer 530° and V/III ratio 50:12.5 (sample No. 4). The red circles and blue solid lines are the experimental and the Gaussian fitted curves, respective. The integration data of each diffraction peaks was calculated from the area under the Gaussian fitted curves.

the value of f_n , which is corresponded to scattering strength of n -th atom, depends on both θ and λ of incident X-ray beam [37]. Table 5.1 shows atomic scattering factors of Ga and N atoms [35], which are used in our calculation. For low scattering angles, the atomic scattering factor can be seen to reach values close to the atomic number as seen in Fig. 5.4. According to the coordinate of all the atoms, the structure factor can be calculated. In the case of epitaxial layer, $P = 1$. The Lorentz polarization factor can be denoted as

$$L_p = \frac{1 + \cos^2 2\theta}{\sin^2 \theta \cos \theta}, \quad 5.3$$

where θ is being Bragg's angle of the (hkl) reflection. In addition, as the temperature of the crystal is increased, the intensity of the Bragg reflected X-ray decreases as an exponential decay. This is so called temperature factor. Debye and Waller showed that the temperature factor depends on the Boltzmann constant (k_B), temperature (T), mass of an atom (M), lattice phonon frequency (ω) and reciprocal lattice vector (\vec{G} , where $|\vec{G}| = 1/d_{hkl} = \sin\theta/\lambda$) and it can be denoted as follows [38].

$$e^{-2M} = \exp\left(-\frac{k_B T}{M\omega^2} G^2\right), \quad 5.4$$

the exponential factor “ $2M$ ” is so called Debye-Waller factor.

As a result, the calculation values of the relative XRD intensities from one plane for several GaN planes are shown in Table 5.2 [19]. The α values, which are the ratio of the integrated XRD intensity from the summation of those from the hexagonal (10-11) planes to the cubic (002) plane, were calculated to be 1.07 for GaN. To estimate the amount of hexagonal phase inclusion in the c-GaN layer, Eq. 5.1 is simplified. Thus, the irradiated volume is

$$V = \frac{I}{I_0 \times |F(hkl)|^2 \times P \times L_p \times N^2 \times e^{-2M}}. \quad 5.5$$

So, the volume ratio of hexagonal phase to cubic phase can be expressed as

$$\frac{V_h}{V_c} = \frac{I_h}{I_c} \frac{I_{0-c} \times |F(hkl)|_c^2 \times P_c \times L_{p-c} \times N_c^2 \times e_c^{-2M}}{I_{0-h} \times |F(hkl)|_h^2 \times P_h \times L_{p-h} \times N_h^2 \times e_h^{-2M}}, \quad 5.6$$

$\sin \theta/\lambda$ (\AA^{-1})	Atomic scattering factor [$f(\sin \theta/\lambda)$]										
	0.0	0.1	0.2	0.3	0.4	0.5	0.6	0.7	0.8	0.9	1.0
Ga	31	27.8	23.3	19.3	16.5	14.5	12.7	11.2	10	8.9	7.9
N	7	5.8	4.2	3	2.3	1.9	1.65	1.54	1.49	1.36	1.29

Table 5.1: Atomic scattering factors for Ga and N atom, which used in our calculation [35].

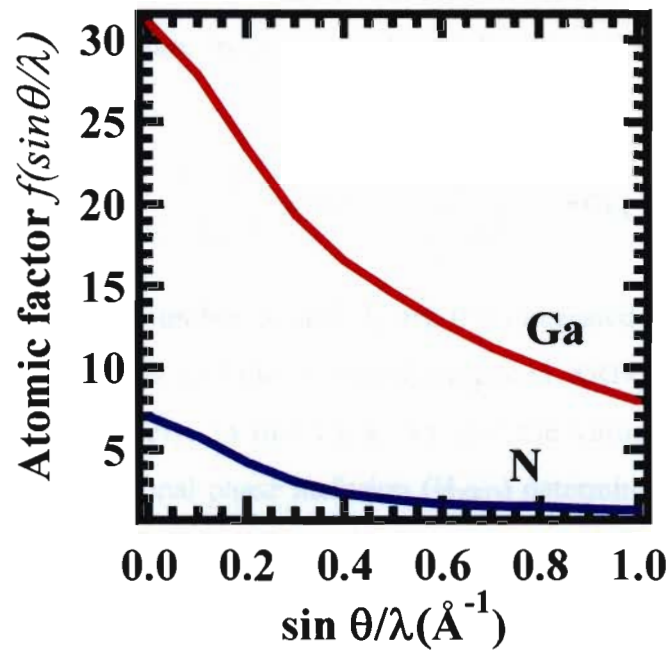


Figure 5.4: Atomic scattering factor for Ga and N atom as a function of $\sin \theta/\lambda$.

Structures	Planes	θ (deg.)	I (10^6 cps.)	$I/I_{c-002} = \alpha$
Cubic	(111)	17.2	18.8	2.35
	(002)	20	7.98	1
	(220)	28.9	4.86	0.61
	(311)	34.5	2.10	0.26
	(222)	36.3	1.33	0.17
Hexagonal	(10-10)	16.1	7.60	0.95
	(0002)	17.3	18.5	2.32
	(10-11)	18.4	8.47	1.07
	(10-12)	24.2	1.63	0.20
	(11-20)	28.9	4.84	0.61

Table 5.2: Theoretical XRD intensities from several cubic and hexagonal phase for GaN crystal.

where h and c denote hexagonal and cubic phase structure, respectively. Finally, the amount of hexagonal phase inclusion in the total volume, $(V_h)_T$, can be calculated using

$$(V_h)_T \% = \frac{V_h/V_c}{1+V_h/V_c} \times 100\% = \frac{I_h}{I_h + \alpha \bar{I}_c} \times 100\%, \quad 5.7$$

where α is the weight number. I_h and \bar{I}_c are the integrated XRD intensities from hexagonal (10-11) planes and the averaged integrated XRD intensities from cubic (002) planes, respectively. In our work, we use the value of $\alpha = 1.07$ for the GaN crystal, thus, hexagonal phase inclusion (H_{XRD}) determined by Eq. 5.7 become:

$$H_{XRD} = \frac{I_h}{I_h + 1.07 \cdot \bar{I}_c} \times 100\%. \quad 5.8$$

From Eq. 5.8, we demonstrate that the amount of hexagonal phase inclusion in the c-GaN layer can be estimated using the ratio of integrated XRD intensity from the cubic (002) plane to the summation of those from the hexagonal (10-11) planes measured by ω -scan. Then, Eq. 5.8 was used to estimate volume ratio of hexagonal phase, namely hexagonal phase inclusion. As shown in Table 5.3, hexagonal phase inclusion amounts of 25-92% was established. It is found that amount of hexagonal phase inclusion is sensitive on the growth temperature of buffer layer. While, less influence of V/III ratio was observed.

Sample No.	Thickness (μm)	V/III ratios Buff.: layer	T_g buffer ($^{\circ}\text{C}$)	H_{XRD} (%): c-phase purity (%)	H_{Raman} (%)
1	1.50	100: 25	550	25 : 75	17
2	2.05	100: 25	575	32 : 68	18
3	1.28	100: 25	600	36 : 64	20
4	1.61	50: 12.5	530	27 : 73	18
5	8.87	50: 12.5	550	26 : 74	24
6	2.55	50: 12.5	575	85 : 15	68

Table 5.3: Amounts of hexagonal phase inclusion determined by HRXRD (H_{XRD}) and Raman scattering (H_{Raman}) in c-GaN layers on GaAs (001) substrates with various growth conditions.

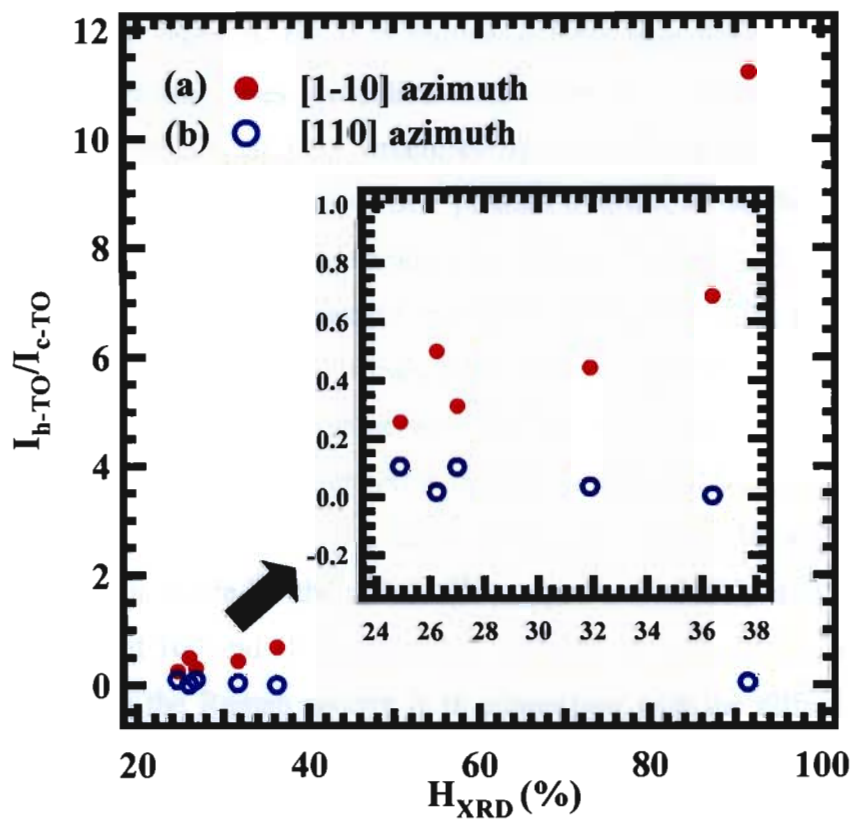


Figure 5.5: $I_{h(10-11)}/I_{c(002)}$ as a function of hexagonal phase inclusion (%) of c-GaN layers on GaAs (001) substrates for (a) [1-10] azimuth and (b) [110] azimuth axes.

In addition, as shown in Fig. 5.5, we found out that the generation of hexagonal phase inclusion in c-GaN exhibits anisotropic characteristic. Only the $\{111\}$ planes that perpendicular to the $[1-10]$ direction is preferred hexagonal phase generation. Since, integrated intensity of hexagonal (10-11) obtained from the $[110]$ azimuth axis is less sensitive to amount of hexagonal phase inclusion.

5.1.3 Correlation between vibrational properties and hexagonal phase generation

In this part, we evaluated the possible impact of the growth conditions on the vibrational properties in the c-GaN layers using Raman spectroscopy. Raman scattering with incident light wavelength 514.5 nm is used to study the regions of thin c-GaN layers at room temperature. The number of samples used in this study are 6 samples. Raman spectra were recorded from 3 different areas (3 spots) for each sample. Figure 5.6 shows Raman spectra of the c-GaN layers on GaAs (001) substrates grown under V/III ratios of buffer and main layers are 100 and 50 (red line) and 50 and 12.5 (blue line). The Raman intensity is normalized with respect to the cubic-LO Raman intensity for each sample and the base lines are subtracted. The black- and green-dash lines are indicated the characteristic phonon frequencies of cubic [21] and hexagonal [21] structures of the GaN crystals, respectively. For reference, values of these characteristic phonon frequencies for both the cubic and hexagonal c-GaN crystals have already presented in Table 2.1. It is found that the cubic LO phonon is clearly observed in all the c-GaN layers. On the other hand, as expected, the occurrence of the h-GaN related Raman features near 568 [31] due to the incorporation of hexagonal phase was clearly observed as shown in Fig. 5.6. This phonon mode is connected to transverse optical phonon (h-TO). Compared to the c-GaN layer grown with lower V/III ratios, Raman spectra exhibit a less influence of hexagonal phonon mode for the c-GaN films grown with V/III ratios of buffer layer and main layer of 100 and 50 (samples No. 1, 2 and 3). The results demonstrate that the difference in the Raman spectra is in connection with the different amounts of hexagonal phase inclusion in the c-GaN films. Based on HRXRD and Raman scattering measurements, the grown c-GaN layers also contain some amount of inclined hexagonal subdomains.

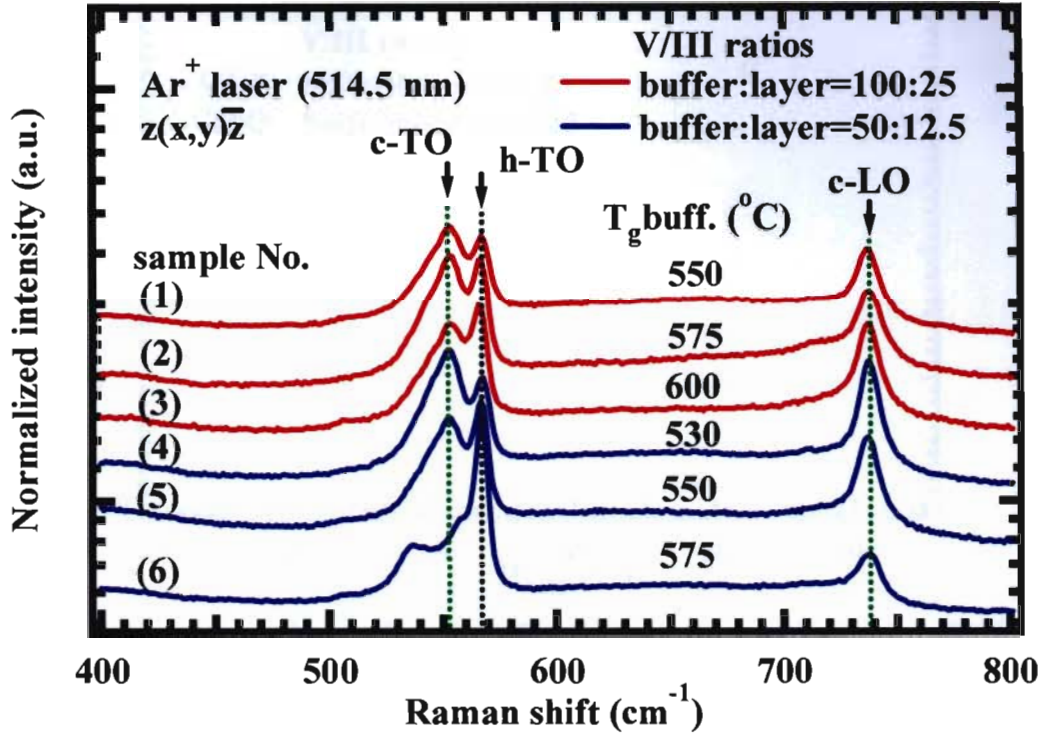


Figure 5.6: Raman spectra of the c-GaN films on GaAs (001) substrates grown with different growth conditions. Green-dotted lines and black-dotted lines indicate the characteristic phonon frequencies of c-GaN and h-GaN phase, respectively.

Under these observations, thus, we found correlation between amount of hexagonal phase inclusion and the intensity ratio of integrated Raman scattering intensities of c-TO phonon (I_{c-TO}) and h-GaN related h-TO phonon (I_{h-TO}) modes (I_{h-TO}/I_{c-TO}) as a linear dependence as shown in Fig. 5.7. Noted that the integrated Raman intensities of c-TO and h-TO obtained by subtracting the base lines and then fit the spectrum with Gaussian-line shape, as shown in Fig. 5.8.

It is known that the integrated intensity of c-TO (I_{c-TO}) in c-GaN layer is proportional to the cubic phase component and that of h-TO (I_{h-TO}) is proportional to the hexagonal phase component. Then hexagonal phase inclusion (H_{Raman}) from the Raman scattering measurements can be calculated as follows;

$$H_{Raman} = \frac{I_{h-TO}}{I_{h-TO} + I_{c-TO}} \times 100\%. \quad 5.9$$

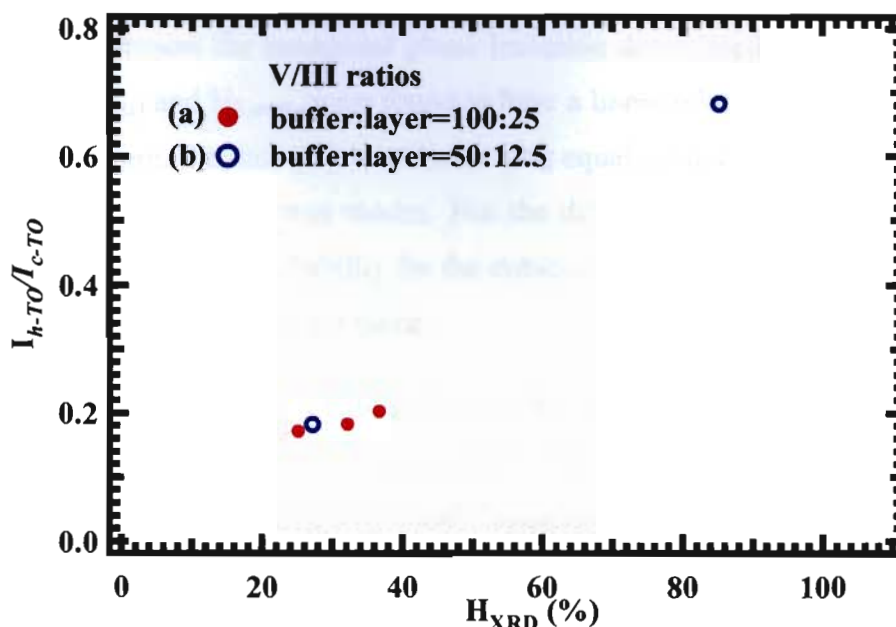


Figure 5.7: I_{h-TO}/I_{c-TO} ratio as a function of hexagonal phase inclusion in c-GaN layers on GaAs (001): (a) V/III ratios of buffer and main layers are 100 and 25, respectively, and (b) V/III ratios of buffer and main layers are 50 and 12.5, respectively.

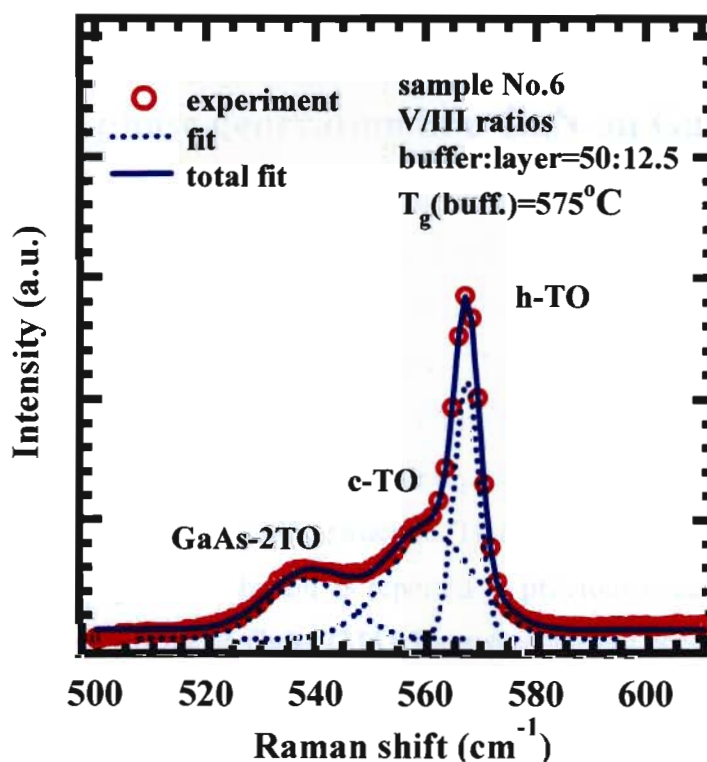


Figure 5.8: Raman spectra of the c-GaN films on GaAs (001) substrates grown with V/III ratios of buffer and main layers are 100 and 25, respectively, at growth temperature of buffer layer of 575°C. Red circle, blue-dashes line and blue solid line are represented an experiment, fitting and total fitting, respectively.

We represent the hexagonal phase inclusion determined by using HRXRD as H_{XRD} . The H_{XRD} and H_{Raman} , were found to have a linear relationship as shown in Fig. 5.9. In this figure, the data points are assuming equal scattering probability for cubic and hexagonal related phonon modes. But the difference between H_{Raman} and H_{XRD} indicates that scattering probability for the cubic-related phonon mode lower than that of the hexagonal related phonon mode.

The average H_{Raman} calculated using the Eq. (5.9) as a function of H_{XRD} is displayed in Fig. 5.9. The data points were obtained giving the best fit; $H_{Raman} = 2.4 + 0.5H_{XRD}$. Table 5.3 shows H_{XRD} and H_{Raman} calculated for each c-GaN layers. We show that a linear dependence of H_{Raman} on H_{XRD} , may provide a useful calibration method to determine the hexagonal phase inclusion in c-GaN layers by using Raman spectroscopy technique. Thus, we applied this method to estimate amount of hexagonal phase inclusion in c-GaN layer on GaAs (311) substrates, which will be discussed later in the next section.

5.2 Hexagonal phase generation in c-GaN on GaAs (311)

It is well known that there are four similar $\{111\}$ planes in the cubic noncentrosymmetric structure; (111) and (1-1-1) planes are along the [1-10] axis and other (1-11) and (-111) planes are along the [110] axis. However, as we described in Chapter II, we can observe only the symmetric (311) and (200) reflections of c-GaN layers grown on GaAs (311) substrates due to limitation of HRXRD instrument. This makes a lack of X-ray diffraction from the hexagonal (10-11) planes connected with the four similar $\{111\}$ planes in cubic structure. Thus, the method used to estimate an amount of hexagonal phase inclusion as reported in previous section cannot used to estimate for the case of layer on GaAs (311). Raman scattering becomes very valuable in proven generation of hexagonal phase in c-GaN layers on GaAs (311) substrates. For example, our report in previous section showed a useful calibration method to determine the hexagonal phase inclusion in c-GaN layers by using Raman spectroscopy technique.

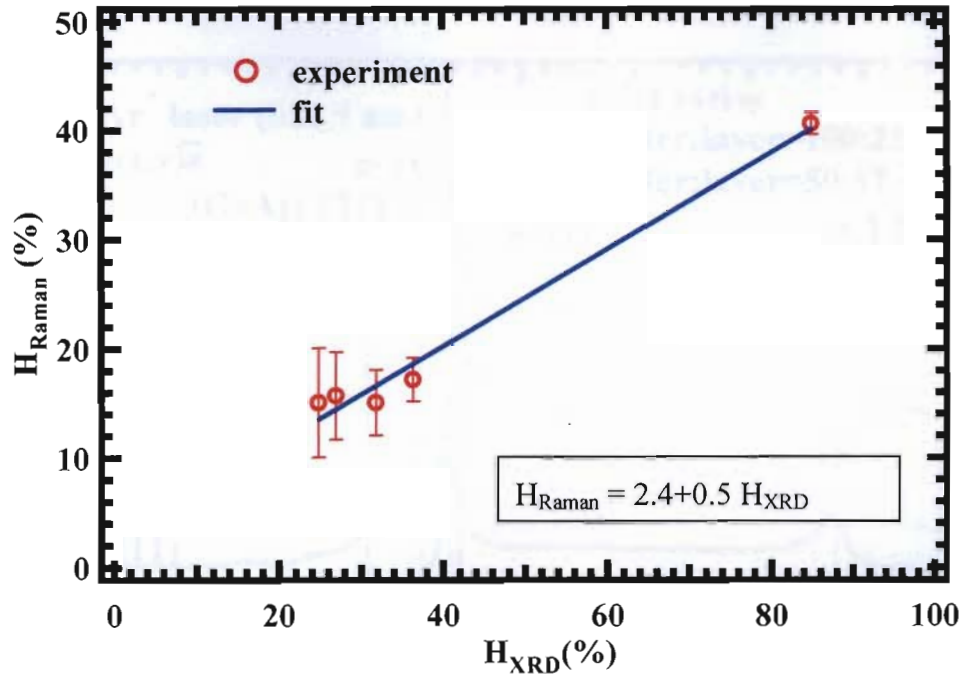


Figure 5.9: H_{Raman} as a function of the H_{XRD} , from our experiment. The data points are average data obtained from 3 spots on the sample. Error bars are standard deviations.

Figure 5.10 shows room-temperature Raman scattering spectra of the c-GaN layers on GaAs (311) substrates grown under V/III ratios of buffer and main layers are 100 and 25 (red line) and 50 and 12.5 (blue line). The Raman intensity is normalized with respect to the cubic-LO Raman intensity for each sample and the base lines are subtracted out. The black- and green-dotted lines are indicated the characteristic phonon frequencies related to cubic and hexagonal structures of the GaN crystals, respectively. The c-LO phonon is also clearly seen for all the c-GaN layers as observed in the case of c-GaN on GaAs (001). As we expected, the occurrence of the h-TO phonon mode near 568 [31] due to the incorporation of hexagonal phase is seen in Fig. 5.10. Compared to the c-GaN layer on GaAs (001), Raman spectra exhibit a stronger intensity of h-TO phonon mode. The result suggests that the difference in the Raman scattering intensity is in connection with the different amounts of hexagonal phase inclusion in the c-GaN films.

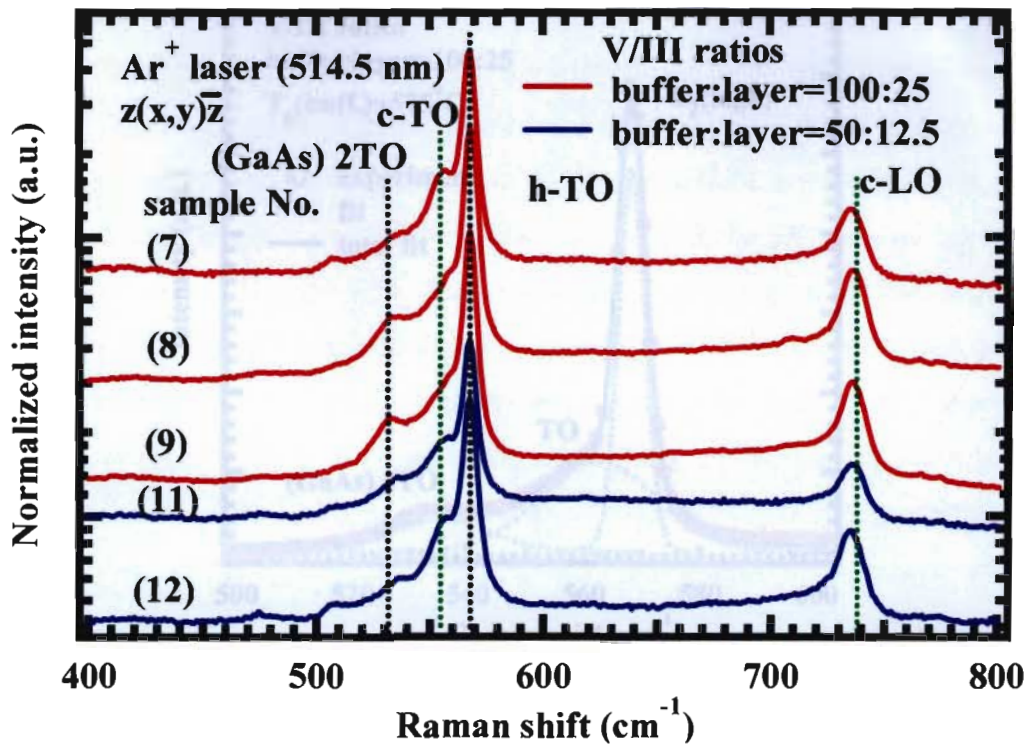


Figure 5.10: Raman spectra of the c-GaN films on GaAs (001) substrates grown with different growth conditions. Red-dotted lines and black-dotted lines indicate the characteristic phonon frequencies of c-GaN and h-GaN phase, respectively.

To determine amount of hexagonal phase inclusion in c-GaN layers on GaAs (311) substrates, Eq. 5.9 was used. Figure 5.11 show the integrated Raman intensities of c-TO and h-TO obtain by subtracted out the base lines and then fited the spectrum with Gaussian-line shape. All determined results of $I_{h\text{-TO}}/I_{c\text{-TO}}$ and H_{Raman} are listed in Table 5.4. Unfortunately, compared to c-GaN layers on GaAs (001) substrates, larger amounts of hexagonal phase inclusion were established for c-GaN layers on GaAs (311) substrates. As shown in Table 5.3, hexagonal phase inclusion amounts of 25-85% was obtained by this method. The results surprised us that the generation of hexagonal phase in c-GaN layer on GaAs (311) is less influenced by the growth conditions. This is due to an insufficient of the layer quality.

Our results demonstrated that not only the substrate surface influenced on the generation of hexagonal phase in c-GaN layers. The growth conditions play as a key to reduce the amount of hexagonal phase inclusion in the c-GaN grown layer

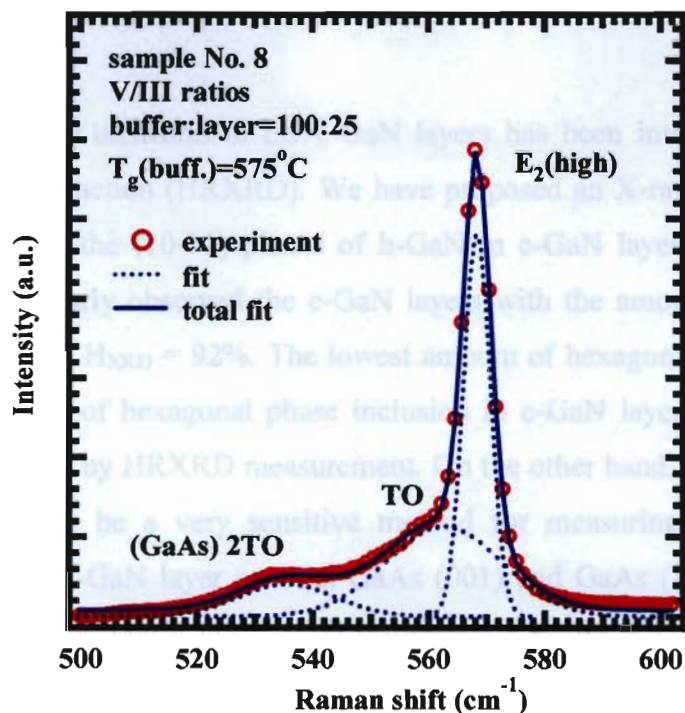


Figure 5.11: Raman spectra of the c-GaN films on GaAs (311) substrates grown with V/III ratios of buffer layer = 100 and main layer = 25 and at growth temperature of buffer layer = 575°C. Red circle, blue-dashes line and blue solid line is experiment, fitting and total fit, respectively.

Sample No.	V/III ratios Buffer:layer r	T _g buffer layer (°C)	Thickness (μm)	I _{h-TO} /I _{c-TO}	H _{Raman} (%)	Estimated hexagonal phase inclusion (%)
7	100:25	550	3.33	0.85	46	87
8	100:25	575	3.38	0.99	50	95.2
9	100:25	600	2.25	0.96	48	91.2
10	50:12.5	530	1.64	No Data	No Data	No Data
11	50:12.5	550	1.48	0.65	40	75
12	50:12.5	575	1.64	0.84	46	87

Table 5.4: Ratios of I_{h-TO}/I_{c-TO} and H_{Raman} for c-GaN layers on GaAs (311) substrates with different growth conditions. Hexagonal phase inclusion was estimated using linear fit, H_{Raman} = 2.4+0.5H_{XRD}, obtained from Fig. 5.9.

5.3 Summary

The hexagonal phase inclusion in the c-GaN layers has been investigated by high resolution X-ray diffraction (HRXRD). We have proposed an X-ray RSM applied in the determination of the (10-11) planes of h-GaN in c-GaN layers on GaAs (001) substrates. It has clearly observed the c-GaN layers with the amounts of hexagonal phase inclusion up to $H_{XRD} = 92\%$. The lowest amount of hexagonal phase inclusion is 25%. The amount of hexagonal phase inclusion in c-GaN layers on GaAs (311) cannot be determined by HRXRD measurement. On the other hand, Raman scattering have seen proven to be a very sensitive method for measuring an existence of hexagonal phase in c-GaN layer on both GaAs (001) and GaAs (311) substrates. It was found that, all the c-GaN layers used in this study exhibit high incorporation of hexagonal phase GaN. The hexagonal phase inclusion in the c-GaN layers determined by Raman spectroscopy technique, H_{Raman} , exhibits a linear dependence on the H_{XRD} . The best fit yields $H_{Raman} = 2.4 + 0.5 H_{XRD}$. A linear dependence of H_{Raman} on H_{XRD} , provides a useful calibration method to determine the amount of hexagonal phase inclusion in c-GaN layers by using Raman spectroscopy technique.

CHAPTER VI

Conclusion

In this thesis, strain and hexagonal phase inclusion in MOVPE grown c-GaN layers on GaAs (001) and GaAs (311) substrates have been investigated. The goal of this thesis is to compare the strain and hexagonal phase generation in the c-GaN layers grown on the GaAs (001) and the GaAs (311) substrates, emphasized on the effect of growth conditions, such as V/III ratios of c-GaN buffer and c-GaN main layers and the growth temperature of buffer layer. High resolution X-ray diffraction (HRXRD) and Raman scattering spectroscopies on c-GaN layers are described.

Strain in c-GaN layers grown on GaAs (001) substrates was measured by a high resolution X-ray diffraction method using $2\theta/\omega$ -scan and RSM modes. Residual strain in the grown layers was in compression, contrary to the predicted tensile strain caused by a large lattice mismatch between c-GaN and GaAs substrates (~20%). It was also found that the relief of strain in the GaN films has a complicated dependence on the growth conditions. We interpreted this as the interaction between the lattice mismatch and thermal mismatch stresses. The fully relaxed lattice constants of cubic GaN are determined to be 4.5045 ± 0.021 Å, which is in agreement with the theoretical prediction of 4.503 Å.

Then, the lattice spacings and residual strain of c-GaN layers grown on GaAs (311) substrates were reported. In our samples, compressive strain existed in the GaN layers. The tensile stresses caused by lattice mismatch are not completely relieved with increasing thickness, and also have a complicated dependence on the growth conditions. As the case of c-GaN layers on GaAs (001) substrates, they partially counteract the compressive strain formed upon cooling due to the mismatch of thermal expansion coefficients. The residual compressive strain emerges as the result of interaction between lattice mismatch and thermal mismatch.

The c-GaN layers have been studied by Raman scattering spectroscopy. It was found that, c-GaN layers have a component of hexagonal phase. And, in all the hexagonal incorporating films, a hexagonal phase-related transverse optical (h-TO) phonon is observed at Raman frequency of 568 cm^{-1} . The ratio of integrated Raman scattering intensities of c-TO phonon and h-GaN related h-TO phonon modes (I_{h-TO}/I_{c-TO}) is proportional to the hexagonal phase inclusion. The hexagonal phase inclusion in the c-GaN layers determined by Raman spectroscopy technique (H_{Raman}), exhibits a linear dependence on the hexagonal phase inclusion (H_{XRD}) determined using HRXRD. The best fit yields $H_{\text{Raman}} = 0.5 H_{\text{XRD}} + 2.4$. A linear dependence of H_{Raman} on H_{XRD} , provides a useful calibration method to determine the hexagonal phase inclusion in c-GaN by using Raman spectroscopy technique.

HRXRD and Raman scattering spectroscopes are also used to investigate the hexagonal phase generation in the c-GaN layers grown on GaAs (311) substrates. Unfortunately, an existence of hexagonal phase cannot be confirmed by HRXRD due to the limit of the instrument. Thus, RSM in HRXRD cannot be used for estimate amount of hexagonal phase in c-GaN on GaAs (311) substrates. But, a strong intensity of h-TO Raman spectra indicated a large incorporation of hexagonal phase in the c-GaN layers. Thus, we applied this method to estimate amount of hexagonal phase inclusion in c-GaN layer on GaAs (311) substrates and found out that incorporation of hexagonal phase in c-GaN layer on GaAs (311) is higher than in the case of the c-GaN layer on GaAs (001).

As shown by these results, the hexagonal phase generation in the c-GaN layers grown by MOVPE is in connection with the generation of stacking faults and/or hexagonal phase subdomains. The growth conditions, such as growth temperatures and the V/III ratios of the cubic buffer layer are mainly affecting parameters, which results in the generation of hexagonal phase and strain of the c-GaN layers. The results obtained here can not only be to interpret the c-GaN layers; but also be extended to explain the structural properties of other novel semiconductors. Hopefully, the obtained information is very useful to the full fill understanding of the hexagonal phase formation mechanism for further device improvemens. Further work is still necessary to fully clarify the affecting parameters on the hexagonal phase generation in the growth of epitaxial cubic III-nitride films.

REFERENCES

- [1] Y. J. Hsu, L. S. Hong, J. C. Jing, and J. C. Chang. Effects of hydrogen on GaN metalorganic vapor-phase epitaxy using tertiarybutylhydrazine as nitrogen source. *J. Crystal Growth* **266** (2004): 347.
- [2] J. Wu, M. Kudo, A. Nagayama, H. Yaguchi, K. Onabe, and Y. Shiraki. Selective growth of cubic GaN on patterned GaAs (100) substrates by metalorganic vapor phase epitaxy. *Phy. Stat. sol.* **176** (1999): 558.
- [3] H. Chen, Z.Q. Li, H.F. Liu, Wan, M.H. Zhang, Q. Huang, J.M. Zhou, Y.Luo, Y.J. Han, K. Tao, and N. Yang. Controllable cubic and hexagonal GaN growth on GaAs (001) substrates by molecular beam epitaxy. *J. Crystal Growth* **230** (2001): 415.
- [4] K. Yasui, K. Kanauchi, and T. Akahane, Growth of c-GaN films on GaAs (100) using hot-wire CVD. *Thin Solid Films* **430** (2003): 178.
- [5] S. Lazar, C. Hebert, and H.W. Zandbergen. Investigation of hexagonal and cubic GaN by high-resolution electron energy-loss spectroscopy and density functional theory. *Ultramicroscopy* **98** (2004) 249.
- [6] L. Liu, and J.H. Edgar. Substrates for gallium nitride epitaxy. *Materials Science and Engineering R* **37** (2002) 61.
- [7] H. Okumura, K. Ohta, G. Feuillet, K. Balakrishnan, S. Chichibu, H.Hamaguchi, P. Hacke and S. Yoshida. Growth and characterization of cubic GaN. *Journal of Crystal Growth* **178** (1997): 113.
- [8] I. H. Lee, and S. M. Park. Deposition of cubic GaN films by reactive laser ablation of liquid Ga target in ammonia. *Bull. Koren Chem. Soc.* **21/11** (2000): 1065.
- [9] Chin-Yu Yeh, Z. W. Lu, S. Froyen, and Alex Zunger. Zinc-blende-wurtzite polytypism in semiconductors. *Phys. Rev. Lett.* **24/25** (1992): 10094.

- [10] T. Ohachi, T. Kikuchi, K. Miyauchi, Y. Ito, R. Takagi, M. Hogiri, K. Fujita, O. Ariyada, and M. Wada. Control of nitrogen flux for growth of cubic GaN on 3C-SiC/Si by RF-MBE. *Journal of Crystal Growth* **275** (2005): e1197.
- [11] Ying-G. Yang, Hong-L. Ma, Cheng-S. Xue, Xiao-T. Hao, Hui-Z. Zhuang, and J. Ma. Characterization of GaN films grown on silicon (111) substrates. *Physica B* **325** (2003): 230.
- [12] S. Suandon. *Structural property analysis of GaN grown on GaAs by MOVPE using transmission electron microscopy*. Master's thesis, Department of Physics, Faculty of Science, Chulalongkorn University, 2005.
- [13] X. Wang, and A. Yoshigawa. Molecular beam epitaxy growth of GaN, AlN InN. *Progress in Crystal Growth and Characterization of Materials* **48/49** (2004): 42.
- [14] D. P. Xu, Y. T. Wang, H. Yang, S. F. Li, D. G. Zhao, Y. Fu, S. M. Zhang, and R. H. Wu. Anomalous strains in the cubic-phase GaN films grown on GaAs (001) by metalorganic chemical vapor deposition. *Journal of Applied Physics* **88** (2000): 3762.
- [15] D. Keith Brown, and Brian K. Tanner, *High resolution X-ray Diffractometry and Topography*. UK: T. J. International Ltd, 1998.
- [16] S. Kuntharin. *Structural analysis of cubic InN films grown by molecular beam epitaxy*. Master's thesis, Department of Physics, Faculty of Science, Chulalongkorn University, 2007.
- [17] K. Uesugi, N. Morooka, and I. Suemune. Reexamination of N composition dependence of coherently grown GaNAs band gap energy with high-resolution X-ray diffraction mapping measurements. *Appl. Phys. Lett.* **74** (1999): 1254.
- [18] Z. X. Qin, H. Nagano, Y. Sugure, A. W. Jia, M. Kobayashi, Y. Kato, A. Yoshikawa, and K. Takahashi. High-resolution X-ray diffraction analysis of cubic GaN grown on (001) GaAs by RF-radical source molecular beam epitaxy. *Journal of Crystal Growth* **189/190** (1998): 425.

- [19] H. Tsuchiya, K. Sunaba, S. Yonemura, T. Suemasu, and F. Hasegawa. Cubic dominant GaN growth on (001) GaAs substrates by hydride vapor phase epitaxy. *Jpn. J. Appl. Phys.* **36** (1997): L1.
- [20] C.-L. Wu, C.-H. Shen, H. Y. Chen, S.-J. Tsai, H.-W. Lin, H.-M. Lee, S. Gwo, T.-F. Chuang, H.-S. Chang, and T.-M. Hsu. The effects of AlN buffer on the properties of InN epitaxial films grown on Si (111) by plasma-assisted MBE. *Journal of Crystal Growth* **288** (2006): 247.
- [21] H. F. Liu, H. Chen, Z.Q. Li, L. Wan, Q. Huang, J. M. Zhou, N. Yang, K. Tao, Y. J. Han, and Y. Luo. MBE growth and Raman studies of cubic and hexagonal GaN films on (001)-oriented GaAs substrates. *Journal of Crystal Growth* **218** (2000): 191.
- [22] M. Balkanski, and R. F. Wallis, *Semiconductor Physics and Applications*. UK: Oxford University Press, 2000.
- [23] M. Kuball. Raman spectroscopy of GaN, AlGa_N and AlN for process and growth monitoring/control. *Surface and Interface Analysis* **31** (2001): 987.
- [24] X. L. Sun, Hai Yang, L. X. Zheng, D. P. Xu, J. B. Li, Y. T. Wang, G. H. Li, and Z. G. Wang. Stability investigation of cubic GaN films grown by metalorganic chemical vapor deposition on GaAs (001). *Appl. Phys. Lett.* **74** (1999): 2827-2829.
- [25] C. A. Arguello, D. L. Rousseau and S. P .S. Porto. First-order Raman effect in wurtzite-type crystals. *Phys. Rev.* **181** (1969): 1351.
- [26] M. Kaball, J. W. Pomeroy, M. Wintrebert-Fouquet, K. S. A. Butcher, Hai Lu, and W. J. Schaff. A Raman spectroscopy student of InN. *Journal of Crystal Growth* **269** (2004): 59.
- [27] H. D. Jung, and N. Kumagai. Optical anisotropy and Surface morphology of InGaAs lattice-mismatched with GaAs (001). *J. Appl. Phys.* **84** (1998): 5497.

- [28] H. Okumura, H. Hamaguchi, G. Feuillet, Y. Ishida, and S. Yoshida. MOCVD growth of cubic GaN on 3C-SiC deposited on Si (100) substrates. *Appl. Phys. Lett.* **72** (23) (1998): 3056.
- [29] A. Trampert, O. Brandt, H. Yang, and K. H. Ploog. Growth of cubic GaN on Si(001) by plasma-assisted MBE. *Appl. Phys. Lett.* **70** (1997): 583.
- [30] O. brandt, H. Yang, A. Trampert, M. Wassermeier, and K. H. Ploog. Ga-terminated β -GaN(001) surface reconstructions studied by scanning tunneling microscopy. *Appl. Phys. Lett.* **71** (1997): 473.
- [31] G. W. G. van Dreumel, J. G. Buijnsters, T. Bohnen, J. J. ter Meulen, P. R. Hageman, W. J. P. van Enkevort, and E. Vlieg. Growth of GaN on nanocrystalline diamond substrates. *Diamond & Related Materials*. In press.
- [32] H.-H. Huang, C.-LiChao, T.-WeiChi, Y.-LinChang, P.-ChunLiu, L.-WeiTu, J.-DarTsay, H.-ChungKuo, S.-JenCheng, and W.-ILee. Strain-reduced GaN thick-Film grown by hydride vapor phase epitaxy utilizing dot air-bridged structure. *Journal of Crystal Growth*. In press.
- [33] S. Gautier, C. Sartel, S. Ould-Saad, J. Martin, A. Sirenko, and A. Ougazzaden. GaN materials growth by MOVPE in a new-design reactor using DMHy and NH₃. *Journal of Crystal Growth* **298** (2007): 428.
- [34] C. Lin, G. Yu, X. Wang, M. Cao, H. Lu, H. Gong, M. Qi, and A. Li. Hydride vapor phase epitaxy growth of high-quality GaN Film on in situ etched GaN template. *Materials Letters* **63** (2009): 943
- [35] บัญชา ธนบุญสมบัติ. การศึกษาวัสดุโดยเทคนิคดิฟแฟรคชัน. กรุงเทพฯ: สำนักพิมพ์สมาคมส่งเสริมเทคโนโลยี (ไทย-ญี่ปุ่น), 2537.
- [36] B. D. Cullity. Elements of X0ray diffraction. London: Addison-wesley, 1956.
- [37] Mario Birkholz. Thin Film Analysis by X-Ray Scattering. Berlin: wiley-VCH, 2006.

- [38] Charles Kittel. Introduction to Solid State Physics. California: John Wiley & Sons, 1996.
- [39] K. Kim, W. Lambrecht, and B. Segall. Electronic structure of GaN with strain and phonon distortions. *Phys. Rev. B* **50** (1994): 1502.
- [40] F. Ben kabou, P. Becker, M. Certier, and H. Aourag. Method for measurement of lattice parameter of cubic GaN layers on GaAs (0 0 1). *Phys. Status Solidi B* **209** (1998): 223.
- [41] M. R. Nardelli, K. Rapcewicz, and J. Bernhole. Strain effects on the interface properties of nitride semiconductors. *Phys. Rev. B* **55** (1997): R7323.

APPENDIX

Regional Conference Presentations

1. **N. Discharoen**, S. Sanorpim, R. Katayama and K. Onabe, 'Strains in the cubic-phase GaN films grown on GaAs (001) by metalorganic vapor phase epitaxy' *Siam Physics Congress (SPC 2008)*, Thailand, March 20-22, 2008. (oral presentation)

2. **Nuttapong Discharoen**, Sakuntam Sanorpim, Ryuji Katayama and Kentaro Onabe, 'HIGH RESOLUTION X-RAY DIFFRACTION OF GaN GROWN ON GaAs (001) VIA METAL-ORGANIC VOPOR PHASE EPITAXY' *THE 34th CONGRESS on SCIENCE and TECHNOLOGY of THAILAND (STT 34)*, Queen Sirikit National Convention Center, Bangkok, Thailand, October 31-November 2, 2008. (oral presentation)

VITAE

Mr. Nuttapon Discharoen was born on march 22, 1982 in Pitsanuloke, Thailand. He received his Bachelor degree of Science in Physics from Naresuan University in 2004, and continued his Master's study in 2005.